The Dissertation Committee for Colin Healey Smith certifies that this is the approved version of the following dissertation:

Studies of Rich and Ultra-Rich Combustion for Syngas Production

Committee:

Janet Ellzey, Supervisor

Ofodike A Ezekoye

Carlos H Hidrovo

Halil Berberoglu

Laxminarayan L Raja

Studies of Rich and Ultra-Rich Combustion for Syngas Production

by

Colin Healey Smith, B.S.; M.S.E.

Dissertation

Presented to the Faculty of the Graduate School of

The University of Texas at Austin

in Partial Fulfillment

of the Requirements

for the Degree of

Doctor of Philosophy

The University of Texas at Austin

December 2012

Dedication

To my family

Acknowledgements

I was born with near-perfect parents who, crucially, have always been tremendously supportive and always allowed me to think and express myself freely. Another accident of birth is having my sister who has been a source of inspiration, and my older brothers who have been generous. I have been tremendously lucky to cross paths with some brilliant, well-rounded, challenging people who have contributed a tremendous amount to my growth as a person and as an engineer/scientist. I cannot imagine life, never mind finishing this degree, without my best friends: Richard Sweeney, Kurt Lavetti, Michael Sienkiewicz, Paul White, Brent Castle and Conan Zhang. These people have made me who I am, and though there are seven billion people on this planet, I really feel I've come across some of the very best.

I've also been lucky to have some tremendous personal, academic and professional support through the years. Cathy Salvo and Joel Herskowitz have been major influences in my life, and I will never forget their generosity and caring. At Cornell Frederick Gouldin, Matthew Miller, Charles Sinclair and Elizabeth Fisher taught me incalculably valuable lessons in life, science and research. Adam Art was the only reason my time at Raytheon was more than bearable.

At UT I've had the pleasure of working with some very talented and driven undergraduate researchers. Daniel Pineda, Casey Zak, Liane Miller and Tommy Browder deserve a tremendous amount of credit for the work reported in this document. I'm lucky to have joined the same research group as Ingmar Schoegl, who taught me so much, Daniel Leahey who is a great friend and co-author, and Erica Belmont who has been a pleasure to work alongside. Brian Carroll, Patrick Jurney, Mohammad Mehrmohammadi, Esfandiar Khatiblou, Stuart Cohen, Michael Pierce, Amanda Lanza, Thomas Lewis, Ben

Gully and Todd Davidson are all good friends and helped me along, in various ways, in my research and learning. I acknowledge my committee, Dr. Ezekoye, Dr. Hidrovo, Dr. Berberoglu and Dr. Raja for their guidance and useful criticism. Dr. Ezekoye, in particular, has had a great influence on me, and I will always look up to him. Other professors at UT have aided me in various ways. Dr. Clemens, Dr. Bogard, Dr. Schmidt, Dr. Hall, Dr. Howell, Dr. Matthews, Dr. Kovar and Dr. Webber have always been willing to chat with me about research, fluid mechanics, ceramic materials, radiation or whatever. Dr. Webber co-advised me for my MS degree, and I owe him a great debt for his support, encouragement and advice throughout my entire time at UT.

Selecting an advisor is a decision quite fraught with uncertainty, so without knowing quite what I was getting into, I became Dr. Ellzey's student; what a great stroke of luck. Dr. Ellzey is unbelievably wise, smart and patient. Critical to my development as a researcher, she allowed me to make mistakes from which I would learn, but not to make mistakes that would really set me back. Very important to me, she gave me the freedom to experiment in the lab and even to take philosophy classes, which kept me sane during five years of Thermal/Fluid Systems. Though extraordinarily busy even for a Professor, she always spent the time to know what I was working on and help me come up with ideas and work through technical problems. She also managed to weather my organizational skills, procrastination and sometimes lazy writing. Put simply and honestly, I cannot imagine having a better advisor than Dr. Ellzey.

I admit that I chose to work hard to write this dissertation and finish this degree. However, as I've described, the path was pretty easy given all of the good fortune I've stumbled upon. And that means I have to acknowledge the role of luck in my completing this work.

Studies of Rich and Ultra-Rich Combustion for Syngas Production

Colin Healey Smith, PhD

The University of Texas at Austin, 2012

Supervisor: Janet L. Ellzey

Syngas is a mixture of hydrogen (H_2), carbon monoxide (CO) and other species including nitrogen (N_2), water (H_2O), methane (CH_4) and higher hydrocarbons. Syngas is a highly desired product because it is very versatile. It can be used for combustion in turbines or engines, converted to H_2 for use in fuel cells, turned into diesel or other high-molecular weight fuels by the Fischer-Tropsch process and used as a chemical feedstock. Syngas can be derived from hydrocarbons in the presence of oxidizer or water as in steam reforming. There are many demonstrated methods to produce syngas with or without water addition including catalytic methods, plasma reforming and combustion.

The goal of this study is to add to the understanding of non-catalytic conversion of hydrocarbon fuels to syngas, and this was accomplished through two investigations: the first on fuel conversion potential and the second on the effect of preheat temperature.

A primarily experimental investigation of the conversion of jet fuel and butanol to syngas was undertaken to understand the potential of these fuels for conversion. With these new data and previously-published experimental data, a comparison amongst a larger set of fuels for conversion was also conducted. Significant soot formation was observed in experiments with both fuels, but soot formation was so significant in the jet

fuel experiments that it limited the range of experimental operating conditions. The comparison amongst fuels indicated that higher conversion rates are observed with smaller molecular weight fuels, generally. However, equilibrium calculations, which are often used to determine trends in fuel conversion, showed the opposite trend.

In order to investigate preheat temperature, which is one important aspect of non-catalytic conversion, experiments were undertaken with burner-stabilized flames that are effectively 1-D and steady-state. An extensive set of model calculations were compared to the obtained experimental data and was used to investigate the effect of preheat temperatures that were beyond what was achievable experimentally. Throughout the range of operating conditions that were tested experimentally, the computational model was excellent in its predictions. Experiments where the reactants were preheated showed a significant expansion of the stable operating range of the burner (increasing the equivalence ratio at which the flame blew off). However, increasing preheat temperature beyond what is required for stabilization did not improve syngas yields.

Table of Contents

Table of Contents

1 INTRODUCTION

1.1 Combustion and Syngas

Combustion can be described both by its physics and by its use. Figure 1 describes combustion from the point of view of a user. There are mass and energy inputs to a combustion process and mass and energy products, which have various uses. The most common use for combustion is to produce high temperature gases (sensible enthalpy) for power production and process heat. Another use of combustion is to produce valuable chemical species that may be used for fuel or as a chemical feedstock. This document describes an investigation of converting fuels to a valuable product, syngas, by combustion.

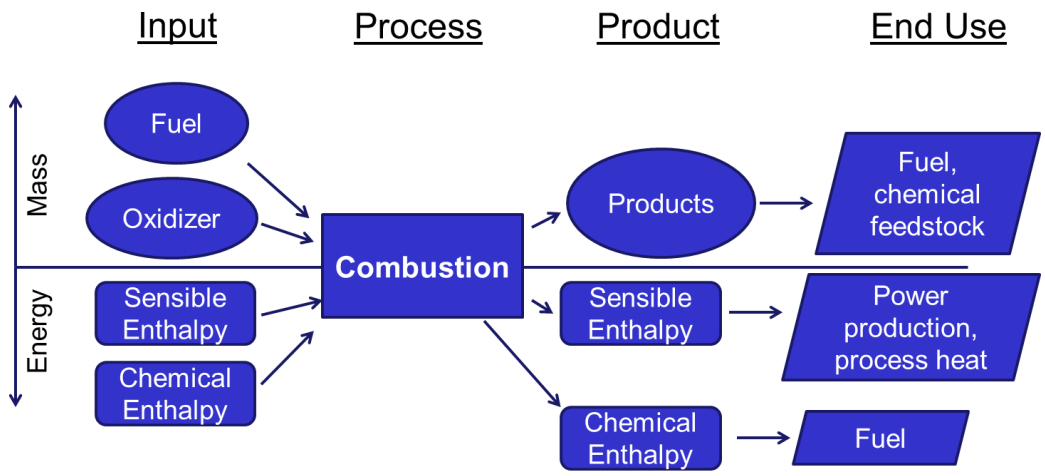

Figure 1. Combustion uses

Syngas is a mixture of hydrogen (H_2), carbon monoxide (CO) and other species including nitrogen (N_2), water (H_2O), methane (CH_4) and higher hydrocarbons. Syngas is a highly desired product because it is very versatile. It can be used for combustion in

turbines or engines, converted to H_2 for use in fuel cells, turned into diesel or other high-molecular weight fuels by the Fischer-Tropsch process and used as a chemical feedstock [1].

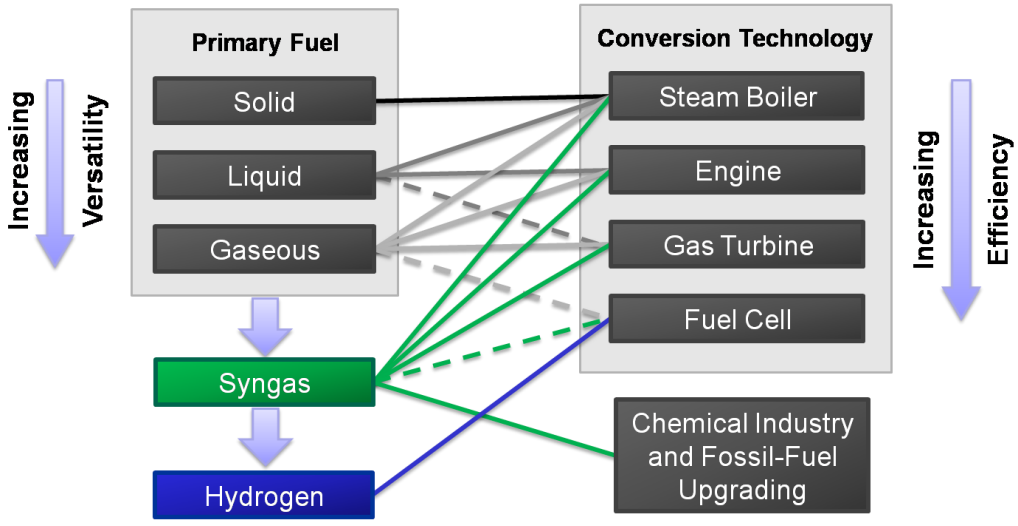

Figure 2. Fuel versatility and conversion technology efficiency [2]. Image from [3]

Various types of fuels and their respective applications are shown in Figure 2. In this figure, the lines that link the fuels with the conversion technologies indicate which fuels may be used with which conversion technologies. Solid lines indicate that a fuel can easily be used with a particular technology and dashed lines indicate that a fuel can be used with a conversion technology in some cases. Solid fuels are only appropriate when the heat source can be isolated from all moving parts such as for steam boilers whereas liquid fuels can be injected into the combustion chamber as in engines and gas turbines. Gaseous fuels, including syngas and hydrogen, may be used in all of these applications.as

well as in fuel cells. In addition to being a fuel for power generation devices, syngas is a feedstock for chemical processing and the petrochemical industry.

Syngas can be derived from hydrocarbons in the presence of oxidizer or water as in steam reforming [4]. There are many demonstrated methods to produce syngas with or without water addition including catalytic methods [5], plasma reforming [6] and combustion [7]. A recent review of these methods can be found in the literature [8].

Catalytic conversion is the most popular method for converting fuels to syngas. In particular, catalytic steam reforming of methane is relatively well-understood and efficient [1]. However, there are drawbacks to using catalysts. They are expensive, prone to degradation, inflexible in feedstock and operating conditions and can be poisoned or deactivated by compounds in the reactants and soot deposition [9-11]. Regardless of conversion method, syngas is produced by reacting rich hydrocarbon air mixtures and the actual degree of conversion is determined by a variety of factors. Equilibrium calculations for a constant pressure, constant enthalpy process are often used to predict the composition of a reacting such mixtures, and these predictions are presented in Figure 3 for ethanol/air a function of equivalence ratio.

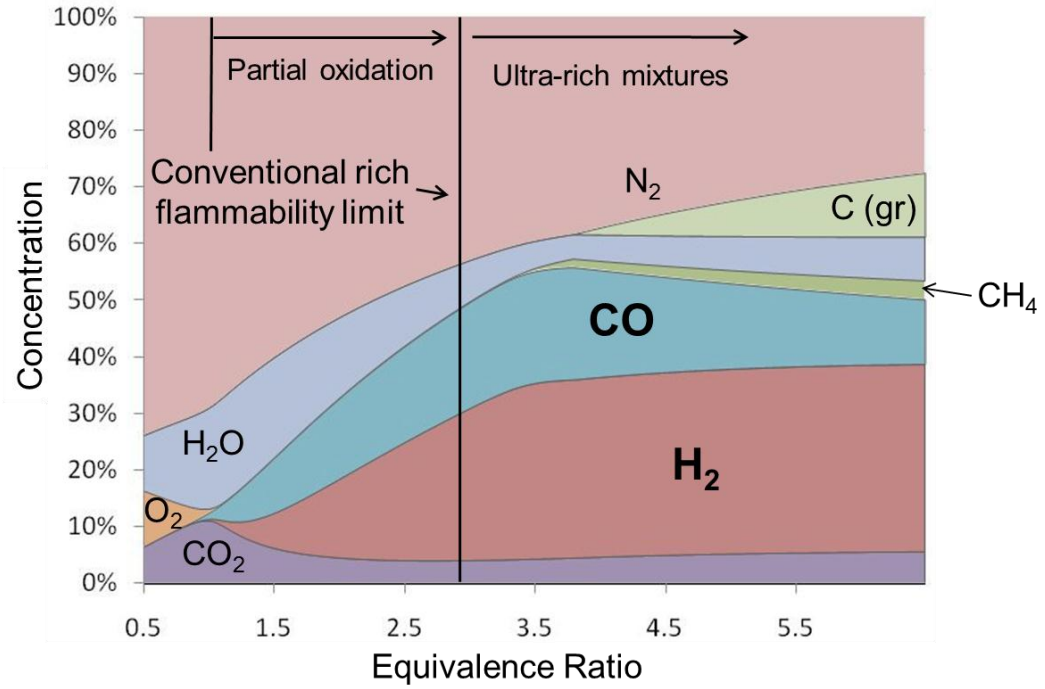

Figure 3. Concentration vs. Equivalence Ratio for ethanol/air (thickness of section in ordinate indicates concentration of species)

Near $\varphi = 1$, almost all carbon and hydrogen are almost entirely converted to CO_2 and H_2O, respectively. At $\varphi < 1$ (lean) oxygen is observed in the product species. At $\varphi > 1$ (rich) CO and H_2 have substantial concentrations. Although equilibrium predicts significant concentrations of these species, very rich mixtures may not release enough heat to produce temperatures high enough for self-sustained chemical reaction. To maximize syngas production, then, reaction rates must be increased for self-sustaining reaction of the mixture.

1.1 Flammability and Stability Limits

The conventional flammability limits, the minimum and maximum equivalence ratios beyond which self-sustained combustion is not attained, are determined experimentally in an apparatus similar to that shown in Figure 4. In an experiment, a cylindrical vessel is filled with a mixture of oxidizer and fuel at a determined temperature and pressure. The mixture is ignited at the bottom of the vessel, and observation is made of the propagation or lack of propagation of a flame down the length of the tube. The mixture at the given temperature and pressure is deemed flammable if a flame propagated the length of the reactor and not flammable if it did not. For a given temperature and pressure there exist two flammability limits: lean and rich.

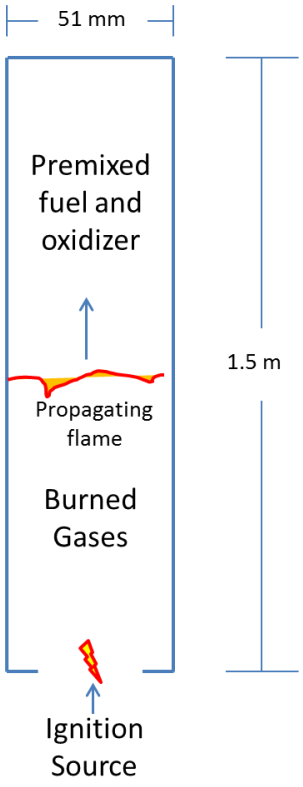

Figure 4. Graphic describing device for measuring the flammability limits of gas mixtures

This type of apparatus has been used to determine the flammability of many fuels under various conditions, and the most comprehensive list of flammability limits is reported in the US bureau of mines survey [12]. For reference, some typical flammability limits are given in Table 1 in terms of the conventional definition of equivalence ratio and the normalized equivalence ratio. The (conventional) equivalence ratio is defined as:

$$\varphi = \frac{\frac{N_{Fuel}}{N_{oxidizer}}}{\left(\frac{N_{Fuel}}{N_{oxidizer}}\right)_{stoichiometric}} \quad (1)$$

where the stoichiometric ratio is the ratio of fuel to oxidizer that would produce only H_2O and CO_2 as products.

Under this definition, the equivalence ratio varies from 0 (pure oxidizer) to infinity (pure fuel) with $\varphi = 1$ indicating stoichiometric (neither lean nor rich). A less often used definition of equivalence ratio is a normalization of the traditional definition:

$$\Phi = \frac{\varphi}{1 + \varphi} \tag{2}$$

Under this definition, at stoichiometric $\Phi = 0.5$, for pure fuel $\Phi = 1$, and for pure oxidizer $\Phi = 0$.

Table 1. A selection of flammability limits for fuels mixed with air at standard temperature and pressure

Fuel	**Lean (conventional)**	**Lean (normalized)**	**Rich (conventional)**	**Rich (normalized)**
Methane [13]	0.5	0.33	1.67	0.625
Propane [13]	0.56	0.36	2.7	0.73
N-heptane [14]	0.58	0.37	3.77	0.79
Ethanol [13]	0.41	0.29	2.8	0.74
Butanol [14]	0.5	0.33	3.9	0.8
Jet fuel [15]	0.55	0.35	4.0	0.8

The rich flammability limits differ significantly amongst the fuels while the lean limits differ less substantially, however this is a result of the definition of equivalence ratio rather than an important physical phenomenon. For the normalized equivalence ratios, the rich and lean limits are seen to be fairly symmetric about 0.5 (Table 1), and

though there is more variance in the rich limits amongst the fuels than seen in the lean limits, the difference is much less pronounced in the normalized form.

There is no general theory of flammability limits though the analysis of Williams based on energy considerations is illuminating [16]. The adiabatic flame temperature is a critical parameter in determining the extinction conditions, which determine the flammability limits. Near stoichiometric the adiabatic flame temperature is maximum, and it decreases on either side of stoichiometric. If the adiabatic flame temperature of a mixture is low enough a flame will not propagate down a flammability tube and the flammability limit is established. Given the dependence of flammability limits on the adiabatic flame temperature, there is one obvious way to broaden these limits: to increase the initial temperature of the mixture, thus increasing the adiabatic flame temperature. The dependence of adiabatic flame temperature on reactant temperature is shown in Figure 5 for a methane/air mixture with an equivalence ratio of 1.25:

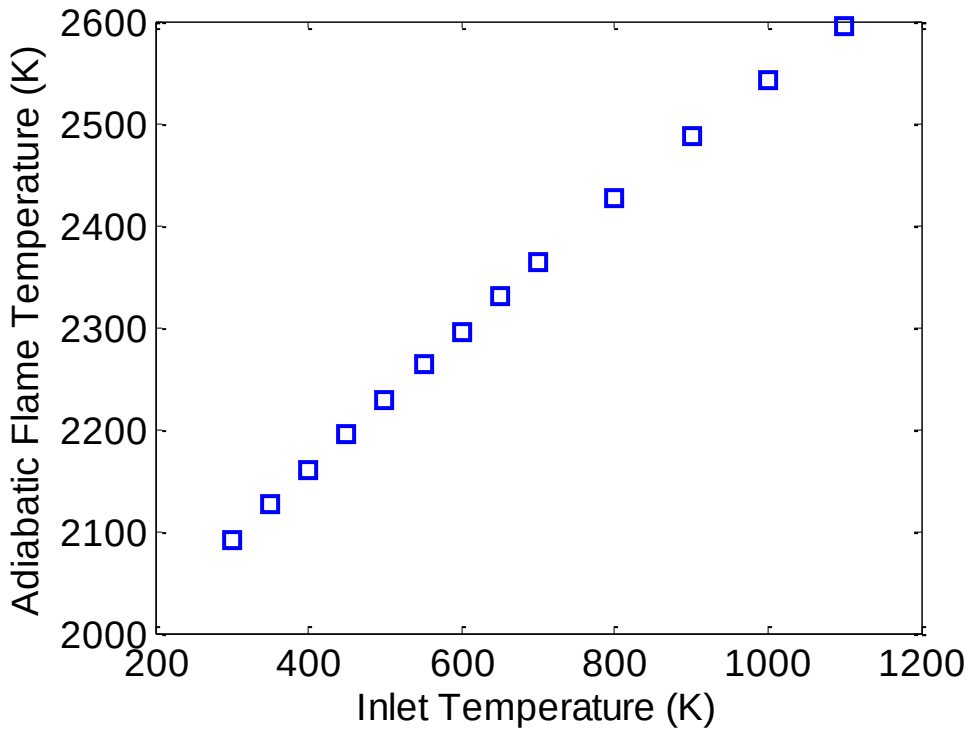

Figure 5. Adiabatic flame temperature vs. reactant temperature for methane/air with φ = 1.25

The adiabatic flame temperature is almost exactly linear for this mixture in the range of reactant temperatures considered. Though preheating always increases the adiabatic flame temperature, this linear dependency is not strictly expected since the specific heat of the products and the distribution of product species depend on the adiabatic flame temperature. The reason for the dependence of flammability limits on adiabatic flame temperature is because reaction rate depends exponentially on the adiabatic flame temperature. Increasing the adiabatic flame temperature through preheat is a means to increase the reaction rate.

Though the adiabatic flame temperature is a critical parameter in determining the flammability limits, transport phenomena are also relevant because the propagation of a flame requires heat and mass transfer. The laminar flame speed of a mixture describes the intensity of combustion as a consequence of both the adiabatic flame temperature and the transport processes. Therefore, the laminar flame speed is also related to the flammability limits; a rule of thumb is that a mixture with a laminar flame speed of 5 cm/s corresponds approximately to a flammability limit [17].

Figure 6 shows how the laminar flame speed varies with inlet temperature for a methane/air mixture having φ = 1.25.

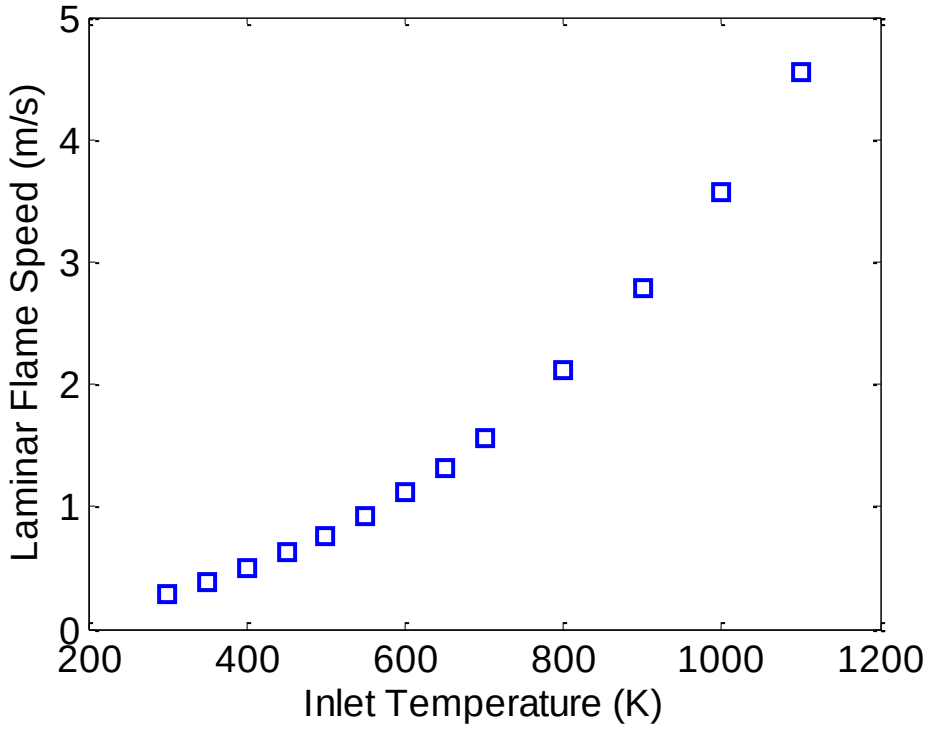

Figure 6. Laminar flame speed vs inlet temperature for methane/air with φ = 1.25

As expected, the laminar flame speed increases with increasing reactant temperature. This increase is nonlinear, unlike the adiabatic flame temperature, indicating that factors other than the adiabatic flame temperature are important in flame propagation. With an increase in preheat temperature from 300 K to 600 K, the adiabatic flame temperature increases by about 200 K, but the laminar flame speed increases by almost 4 times.

Flames propagate through premixed gases, so steady-state operation is achieved by balancing convective motion of premixed gases with the propagation of a reaction zone. The stability limits for a burner are often characterized in terms of flashback and blowoff. Under flashback conditions, the flame speed is less than the convective speed of

the reactants resulting in the upstream propagation of the flame. For the reverse case when the convective speed of the reactants is greater than the flame speed, the flame propagates downstream and "blows off" the burner. Given a burner and a convection condition, flashback and blowoff conditions may be found by varying the mixture equivalence ratio; just like flammability limits, there are typically lean and rich blowoff limits, and if flashback occurs near stoichiometric there are lean and rich equivalence ratios that define the flashback range. The flame temperature strongly influences the flammability limits, so non-adiabatic operation (either heat loss or heat addition) affects the stability conditions.

1.2 Combustion in Heat-Recirculating Reactors

In a "free flame", a reaction zone propagates into a mixture of fuel and oxidizer at a certain speed, the laminar flame speed or laminar burning flux. The products are left at the adiabatic flame temperature if the system is adiabatic. In contrast, in a heat recirculating reactor (Figure 7) the reactants enter, release heat, and the hot products circulate such that heat is transferred to the entering reactants. These preheated reactants produce peak product temperatures that are higher than those in a free flame; that is, the peak temperature is *superadiabatic*. These superadiabatic products lose heat to the entering reactants and are at the adiabatic flame temperature at the exit of the reactor.

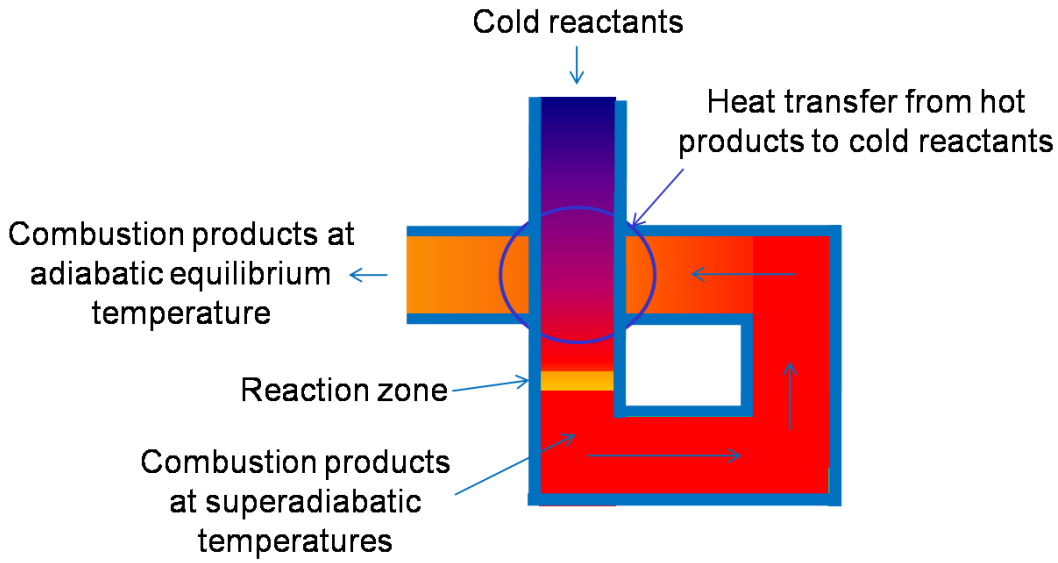

Figure 7. Graphic describing a generic heat-recirculating reactor

Since reactants are preheated before reaching the reaction zone, the flame speeds are increased as shown in Figure 6. This reaction rate and flame speed enhancement allows mixtures with equivalence ratios outside the conventional flammability limits to burn and, if flashback is avoided, produces higher than normal burning fluxes. Both of these properties can be used for interesting applications; therefore a significant amount of work has been done with heat recirculating reactors.

The original idea of a heat recirculating reactor was developed in the 1960's by Felix Weinberg [18, 19] when studying the processes in smoldering cigarettes. Over the next few decades [20-23], he and other researchers advanced the concept from both theoretical and design perspectives. As described by Weinberg [24], there are many possible designs for heat-recirculating reactors. Some of the more theoretical work

focused on combustion in a chamber where conducting rods or plates were introduced [25]. Other designs include a swiss roll reactor [26] and a counterflow reactor [27] where hot products and cool reactants are separated by a conducting wall. These designs feature relatively simple fluid mechanics in contrast to flows that exist in other heat recirculating reactors that are based on flow in porous media [28]. Two types of porous media reactors are often studied: a 2-section burner [29-34] that operates at steady-state with a reaction zone stabilized between two different types of porous media, and a filtration reactor [23, 35-40] with a reaction zone that often propagates relative to a solid porous medium.

The present study is focused on transient filtration combustion which is depicted in Figure 8. The reactor is an insulated cylinder filled with a porous medium, which may be a bed of individual particles [37] or reticulated ceramic foam [41].

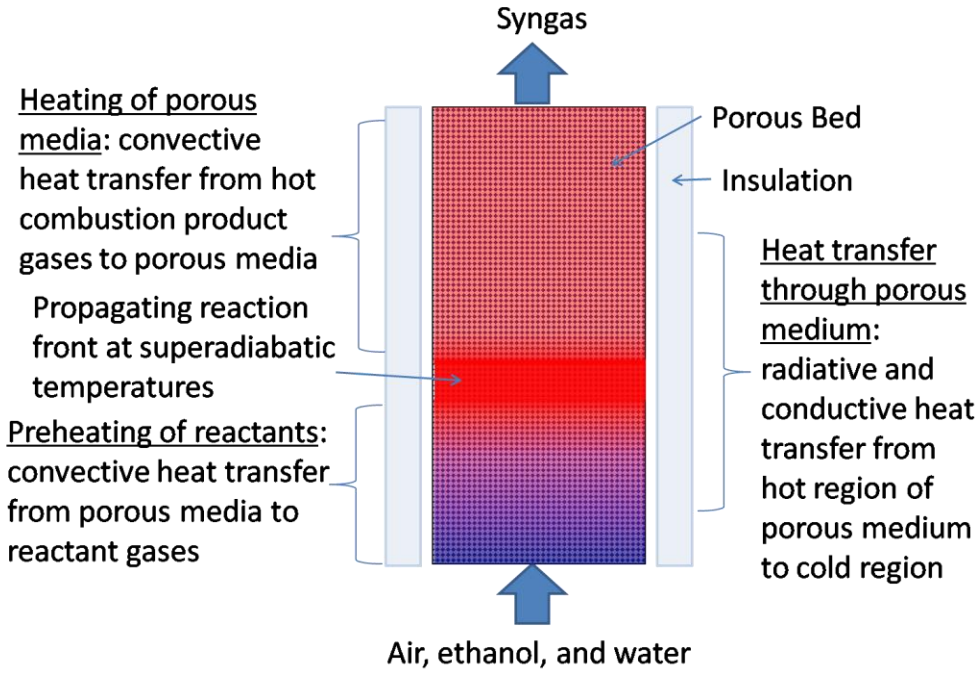

Figure 8. Graphic describing heat transfer processes in filtration combustion

Fuel and oxidizer flow into the reactor and react within the pores resulting in heat transfer to the solid matrix. Due to the temperature gradient, heat is transferred upstream in the solid by conduction and radiation and then transferred to the incoming cold reactants. The front may propagate upstream, downstream or remain stationary depending on operating conditions and the properties of the solid. Maximum propagation speeds observed in the filtration reactors examined in the present study are ~ 4 cm/s which is significantly less than the flow velocities of ~30 cm/s. This propagation results in another heat transfer mechanism because the front is moving through the heated solid.

Figure 9, which is a computational model solution for ethanol/air [42], shows the gas temperature as a function of axial position for four different times. The equilibrium

temperature is ~1700 K, and the superadiabatic temperature spikes can be clearly seen in each curve. The figure also shows that the preheat region expands as the front propagates downstream.

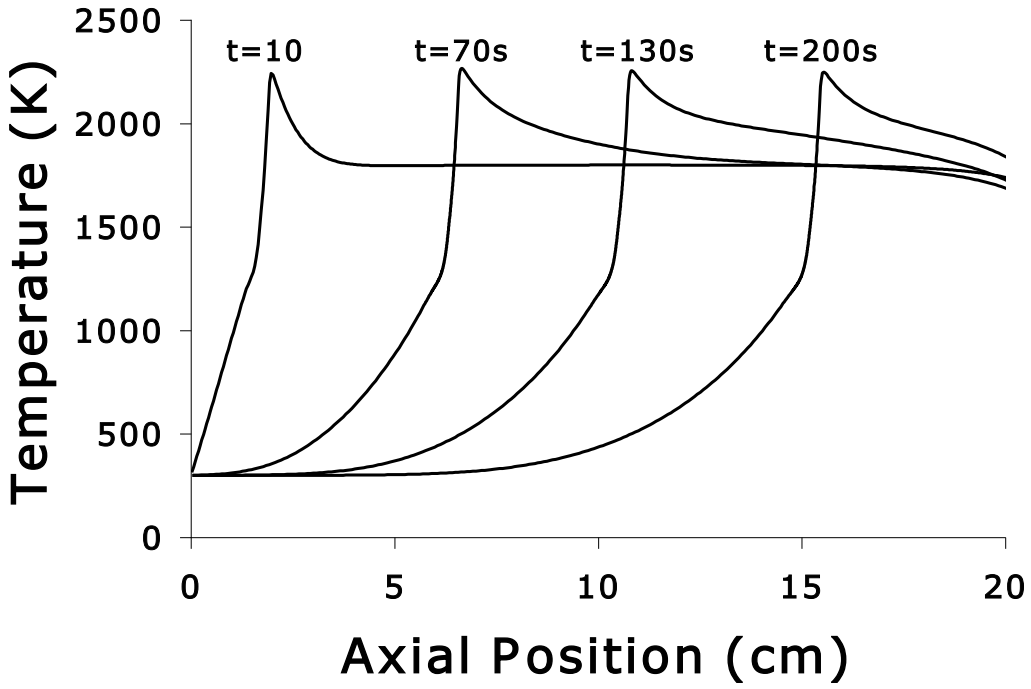

Figure 9. Representative temperature vs. axial position for a reaction zone propagating downstream in a filtration reactor. Figure taken with permission of the author from [42]

The superadiabatic temperatures make possible the combustion of mixtures far outside the conventional flammability limits [43]. Theoretical analysis predicted no flammability limit for filtration combustion [20], and experimental observations have confirmed that stable combustion is achieved at both very rich and very lean conditions [44]. The vast operating range associated with a filtration reactor is a feature that

distinguishes it from other types of heat-recirculating reactors, which typically produce peak temperatures that are only slightly superadiabatic. Filtration combustion has been the topic of multiple review papers [7, 45-47], and the detailed principles of operation can be found in the literature [35, 48, 49].

1.3 The Use of Heat-Recirculating Reactors for Syngas Production

There have been many studies on the conversion of fuel to syngas using heat-recirculating reactors. The earliest research on conversion of fuel to syngas was completed by Kennedy from the University of Illinois at Chicago and coworkers. His group and collaborators published multiple articles starting in 1998 with their study of the conversion of methane to syngas using a filtration reactor [50]. Further studies were conducted on methane [44, 51], hydrogen sulfide [52] and ethane and propane [53]. Conversion rates of methane to CO and H_2 were reported at about 80% and 60%, respectively, and they examined a very wide range of equivalence ratios (2 to 8) and reactor pressures. The conversion rates for ethane and propane were similar to the methane conversion rates with propane having slightly lower conversion. Ellzey and coworkers investigated the conversion of methane [41, 54], ethanol [37] and heptane [39] and several other articles on the conversion of methane have been published more recently [55-58].

Some researchers have investigated the use of porous media reactors that operate at steady-state for the conversion of fuels to syngas. In one design, a reaction stabilizes at the interface of two sections of porous media that have different pore sizes or other properties. The group of Mastorakos at the University of Cambridge experimented with

this type of reactor converting n-heptane and diesel in one study [59] and methanol, methane, octane and petrol in another [31]. A reaction zone also may be stabilized in a diverging channel [7]. Recently, Ellzey and coworkers have published results from the conversion of methane [60] and heptane [61] to syngas in a counterflow reactor. In this design, flames are stabilized in a counterflow heat exchanger in which reactants are preheated by heat transfer from the products in a neighboring channel. These reactors, which operate at steady state, have been shown to successfully convert fuels to syngas. The range of equivalence ratios over which these reactors can operate, however, is significantly smaller than that for filtration reactors.

1.4 Objectives

The primary goal of this study is to add to the understanding of non-catalytic conversion hydrocarbon fuels to syngas. This is accomplished through experiments with two different fuels in a filtration reactor and a comparison of these data with previously-published experimental results with other fuels and equilibrium calculations. The other means of contributing to the primary goal is to investigate the effect of preheat on syngas production in simple, well-controlled burner-stabilized flames.

Jet fuel is widely-used across the world and in particular by the military. Butanol can be produced from renewable sources [62], and is a proposed alternative to hydrocarbon fuels. Though experimentation, the potential of these two fuels to be converted to syngas by a noncatalytic method was investigated. With these data and data from the literature an investigation of the effect of fuel type on syngas production was conducted.

Combustion in heat-recirculating reactors is complex and especially complex in a filtration reactor. Besides the gas phase reaction and transport, there is convection that occurs between the gas and the solid and conduction and radiation within the solid. Preheating of reactants is known to be a critical feature of a heat-recirculating reactor, but temperature is not controlled in these reactors, so the specific effect of the preheat temperature on syngas production is not known. In addition, the complexity of the transport processes makes modeling difficult. Modeling work has shown significant deviations from experimental data in terms of species predictions, but the reasons for this are not known. The second contribution of this study is to understand the effect of preheat on syngas production using flat, burner-stabilized flames. These burners do not have the complex transport processes that occur in heat-recirculating reactors, so comparison with model results can shed light on the reasons for the discrepancies observed in heat-recirculating reactors.

1.5 Methodology

Experimentation with liquid fuels is more difficult than experimentation with gaseous fuels because of the requirement of vaporization and mixing with air. In order to complete the objectives, a new filtration reactor was constructed. This reactor was used to study the transient filtration combustion of jet fuel and butanol. An analysis of the present experimental data and the experimental data from the literature along with equilibrium calculations and the results of computational modeling are used to perform a comparison amongst fuels in terms of conversion potential. This work is discussed in chapter 2.

Flat flames were studied with two burners: a McKenna burner that is often used for model comparison and a ceramic burner that was built to study flat flames with

preheated reactants. Extensive computational simulations were conducted with Cantera and compared with experimental results to further investigate the effect of preheat. This work is discussed in chapter 3.

2 CONVERSION OF JET FUEL AND BUTANOL TO SYNGAS VIA FILTRATION COMBUSTION

2.1 Introduction

Although understanding of the combustion of rich mixtures is lacking, both butanol and jet fuel have been studied extensively at more moderate equivalence ratios (φ). Studies on butanol include basic investigations on flames [63], kinetic modeling [64, 65], combustion in engines [66], and catalytic combustion [67]. At rich conditions where the interest is on the production of syngas, butanol research has focused on equilibrium thermodynamic analysis [68-71], and conversion by catalytic methods [72-74].

At moderate φ, there has been significant work on jet fuel and other high molecular weight fuels over the last two decades. Fundamental work on diffusion flames [75, 76] and kinetic modeling [77, 78] has significantly advanced our understanding of these complex fuels, as has work on cracking [79] and stability [80]. Equilibrium analyses and computational studies [81] have shown the potential for syngas production from jet fuel using various methods including catalysts [5, 11, 82-88] and plasmas [89]. Investigations of noncatalytic reforming have generally focused on reactors with stationary reaction zones [90]. Soot formation is often a consideration when using these fuels and their propensity to soot has been studied in various experimental configurations including diffusion flames [77, 91, 92], pool fires [93, 94], and engine conditions [95-97]. Soot production in premixed flames has also been investigated at moderately rich φ [98,

99], but, as noted in the literature [100], very high equivalence ratios are difficult to study because of flame instability.

As a demonstration and initial investigation of the principle of noncatalytic conversion of jet fuel and butanol to syngas by transient filtration combustion, we performed experiments over a range of rich equivalence ratios and inlet velocities (cold gas). Both fuels are compared for syngas production potential and soot production, and a comparison to other fuels is performed based on data found in the literature.

The following sections describe two sets of experiments. In one set jet fuel was tested in multiple different types of porous media with significant degradation of porous media observed. Soot formation was also observed at levels that produced reactor clogging. Degradation and massive soot production were phenomena unique to jet fuel. In the second set of experiments, the reactor was redesigned; both jet fuel and butanol were successfully converted to syngas, though soot production remained an obstacle.

2.2 Initial Experiments with Jet Fuel

Initial experiments with jet fuel were attempted with multiple types of porous media. The initial attempts showed that certain types of porous media degraded during the combustion process. Experiments described in this section were performed with three different reactors: a packed bed of aluminum oxide pellets, YZA (yttria stabilized zirconia/alumina) porous ceramic and ZTM (zirconia toughened mullite) reticulated porous ceramic.

3.2.1 EXPERIMENTAL APPARATUS FOR INITIAL EXPERIMENTS

The experimental apparatus (Figure 10) consisted of the reactor, the fuel vaporization system, the reactant delivery system and the data acquisition system.

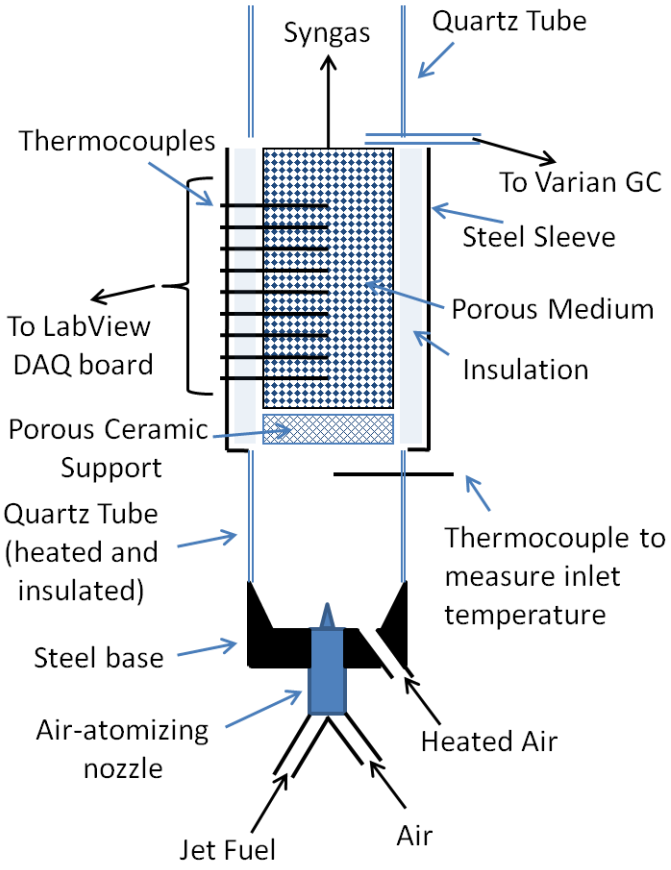

Figure 10. Experimental apparatus used in initial experiments with jet fuel

The reactor was an insulated cylinder of porous media, 20 cm long and 5.59 cm in diameter. In our previous work in filtration combustion, various materials were used as the porous medium. Alumina pellets of 3 mm in diameter have been successfully used by

the Ellzey group [37, 39] and others [50, 52] for various fuels. Two other materials YZA (yttria stabilized zirconia/alumina) ceramic foam and ZTM (zirconia toughened mullite) ceramic foam were also tested as porous media. Both YZA and ZTM have been used in previous experimental work in our group [101, 102] for radiant burners operating at lean conditions. YZA has also successfully been used in the Ellzey group for the conversion of methane to syngas [41].

Zirconia (ZrO_2), alumina (Al_2O_3) and mullite ($Al_6Si_2O_{13}$) have melting points of 2717˚C [103], 2072˚C [104], 1840˚C [105], respectively, and temperatures in the type of reactor that is employed here typically reach no more than 1800˚C. However, Mathis [106] noted with regard to the ceramics (YZA and ZTM) that are used in this study that "the manufacturer's specifications indicate that the maximum exposure temperature for YZA and ZTM it is 1870 K and 1920 K, respectively." Since the manufacturer specifies a lower temperature than typical peak temperatures in a reactor like this, material changes or degradation seemed possible, if not likely.

The vaporization system consisted of an air-atomizing nozzle and a quartz chamber for mixing. The atomized fuel droplets, approximately 20 microns in size, were vaporized in a separate heated air stream in the quartz chamber. The base of the chamber, which held the nozzle and air heater, was machined from stainless steel. The outer surface of the quartz chamber was wrapped with resistance heaters and insulation to prevent condensation of the fuel. Portions of the band heaters and insulation were removable so that any potential condensation of the jet fuel could be observed.

The reactant delivery system included a tank, a pump and rotameters for jet fuel and flow regulators for compressed, dry laboratory air. The air entering the nozzle and the air entering the inline air heater were controlled with separate flow regulators.

For these experiments, jet fuel from Berry Aviation at the San Marcos Municipal Airport was used. The fuel is supplied to Berry Aviation by AVFuel Corporation. Since jet fuel can have a varying composition, an average chemical formula must be assumed. In this work a chemical formula of $C_{11}H_{21}$ was used [107]. The density, as measured by a laboratory scale, was 797 kg/m3, and the lower heating value was 43.2 MJ/kg as given by [108].

Measurements included temperatures and exhaust species. The temperatures were measured with 11 B-type thermocouples. The thermocouples were spaced at 1.5 cm intervals with the junctions at the centerline of the reactor for the alumina experiments and at the inside diameter of the alumina insulation for the YZA and ZTM experiments. Additionally, the temperature of the reactant mixture was measured with a K-type thermocouple just before entry to the reactor. The exhaust species were measured by a Varian, Inc. gas chromatograph (GC), which was calibrated to measure the following species: hydrogen, oxygen, nitrogen, methane, carbon dioxide, carbon monoxide, ethylene, ethane, acetylene, propane, iso-butane, n-butane, iso-pentane, n-pentane and n-hexane.

2.2.1 EXPERIMENTAL METHOD

In the experiments, jet fuel and air were controlled to flow into the reactor in mixtures with specific equivalence ratios and inlet velocities. During the experiments, the vaporization chamber was frequently monitored for condensation. If condensation was observed, the measurements were discarded and the temperature of the heated air stream was increased. The temperature of the inlet mixture was between 170˚C and 200˚C as measured by the thermocouple placed before entry to the reactor. The inlet velocity is defined as:

$$inlet\ velocity\ (V) = \frac{R \times T \times \sum \dot{N}}{P \times A} \tag{3}$$

Where A is the cross-sectional area of the reactor, R is the universal ideal gas constant, T is the temperature, P is the pressure, and $\sum \dot{N}$ is the total molar flow rate of air and jet fuel.

Important metrics for syngas production are the hydrogen yield and the carbon monoxide yield. These metrics, defined below, describe how effectively the reactor converts hydrogen and carbon bound in the fuel to diatomic hydrogen and carbon monoxide, respectively.

$$hydrogen\ yield\ = \ 100 \times \frac{2 \times \dot{N}_{H_2}}{N_H \times \dot{N}_{Fuel}} \tag{4}$$

$$carbon\ monoxide\ yield = \ 100 \times \frac{\dot{N}_{CO}}{N_C \times \dot{N}_{Fuel}} \tag{5}$$

where the units of $\dot{N}_{Fuel}$, $\dot{N}_{H_2}$ and $\dot{N}_{CO}$ are moles per second and N_H = 21 and N_C = 11 for jet fuel.

The values for the chemical energy conversion efficiency were calculated. This metric describes how much chemical energy in the fuel was converted to chemical energy in a given exhaust species. The energy conversion efficiencies were calculated using the LHV of the individual species as described by the following representative equation for hydrogen:

$$hydrogen\ energy\ conv.\ efficiency = 100 \times \frac{\dot{N}_{H_2} \times LHV_{H_2}}{\mathrm{LHV}_{Fuel} \times \dot{N}_{Fuel}} \quad (6)$$

where LHV values are in units of kJ per mole.

Similarly, the total energy conversion efficiency, a measure of how much energy in the fuel was lost to thermal energy in the process, was calculated as follows:

$$total\ energy\ conversion\ efficiency = 100 \times \frac{\sum_i \dot{N}_i \times LHV_i}{\mathrm{LHV}_{Fuel} \times \dot{N}_{Fuel}} \quad (7)$$

The summation is performed over all gaseous species in the exhaust with positive LHV and with non-negligible concentration (concentration > 0.1%). LHV values were taken from [109].

As mentioned in the introduction, the reaction zone may propagate upstream or downstream or remain stationary relative to the porous medium depending on the operating conditions. To measure the product species for a given set of operating conditions, the GC samples the exhaust gases at least 4 times with each sample requiring 160 seconds. The downstream propagation rate was observed up to about 3 cm/min, so

the 4th sample of the products would take place when the reaction zone is 16 cm downstream from the location of the reaction zone when the first sample was taken. This difference in reaction zone locations between samples also implies a difference in residence times that the gases experience in hot porous media downstream of the reaction zone. Since some reactions that occur in the combustion of mixtures with very high equivalence ratios are slow, the measurements of product species can differ from sample to sample as the reaction zone propagates.

2.2.2 RESULTS AND DISCUSSION FOR INITIAL EXPERIMENTS

2.2.2.1 Experiments with alumina pellets – discussion of materials

Experiments were conducted with porous media consisting of a bed of 3 mm diameter alumina pellets. After continuously burning jet fuel and air mixtures at various equivalence ratios and inlet velocities for approximately 6 hours, the reactor was purged and cooled with N_2 in order to examine soot buildup. Upon inspection, it was found that the alumina pellets had degraded enough to form a large cavity in the packed bed (Figure 11) After removing the top layer of the pellets, a hardened bank of soot-covered alumina pellets was observed (Figure 11 and Figure 12). To remove the pellets shown in the figure, a metal tool with significant applied pressure was required.

Figure 11. Image of alumina pellets - post experiment

Figure 12. Image of alumina pellets - post experiment

A sample of the pellets from the reactor was taken and compared with unused pellets: 373 used pellets and 275 unused pellets were independently weighed and placed in graduated cylinders for a volume estimate. It was found that the used pellets had decreased in weight by 12% and decreased in volume by 53%. These data are shown in Table 2.

Table 2. Weight and Volume of Alumina Pellets

	# of pellets	weight (g)	volume (ml)	weight/pellet (g)	volume/pellet (ml)
Used	373	9.12	7.50	0.02	0.02
New	275	7.70	12.00	0.03	0.04

In addition to finding a mass and volume decrease of the individual pellets, seemingly melted AL_2O_3 was taken from the apparatus (Figure 13). A sample of this material with no visible alumina pellets was analyzed by X-ray diffraction. The material had a major phase of AL_2O_3 (corundum/alumina) and a trace phase of $Al_6Si_2O_{13}$ (mullite). The melting point of alumina is 2072˚C [104] and the melting point of mullite is 1840˚C [105]. The peak temperature measured in the bed during all experimentation was 1689˚C, so melting was not expected. Further experiments are required to determine the reason for the alumina degradation.

Figure 13. Image of degraded alumina pellets

2.2.2.2 Experiments with alumina pellets – discussion of fuel conversion

Although the pellets had clearly degraded throughout the course of these experiments, data for jet fuel reforming was still obtained. These data must be qualified, however, by the fact that the experimental apparatus was changing in time. It is not possible to know when the degradation occurred, and further experimentation is necessary to understand the observed phenomena.

At a constant inlet velocity of 40 cm/s, the equivalence ratio was varied and measurements of exhaust species were taken. Figure 14 shows the hydrogen yield and the carbon monoxide yield as a function of equivalence ratio.

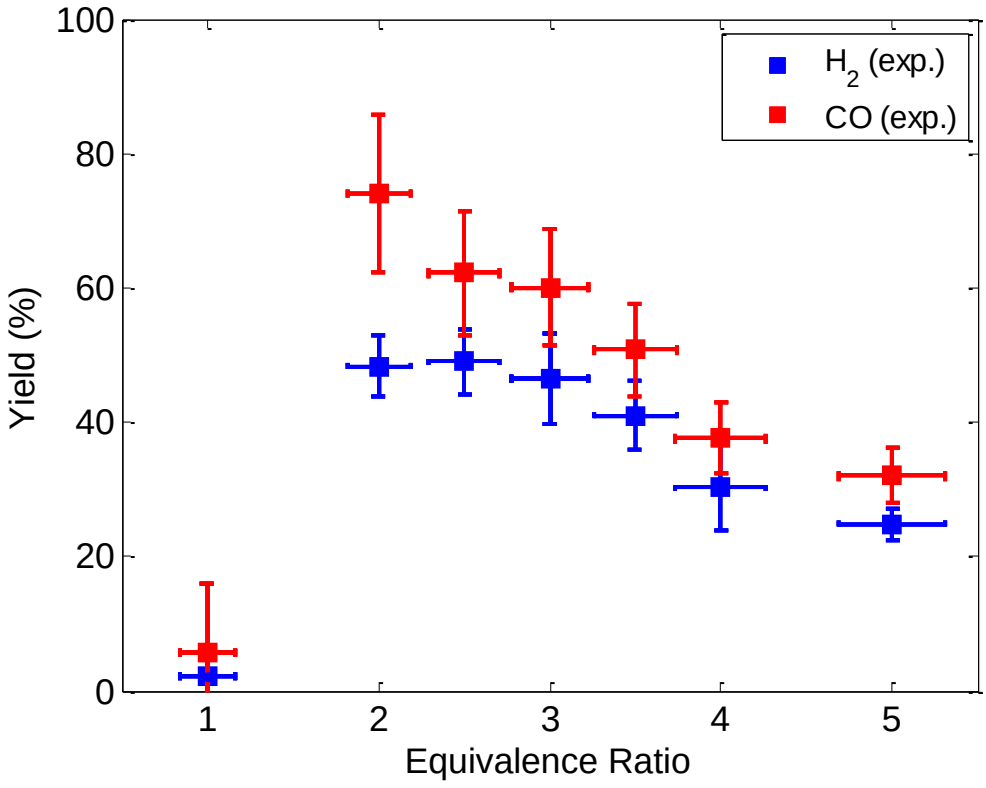

Figure 14. Hydrogen and carbon monoxide yield vs. equivalence ratio - experiments with alumina pellets (V = 40 cm/s)

Near zero hydrogen is observed at an equivalence ratio of 1, and a large jump is seen from equivalence ratios of 1 to 2 in terms of hydrogen and carbon monoxide yield. The carbon monoxide yield peaks at $\varphi = 2$ with a value of about 75%, and the peak hydrogen yield of about 50% occurs at $\varphi = 2.5$. The carbon monoxide yield decreases rapidly with increasing equivalence ratio after the peak, and the hydrogen yield decreases more smoothly. These results are similar in trend and magnitude to our previous results for methane [41], n-heptane [39] and ethanol [37].

Figure 15 shows the energy conversion efficiency as a function of equivalence ratio for hydrogen, carbon monoxide and the total energy conversion efficiency. The total energy conversion efficiency is relatively constant with equivalence ratio at values of $\varphi = 2$ and above except for an anomalous drop at $\varphi = 4$. These data show that about 40% of energy in jet fuel was lost to heat in the conversion process. The conversion of energy in jet fuel to energy in carbon monoxide and hydrogen both decrease after their peaks near $\varphi = 2$. The difference between the total chemical energy and the sum of the hydrogen and carbon monoxide energy is contained in other species, such as methane, ethylene and acetylene, which increase rapidly with increasing equivalence ratio (Figure 16). At $\varphi = 5$, 15% of the energy in jet fuel is converted to energy in methane and 6-7% was converted to both to ethylene and to acetylene.

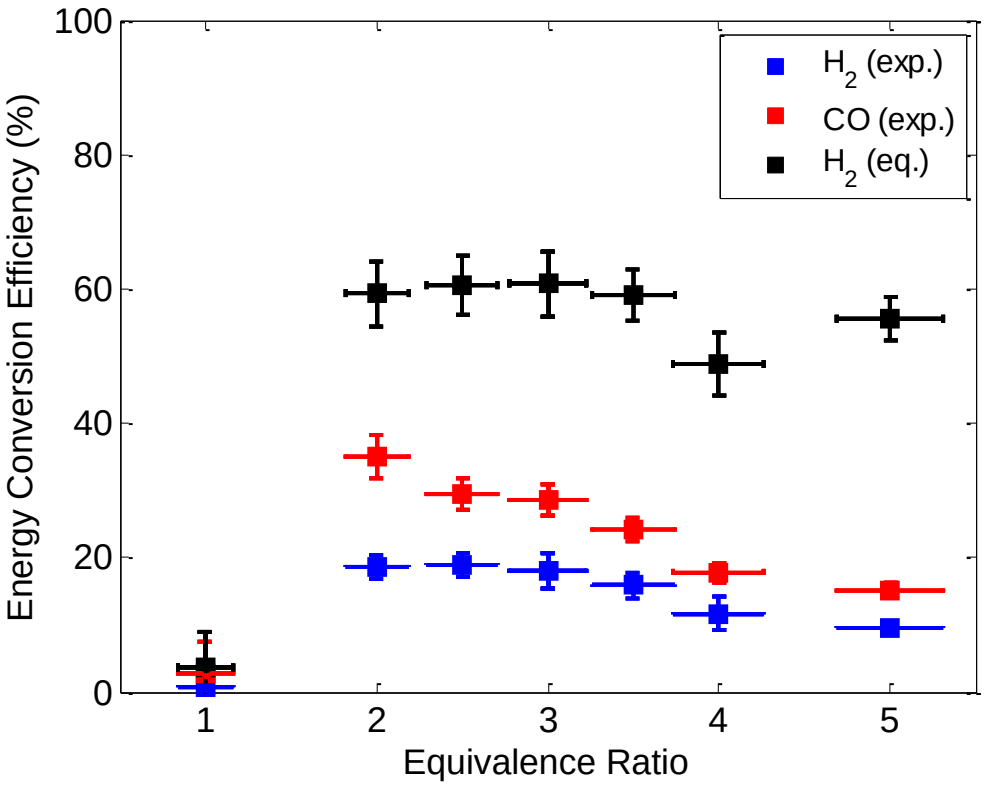

Figure 15. Energy conversion efficiency vs. equivalence ratio - experiments with alumina pellets (V = 40 cms/)

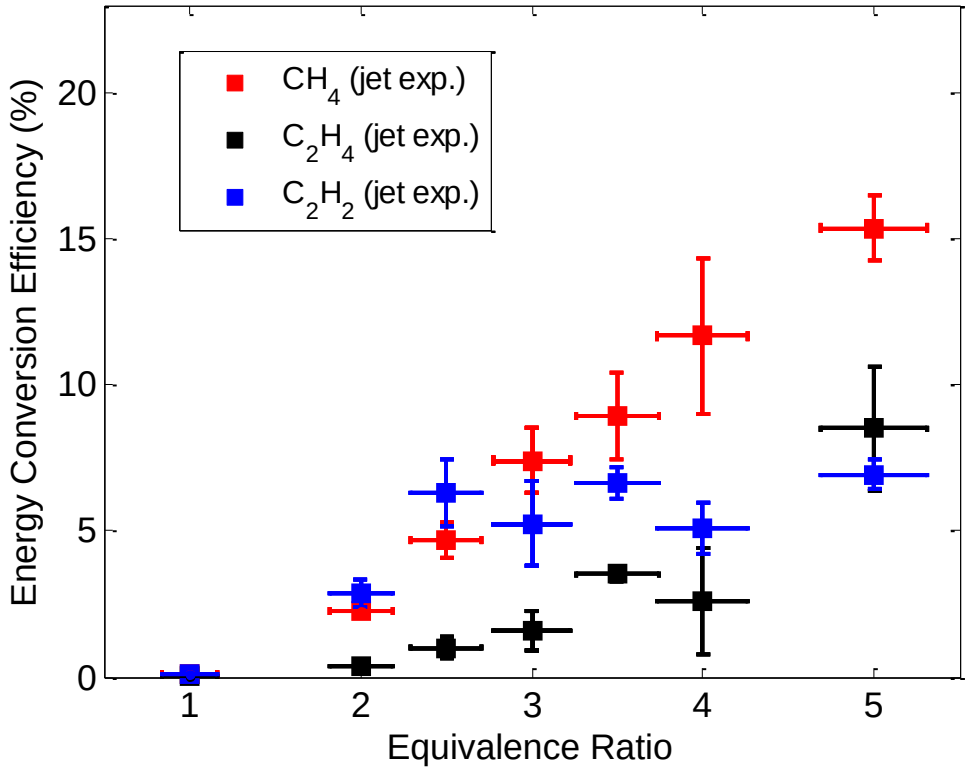

Figure 16. Energy conversion efficiency (minor species) vs. equivalence ratio - experiments with alumina pellets (V = 40 cm/s)

The adiabatic flame temperature of a mixture is not a function of the flow rate (inlet velocity), but the rate of energy input to the system is directly proportional to the inlet velocity. Since the rate of heat loss, by convection and radiation, is proportional to the temperature of the system this heat loss is greatest, as a fraction of the energy input, at the lowest inlet velocities. Therefore the lowest reactor temperatures are expected at the lowest inlet velocities. A suspected consequence of these low temperatures is low yields [39].

Figure 17 shows the carbon monoxide and hydrogen yield as a function of inlet velocity with the equivalence ratio held constant at 3. The lowest yields and lowest temperature (Figure 18) occur at the lowest inlet velocity, 25 cm/s, a trend that has been seen in our previous work

[37, 39, 41]. However, the decrease in yield at velocities higher than 40 cm/s is not consistent with our previous work [37, 39, 41]. In our filtration combustion experiments with other fuels, the yields are almost always increasing with inlet velocity. The decrease in yield is, however, consistent with the peak temperatures measured in the bed (Figure 18). Degradation of the porous media is suspected as the cause of this anomalous behavior, though more testing is required.

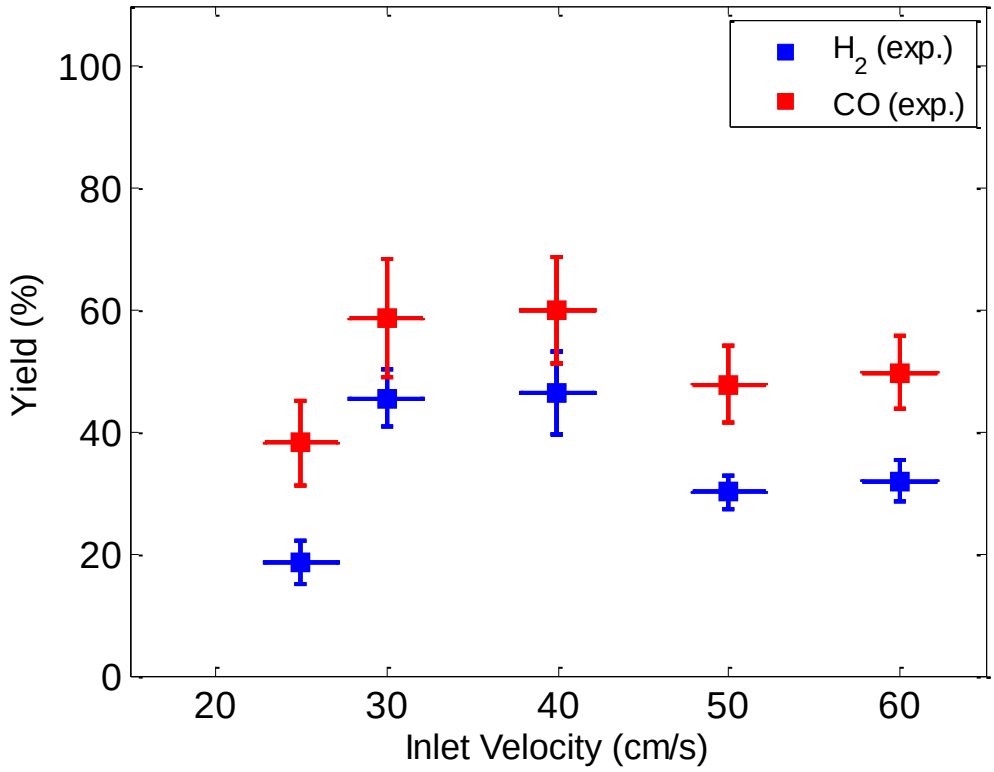

Figure 17. Hydrogen and carbon monoxide yield vs. inlet velocity - experiments with alumina pellets ($\varphi = 3$)

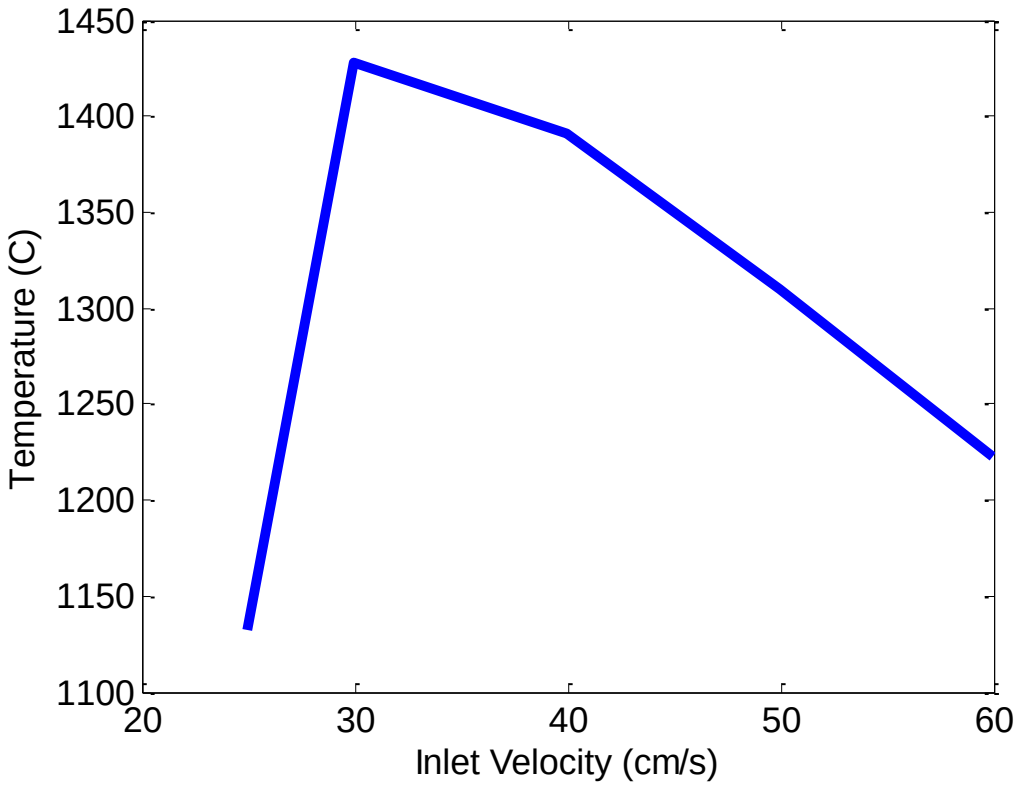

Figure 18. Average peak temperature vs. inlet velocity - experiments with alumina pellets (φ = 3)

2.2.2.3 Experiments with YZA – discussion of materials

After discovering that the alumina pellets were degraded over the range of experimental conditions, another rig was built using a cylinder of YZA reticulated ceramic in place of the alumina pellets. YZA is yttria (Y_2O_3) stabilized zirconia/alumina. Pre-experiment X-ray diffraction showed that the YZA was mostly cubic (tazheranite) zirconia with some alumina and some regular phase (monoclinic baddeleyite) zirconia.

After running experiments for approximately 7 hours, the reactor was purged with air instead of nitrogen gas, burning off any soot that had accumulated in the reactor during experimentation. Since the behavior of the reactor seemed to change over the course of the

experiments (based on real-time observation of temperature and species data), the YZA cylinders were removed and examined for evidence of degradation. It was found that the YZA had degraded from the unused state (left hand side of Figure 19). The image on the right of Figure 19 shows some seemingly melted YZA and/or alumina insulation. The image in Figure 20 shows internal struts that have also seemingly melted. The maximum temperature achieved during the experiments with YZA was 1740˚C as measured by thermocouples placed at the outer edge of the cylinders (as opposed to at the centerline of the reactor as was done with the packed bed of alumina pellets). Samples of the seemingly melted YZA were again examined by X-ray diffraction and the same constituent materials were found as the pre-experiment testing.

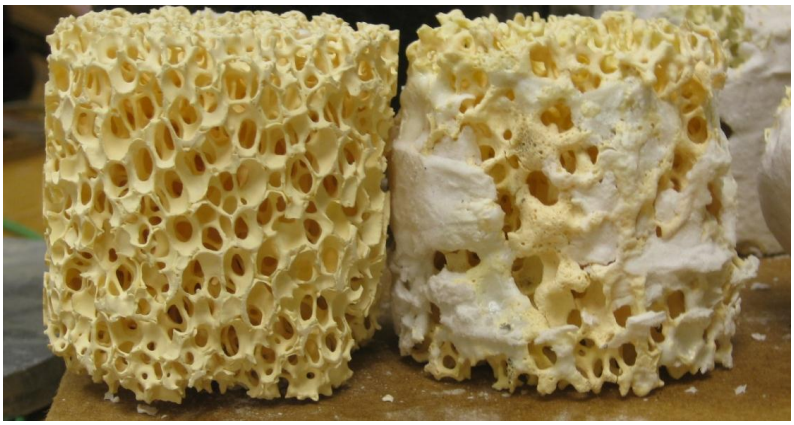

Figure 19. Images of YZA (left: pre-experiment, right: post-experiment)

Figure 20. Image of YZA - post-experiment

2.2.2.4 Experiments with YZA – discussion of fuel conversion

Though the porous media had degraded over the course of the experiments, and it is impossible to know when the degradation occurred, data were still obtained over a range of equivalence ratios and inlet velocities. Again, these results must be qualified by the fact that the experimental apparatus experienced significant structural changes during experimentation.

Figure 21 shows the hydrogen and carbon monoxide yield as a function of equivalence ratio for a constant inlet velocity of 40 cm/s. The peak hydrogen and carbon monoxide yield occurs at the same equivalence ratios that the peaks had occurred at for the experiments with the alumina pellets, though the magnitudes are smaller. Some of the reasons for a lower yield at the same velocity and equivalence ratio include having different material properties (conductivity, tortuosity, albedo, etc.) and having a different residence time (the inlet velocity is defined by the cross-sectional area of the insulating cylinder, not including the porosity of the medium, so equal

inlet velocities for different porous media have equivalent mass flows of air and fuel, but different residence times in the reactor).

The energy conversion efficiency is shown in Figure 22. Similar to the experiments with the alumina pellets, about 45% of the energy in the jet fuel is lost to heat. As the equivalence ratio is increased, more energy is contained in species other than hydrogen and carbon monoxide as shown in Figure 23.

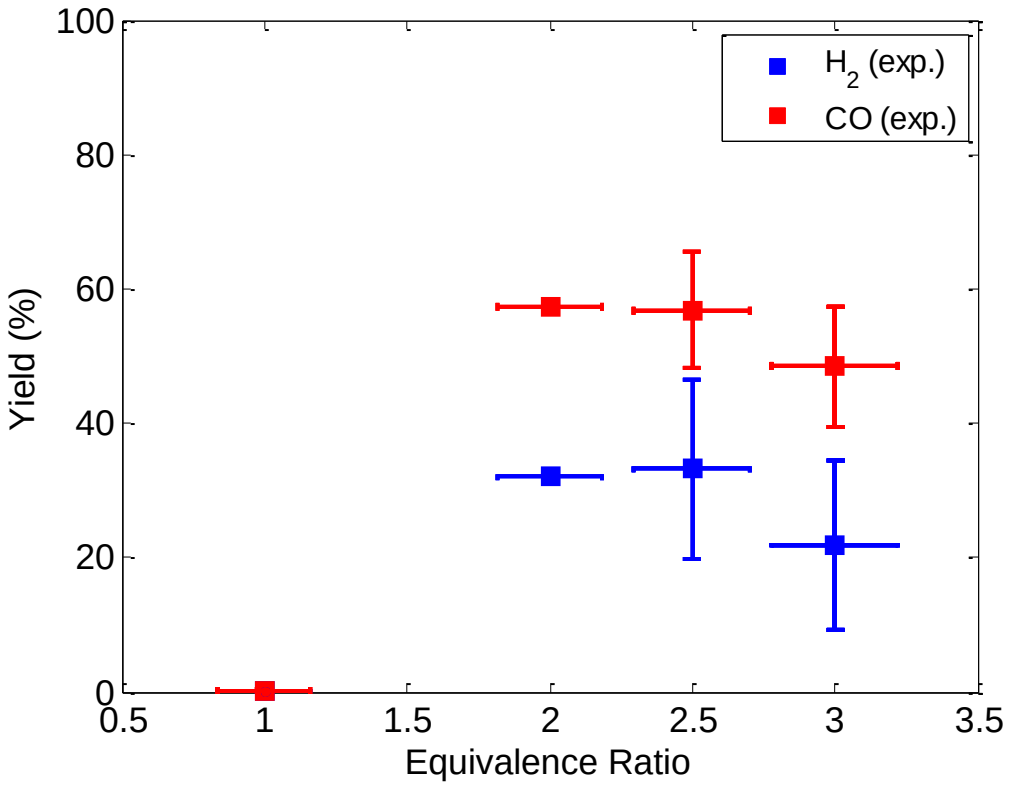

Figure 21. Hydrogen and carbon monoxide yield vs. equivalence ratio - experiments with YZA (V = 40 cm/s)

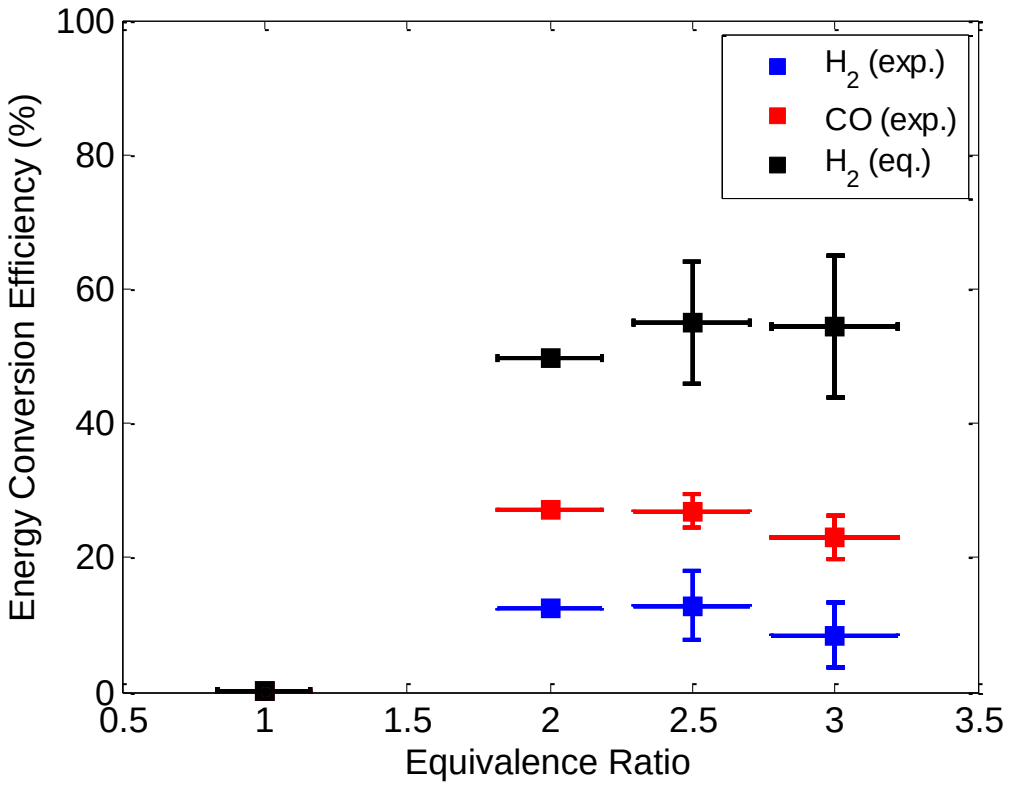

Figure 22. Energy conversion efficiency vs. equivalence ratio - experiments with YZA (V = 40 cm/s)

Holding the equivalence ratio constant at 2.5, the inlet velocity was varied from 30 to 60 cm/s, and the hydrogen and carbon monoxide yields for these conditions are shown in Figure 24. There is little variation in the hydrogen and carbon monoxide yield as inlet velocity is changed, though the hydrogen yield has a fairly noticeable decrease with increasing inlet velocity, again contrary to our previous results with other fuels [37, 39, 41].

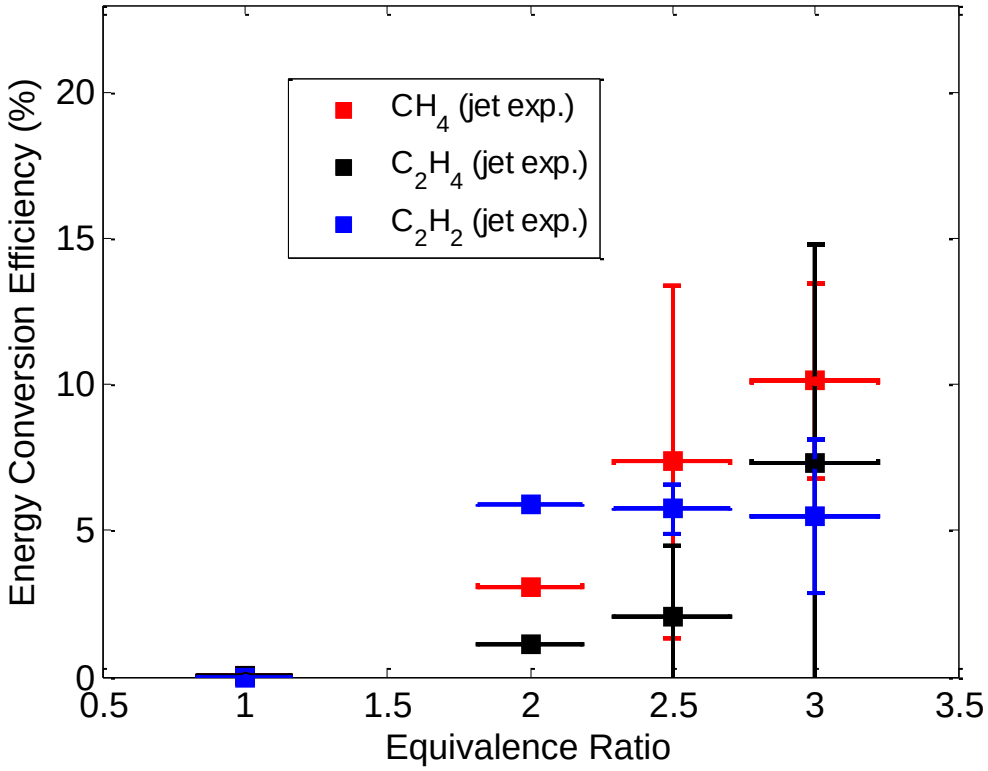

Figure 23. Energy conversion efficiency (minor species) vs. equivalence ratio - experiments with YZA (V = 40 cm/s)

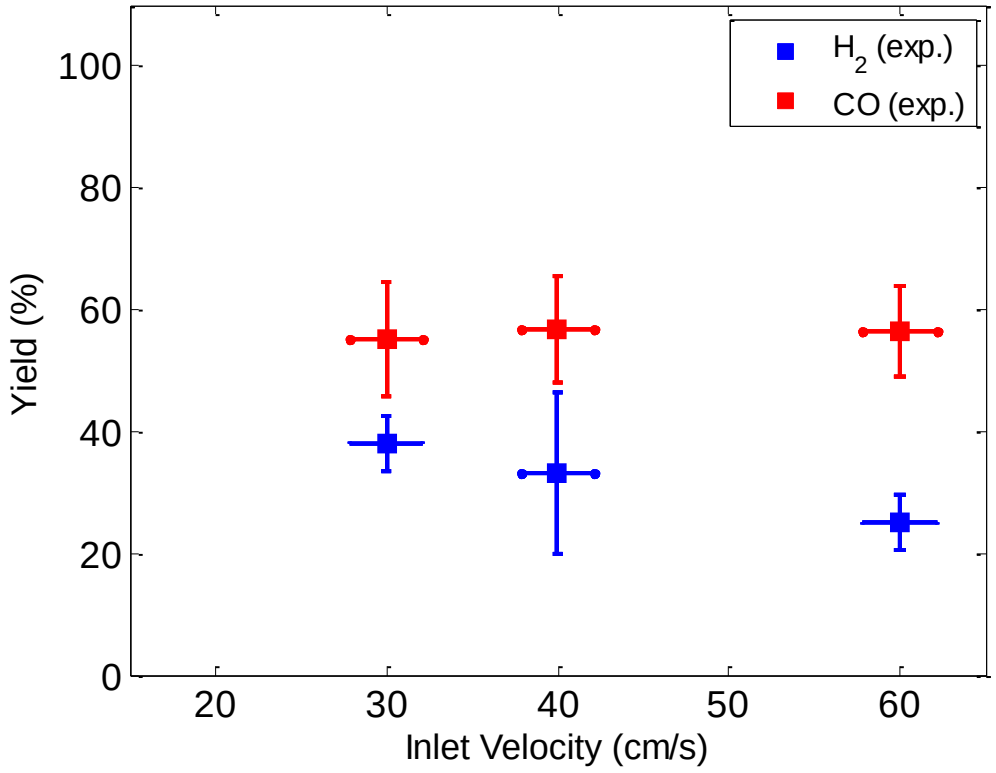

Figure 24. Hydrogen and carbon monoxide yield vs. inlet velocity - experiments with YZA (φ = 2.5)

With the YZA reactor, we were able to gather another set of data; the inlet velocity was held constant at 60 cm/s and the equivalence ratio was varied through the same range as was done while holding the inlet velocity constant at 40 cm/s. These data are shown in Figure 25. Though Figure 24 shows a slight decrease in yield as the inlet velocity is increased and the equivalence ratio is held constant, a comparison between Figure 21, showing yield vs. equivalence ratio at 40 cm/s and Figure 25, shows an overall trend of higher yields at the higher inlet velocity, 60 cm/s. At φ = 2.5 and greater, the yields are lower than the yields at the same equivalence ratio with the velocity at 40 cm/s, but the yields at φ = 2 and 2.25 are significantly higher at 60 cm/s. The unexplainable trends in the data suggest that porous media degradation over the course of experiments may have significantly affected yields.

One other notable result from the YZA data is shown in Figure 26. At an equivalence ratio of 3 and 60 cm/s, a very significant amount of energy in jet fuel is converted to species other than hydrogen and carbon monoxide. About 17% of the energy in jet fuel is converted to methane and about 10% is converted to ethylene.

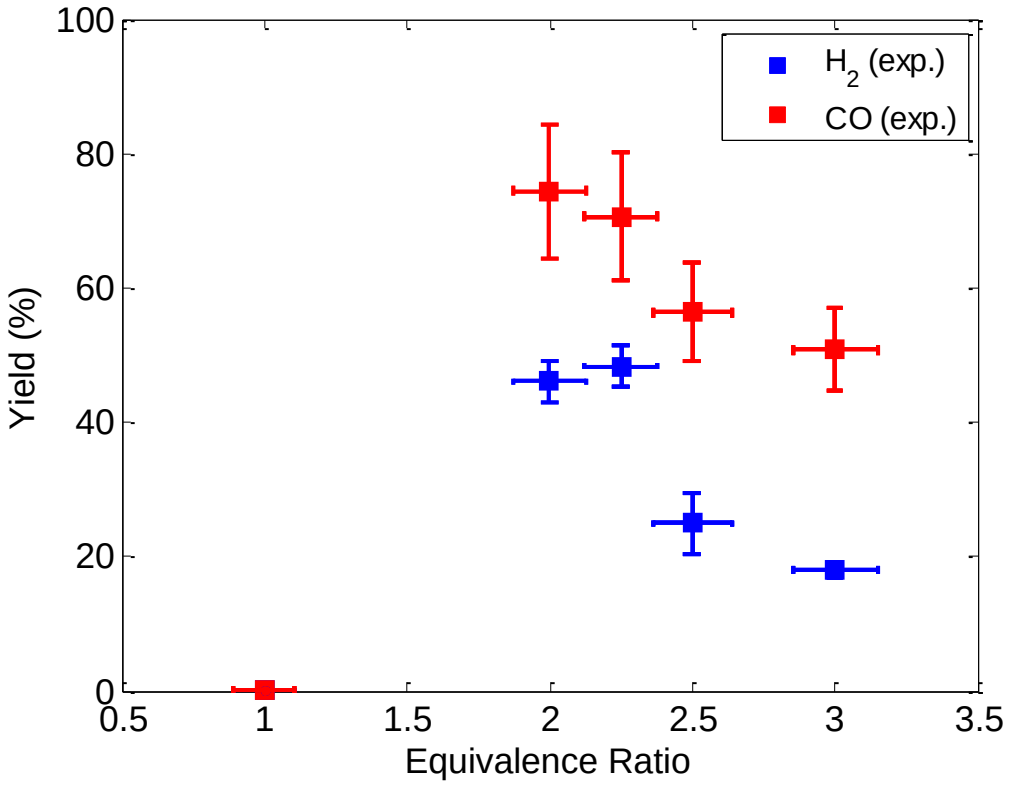

Figure 25. Hydrogen and carbon monoxide yield vs. equivalence ratio - experiments with YZA (V = 60 cm/s)

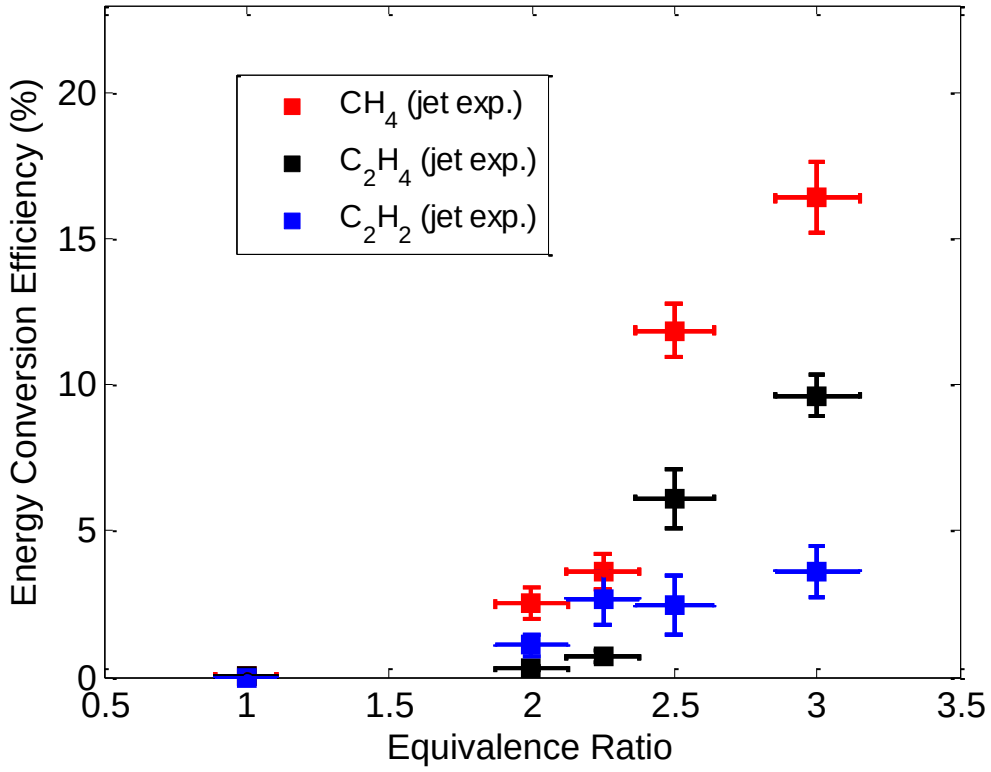

Figure 26. Energy conversion efficiency (minor species) vs. equivalence ratio - experiments with YZA (V = 60 cm/s)

2.3.3.1 Experiments with ZTM – discussion of materials

Lastly, ZTM reticulated ceramic foams of the same size and shape as the YZA were used as a porous medium. ZTM (zirconia toughened mullite) was examined by X-ray diffraction before the experiments, and the constituents were found to be mostly monoclinic ZrO_2 and AL_2O_3 with minor phases of $AL_6Si_2O_{13}$ and cubic ZrO_2. These experiments were performed primarily to determine if this material would also degrade, though species and temperature data were also taken. Experiments were run for

approximately 3 hours until the rig became inoperable (the top piece of ZTM popped out of the top of the reactor, creating a large cavity within the reactor). The rig was purged and cooled with air and disassembled. Significant degradation of the ZTM was observed as shown in Figure 27. Samples of the seemingly melted pieces of material were shown to be, again by X-ray diffraction, equal monoclinic and cubic ZrO_2 with some Al_2O_3. The pre and post usage X-ray diffraction patterns seemed to indicate that the mullite phase had been carried away in the gas flow.

Figure 27. Images of ZTM (left: post-experiment, right: pre-experiment)

2.2.2.5 Experiments with ZTM – discussion of fuel conversion

A limited data set was obtained before the rig had become inoperable. Figure 28 shows the hydrogen and carbon monoxide yield as a function of equivalence ratio at an inlet velocity of 40 cm/s. Consistent with the previously discussed results, the peak yields appeared to occur near an equivalence ratio of 2. The peak hydrogen and carbon monoxide yields, about 47% and 70%, respectively, are also similar in magnitude to the alumina and YZA results.

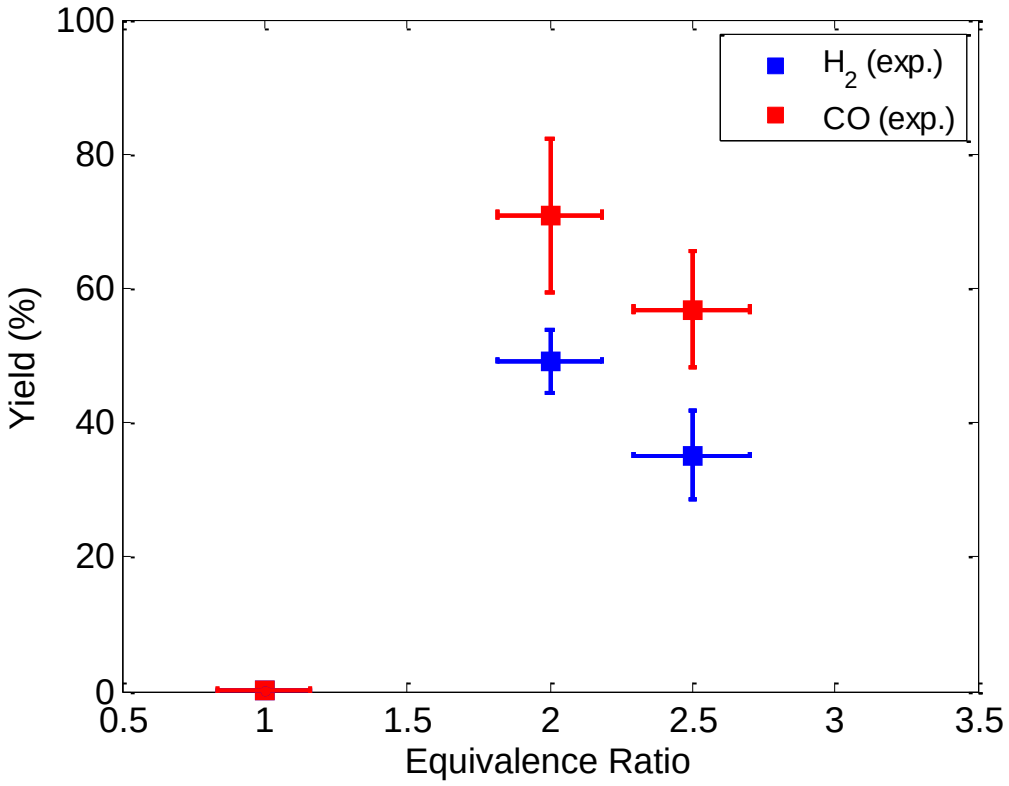

Figure 28. Hydrogen and carbon monoxide yield vs. equivalence ratio - experiments with ZTM (V = 40 cm/s)

2.2.3 CONCLUSIONS FOR INITIAL EXPERIMENTS

The primary conclusion of this work was that the porous media that were used in these tests was unacceptable for long-term use for jet fuel combustion. Even with the observation of degradation, the conversion of jet fuel to syngas was demonstrated. The degradation of the porous media under filtration combustion with jet fuel was unique; it had not been observed in experimentation with other fuels with the same porous media. Though an investigation of the material changes would be interesting, it was decided that experiments would be performed with different porous media in the hope that the conversion of jet fuel and butanol by filtration combustion could be investigated without the complication of phase change or reactions with the porous media. Since the alumina pellets had been most successfully used, new alumina pellets with a high level of purity were obtained and the experiments were attempted again with the new porous media. These experiments are described in the next section (2.3)

Acknowledgements for Work on Initial Experiments

Casey D. Zak, Daniel I. Pineda and Janet L. Ellzey contributed substantially to the work described in this chapter, which is based on a conference publication [110]. I would also like to acknowledge Dr. Steven Swinnea of the Texas Materials Institute for his X-ray diffraction work and Dr. Desiderio Kovar of The University of Texas at Austin for help understanding the materials science aspect of this work.

2.3 Experiments with Re-Designed Experimental Apparatus

2.3.1 EXPERIMENTAL APPARATUS

The re-designed experimental apparatus consisted of the reactor, the fuel vaporization system, the reactant delivery system, and the data acquisition system. A quartz cylinder 5 cm in diameter and 30 cm in length was the reactor and vaporization chamber. The reactor section of the quartz cylinder was filled with alumina (AL_2O_3) spheres of 5 mm in diameter and was insulated on the outside with 2 cm thick alumina. The alumina spheres were 99.5% pure alumina and obtained from Union Process. The relevant properties of the spheres are shown in Table 3. The alumina insulation had holes approximately every 2 cm along the length to allow visual observation of the reaction zone location and soot deposition (Figure 29). Figure 30 shows the details of the filtration reactor, and Figure 31 shows the details of the reactant delivery system.

Figure 29. Image of filtration reactor

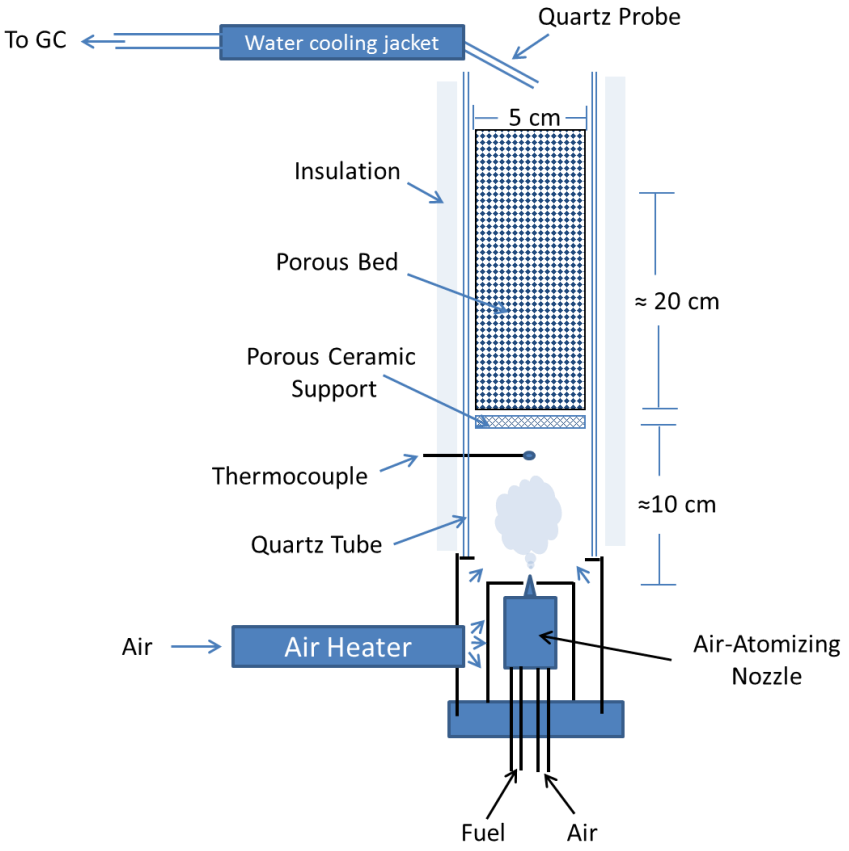

Figure 30. Diagram of re-designed experimental apparatus

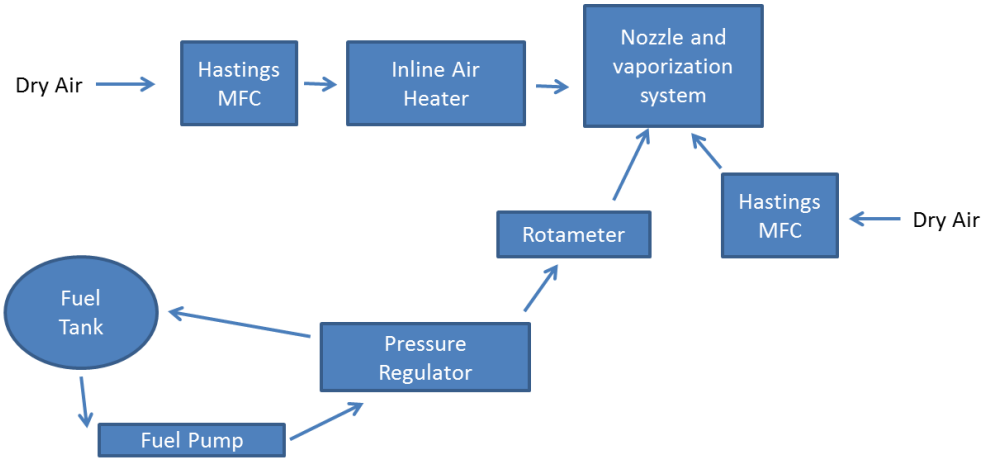

Figure 31. Design of reactant delivery system

Table 3. Properties of alumina spheres [111]

Property	Value
Specific heat [c_s]	1255 J/kg-K
Conductivity [k_s]	1.195 W/m-K
Albedo [ω_λ]	0.8
Extinction Coefficient [β_λ]	100 m^{-1}
Density [ρ_s]	2334 kg/m^3
Pore Diameter	0.005 m
Porosity	0.4

The vaporization system consisted of an air-atomizing nozzle (spraying systems 1/8 JBC-SS with 2050 fluid cap) and the quartz chamber for mixing. The atomized fuel droplets, approximately 20 microns in size, were vaporized in a separate heated air stream in the quartz chamber. The base of the chamber, which held the nozzle and air heater, was machined from stainless steel. The outer surface of the quartz chamber was wrapped with resistance band heaters and insulation to prevent condensation of the fuel. Portions of the band heaters and insulation were removable so that any potential condensation of the jet fuel could be observed. Especially since filtration combustion is a transient process, having visual access to the vaporization chamber was critical. Some operating conditions were not tested (high inlet velocities with high equivalence ratios) because the vaporization system was unable to produce a gaseous stream of reactants. Data is reported under no conditions when accumulation of liquid fuel was observed, and the reactant stream was always transparent (ie: no observable droplets of liquid fuel) before entry into the porous media. The temperature of the inlet mixture was always

between 150˚C and 200˚C as measured by the thermocouple placed before entry to the reactor.

The fuel delivery system included a fuel tank, a pump and rotameters (Cole Parmer) for fuel regulation. The stream of dry laboratory air entering the nozzle was unheated, but an inline air heater (Convectronics Part 007-10135) heated the other stream of air. The air entering the nozzle and the air entering the inline air heater were controlled with separate mass flow controllers (Hastings).

For these experiments, jet fuel from Berry Aviation at the San Marcos Municipal Airport was used. The fuel is supplied to Berry Aviation by AVFuel Corporation. Since jet fuel can have a varying composition, an average chemical formula must be assumed. In this work a chemical formula of $C_{11}H_{21}$ was used [107]. The density, as measured by a laboratory scale, was 797 kg/m3, and the lower heating value was 43.2 MJ/kg as given by [108]. The butanol that was used in this study was obtained from Superior Solvents and Chemicals. The density was measured as 810 kg/m3 and the lower heating value was 33.1 MJ/kg [108].

2.3.2 EXPERIMENTAL PROCEDURE

When a specific operating condition (φ, V) was to be tested, the reaction front was first positioned 5-10 cm from the bottom of the porous medium part of the reactor by igniting a slightly lean flame at the exit of the porous medium and allowing it to propagate upstream. This procedure ensured that any soot that was deposited within the

reactor during operation at the previous condition was completely burned off before the start of the next condition to be tested. Then the flows of fuel and air were set to the desired values, and the location of the reaction zone was monitored visually through the holes in the insulation surrounding the reactor.

The exhaust species were measured by a Varian, Inc. gas chromatograph (GC) that was calibrated to measure the following species: hydrogen, oxygen, nitrogen, methane, carbon dioxide, carbon monoxide, ethylene, ethane, acetylene and select higher hydrocarbons. The GC sampled the exhaust gas for measurement through a water-cooled quartz probe. For every tested condition, the first two measurements were discarded and the rest of the measurements were averaged. Measurement uncertainty was calculated using a Student-t distribution. The contributions to the uncertainty were uncertainty in the GC calibration gases, uncertainty in the GC calibration, and uncertainty in the flow rates of air and fuel. Uncertainties for all calculations were based on sequential perturbation.

2.3.3 RESULTS AND DISCUSSION

In the experiments for each fuel, we obtained one set of data by varying φ and holding V constant and another by varying V while holding φ constant. The experimental operating conditions are described in Table 4.

Table 4. Experimental operating conditions

Fuel	**Equivalence Ratio (φ)**	**Inlet Velocity (V) [cm/s]**
Butanol	1-5	30
Butanol	3	30-60
Jet A	1-3.15	34
Jet A	2.7	34-46

The tested ranges for φ and V were determined by multiple factors. For both fuels, maximum values of V were limited by the rate of downstream reaction zone propagation. Species data are reported from conditions when the GC could sample the exhaust gases at least 4 times, and this was possible only when the downstream propagation rate was less than ~2.5 cm/min. For butanol and jet fuel, the reaction zone remained nearly stationary (the reaction zone remained within 5-10 cm from the bottom of the reactor in the time that 5 samples were taken) relative to the porous media when the operating conditions were $\varphi \approx 2$, $V \approx 32$ so the GC could sample the exhaust gases many times. When φ or V increased from these values, the reaction zone propagated downstream up to ~3 cm/min, and the speed of propagation was higher for jet fuel than for butanol under the near-overlapping tested conditions. The ~2.5 cm/min limit on the propagation speed determined the limiting V for both fuels and the limiting φ for butanol. As described in detail in section 2.3.3.1, soot formation limited the maximum testable φ for jet fuel. The minimum testable V were determined by the minimum flow rates required for safe operation of the inline air heater.

Important metrics for syngas production are the hydrogen yield and the carbon monoxide yield. These metrics, defined below, describe how effectively the reactor converts hydrogen and carbon bound in the fuel to diatomic hydrogen and carbon monoxide, respectively.

$$hydrogen\ yield\ =\ 100 \times \frac{2 \times \dot{N}_{H_2}}{N_H \times \dot{N}_{Fuel}}$$

$$carbon\ monoxide\ yield =\ 100 \times \frac{\dot{N}_{CO}}{N_C \times \dot{N}_{Fuel}}$$

where the units of $\dot{N}_{Fuel}$, $\dot{N}_{H_2}$ and $\dot{N}_{CO}$ are moles per second. N_H = 10 and N_C = 4 for butanol, N_H = 21 and N_C = 11 for jet fuel [107].

We also calculated values for the chemical energy conversion efficiency. This metric describes the percentage of chemical energy in the original fuel that was contained in particular exhaust species. The energy conversion efficiencies were calculated using the LHV of the individual species as described by the following representative equation for hydrogen:

$$hydrogen\ energy\ conversion\ efficiency = 100 \times \frac{\dot{N}_{H_2} \times LHV_{H_2}}{\mathrm{LHV}_{Fuel} \times \dot{N}_{Fuel}}$$

where LHV values are in units of kJ per mole.

Similarly, we calculated the total energy conversion efficiency, the percentage of chemical energy in the original fuel contained in all fuel exhaust species. If all species are at ambient temperature and no energy is lost through heat transfer, then this quantity should be 100%. Values lower than 100% indicated how much energy is associated with

heat losses and the sensible energy of the products. The total energy conversion efficiency was calculated as follows:

$$total\ energy\ conversion\ efficiency = 100 \times \frac{\sum_i \dot{N}_i \times LHV_i}{\mathrm{LHV}_{Fuel} \times \dot{N}_{Fuel}}$$

The summation is performed over all gaseous species in the exhaust with positive LHV and with non-negligible concentration (concentration > 0.1%). LHV values were taken from [109].

For comparison with experimental results, equilibrium values are also presented. We calculated these values for a constant pressure/enthalpy process using the Cantera software suite [112]. Previous work [39, 113] has shown that equilibrium calculations predict trends in exhaust species as a function of reactant composition and can provide insight into the thermodynamic character of the conversion process. All equilibrium calculations included the formation of solid carbon.

2.3.3.1 Soot Investigation

One of the challenges of investigating butanol and jet fuel at rich conditions was the propensity of these fuels to produce soot. For both fuels, when φ was greater than approximately 1.5, soot was observed in the reactor through the holes in the insulation surrounding the reactor and at the exit of the reactor (Figure 32). When the reaction zone propagated downstream soot was observed both upstream (in Figure 32 the reaction zone is at approximately 7 inches and soot can be observed upstream at 6 inches) and downstream of the reaction zone. The highest φ tested with jet fuel was 3.58 because soot

laydown at this equivalence ratio and higher was so great that it clogged the pores of the reactor. With butanol the reactor was not clogged at any tested equivalence ratio, although significant soot was observed. The quantities of soot increased, based on qualitative observation, with increasing φ.

Figure 32. Image of soot through holes in insulation

Figure 33. Images of Soot Formation for Butanol (left) and Jet Fuel (right)

The right hand image in Figure 33 shows the top of the filtration reactor after experimenting with jet fuel/air mixtures with an equivalence ratio of 3.58 and an inlet velocity of 34 cm/s. The following was observed previous to the time this image (right hand image in Figure 33) was taken:

- The reaction zone propagated upstream for the conditions of $\varphi = 0.9$, V=34 cm/s until the reaction was ≈ 7 cm from the bottom of the pellets

- The operating conditions were changed to φ = 3.15, V=34 cm/s, and the reaction zone propagated downstream
- When the reaction zone was 22 cm from the base, the operating conditions were changed to φ = 1.4, V=34 cm/s
- After a short time, the reaction zone appeared to "jump" from ≈ 22 cm from the base to ≈ 7 cm from the base.
- In order to avoid flashback into the mixing/vaporization chamber, the operating conditions were changed to φ = 3.6, V=34 cm/s
- After a short time, the pellets were ejected from the top of the reactor. Then the image in Figure 33 was obtained.

Previous to the observations above, the reactor was operating normally. At high equivalence ratios with jet fuel (φ > 3.15) soot formation is significant enough to clog the pores in the packed bed of alumina pellets and block the flow of the reactants through the reactor. Similar experiments were attempted after rebuilding the reactor and it was found that the reactor could be operated at an equivalence ratio up to 3.15 without clogging, but at φ = 3.58 clogging always occurred. In experiments performed by the authors' research group under similar experimental conditions with other fuels—including ethanol [37] and methane [41], soot deposition was not observed in significant amounts. In experiments with heptane [39, 114], soot was observed, but not at amounts that appear, qualitatively, to those observed in the present experiments with butanol, and especially with jet fuel.

The left hand image in Figure 33 shows the quartz reactor with the insulation removed after an experiment with butanol. At the bottom of the reactor, white alumina

pellets can be seen. The inside of the quartz chamber above these white pellets is black from soot deposition. This image was taken after a filtration wave for an equivalence ratio of 4 and an inlet velocity of 30 cm/s had propagated from the bottom of the reactor to the top. During the propagation of the filtration wave, soot formation was observed through the holes in the insulation that covers the quartz cylinder. Under these conditions (φ = 4, V=30), the reaction zone propagates downstream, and soot was observed on pellets both upstream and downstream of the reaction zone. Because of this phenomenon, the soot-coated porous medium, instead of being inert, acts as a porous solid fuel. This situation complicates the analysis of the results because the effective equivalence ratio at any given time is not known. Soot deposition was observed for experiments with butanol at equivalence ratios of 3 and greater at all inlet velocities.

In order to investigate further the magnitude of soot deposition, a carbon-flow balance was performed from the experimental measurements and equilibrium calculations. Figure 34 shows this carbon balance in terms of the ratio:

$$\frac{carbon\ out}{carbon\ in} = \frac{flow\ rate\ carbon\ atoms\ in\ gaseous\ exhaust}{flow\ rate\ of\ carbon\ atoms\ in\ fuel}$$

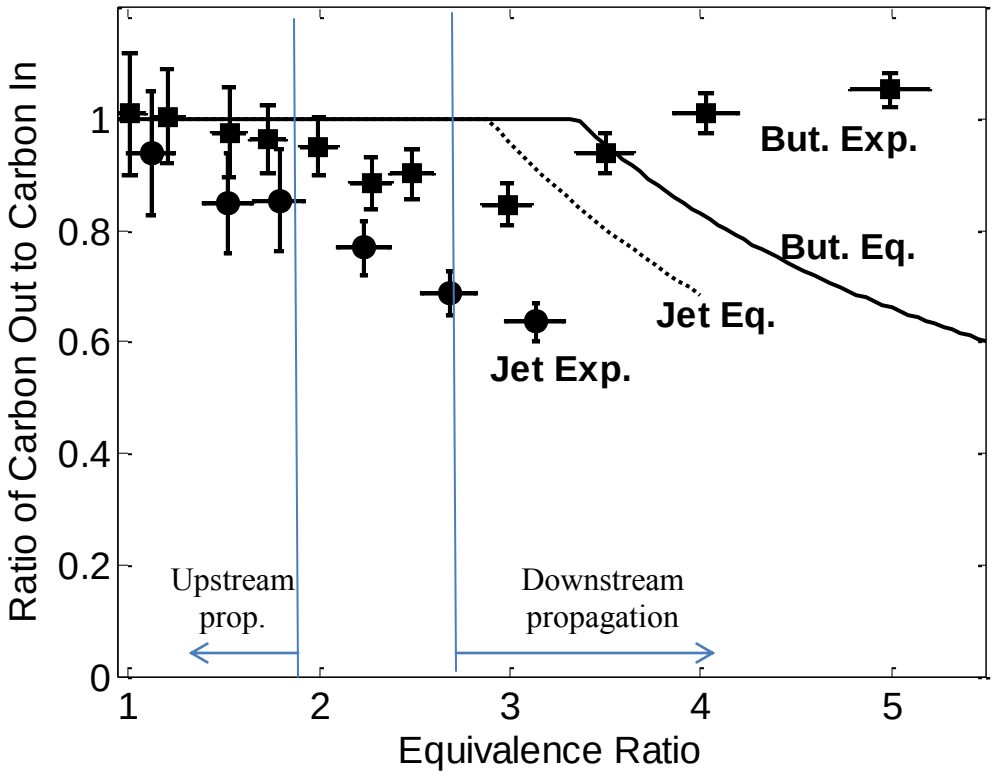

Figure 34. Ratio of carbon out to carbon in vs. equivalence ratio with inlet velocity = 32 ± 2 cm/s. Lines on the figure indicate approximate equivalence ratios at which upstream and downstream propagation occurred.

As shown in the figure, equilibrium predicts that all carbon is in gaseous species until φ ~ 3, above which significant solid carbon formation occurs. In the experiments near stoichiometric conditions, carbon is in gaseous compounds for both butanol and jet fuel. As φ increases, however, the ratio of carbon leaving to carbon entering decreases steadily for jet fuel until the maximum φ tested (3.15) is reached indicating loss to carbon laydown in the reactor. For jet fuel at φ = 3.15, about 40% of the carbon entering the system is deposited in the reactor. These data are consistent with the qualitative

observation of heavy soot deposition and reactor clogging in the experiments with jet fuel. For butanol the ratio decreases until $\varphi = 3$, and then rises again to exceed 1 at $\varphi = 5$.

The carbon ratio greater than 1 is counter-intuitive and initially suggests that carbon is being "created." On closer inspection, however, this is a consequence of the transient nature of filtration combustion. As shown in Figure 9, when the front propagates downstream three important parameters change with time: the residence time of the gas upstream of the reaction increases, the residence time of the gas downstream of the reaction zone decreases, and the preheat region expands. These effects, coupled with the soot deposition complicate the analysis of the experimental results for downstream-propagating reaction zones. As indicated in Figure 34, the reaction zone propagated downstream when φ exceeded 2.5, and this downstream propagation rate increased with equivalence ratio.

Soot is complex, containing a variety of chemical species and structures, including adsorbed hydrocarbons [115]. Since soot is composed mainly of carbon and hydrogen, it, along with adsorbed hydrocarbons, can be oxidized to other species that are measured in the exhaust [99, 116]. One would expect this effect to be particularly pronounced when O_2 is in proximity to surfaces coated with soot at high temperature, and this occurs significantly when the reaction zone propagates downstream as soot was observed upstream of the reaction zone. Soot particles can grow on timescales similar to the residence times in the reactor [117, 118]. Therefore an additional effect of downstream propagation is that hydrocarbon species, particularly acetylene, that contribute to soot growth have less time to do so because their residence time between

the reaction zone and the sampling point decreases with downstream propagation. The carbon balance exceeding 1 at the highest φ is suspected to be the result of the soot consumption/oxidation rate exceeding the soot deposition rate at the time those samples were taken.

The data that were taken when the reaction zone was nearly stationary (φ ~ 2) or upstream propagating (φ < 1.5) are considered as appropriate representations of the conversion potential of these fuels. In these cases, soot is not observed upstream of the reaction zone, and therefore there is no potential for additional fuel species to be added to the gaseous stream. Results in the following sections are presented in terms of yield and energy conversion efficiency, which are defined relative to the known fuel input at the time of sample. The data shown in Figure 34 imply that the yields and energy conversion efficiencies must be interpreted with the carbon flow balance in mind. If there is a net deposition of soot at the time a given sample is taken, this will be reflected in lower yields and energy conversion efficiencies. If the rate of oxidation/consumption exceeds the deposition rate at the time a sample is taken the yields and energy conversion efficiencies will be artificially high.

Not only do the results shown in Figure 34 and our qualitative observation of soot (including complete pore blockage in the jet fuel experiments) have implications for the present work, these data also have important implications for any experimental work with butanol and jet fuel at high φ in premixed combustion. Burning the soot out of the reactor at all conditions was accomplished by burning a lean mixture that propagated upstream though the reactor. For a filtration reactor to be operated in any practical application this

procedure would be required. In addition, such a cleaning procedure would likely be required for other reactors that operate with these fuels at φ greater than about 2.

2.3.3.2 Conversion of Jet Fuel to Syngas

Ideal fuel conversion results in the complete conversion of carbon and hydrogen in the reactants to CO and H_2 in the products, respectively. The yields of these species, then, describe reactor performance relative to the ideal case. The effect of φ on syngas production in terms of H_2 and CO yields is shown in Figure 35.

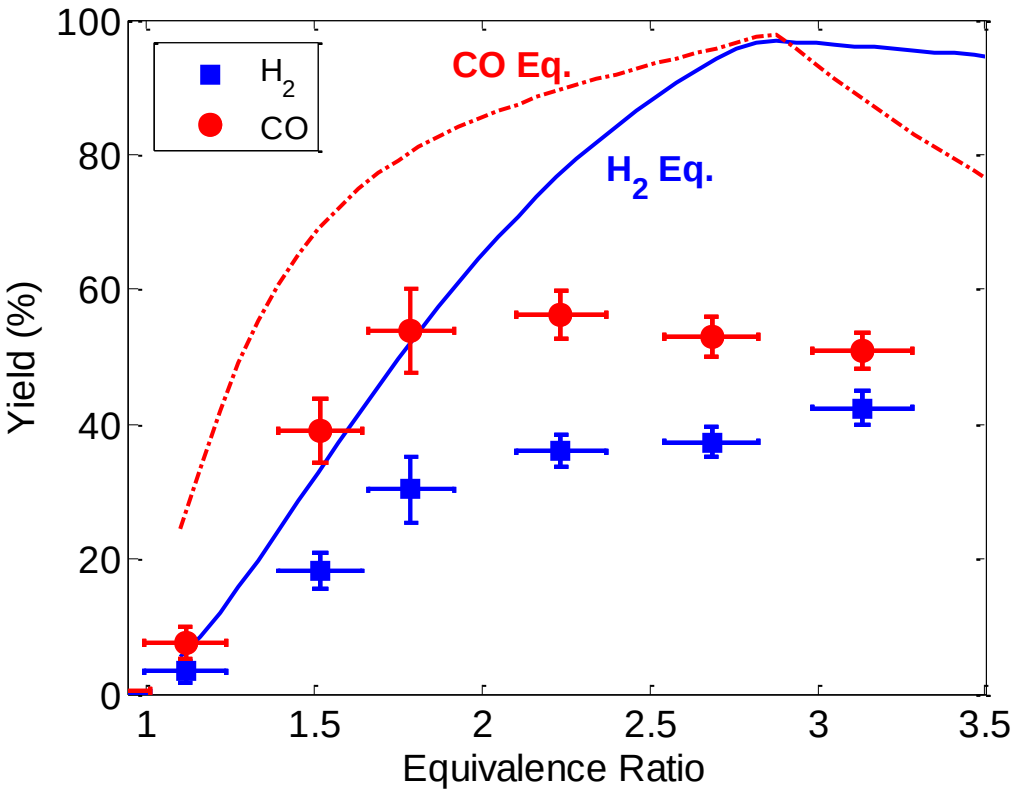

Figure 35. Yield vs. equivalence ratio for jet fuel with inlet velocity = 34 cm/s. Downstream propagation observed for equivalence ratio > 2.5

The yields for CO and H_2 are zero at stoichiometric, and very small for $\varphi = 1.25$. At higher φ the equilibrium values are all higher than the corresponding experimental measurements. The CO yield increases rapidly with φ until $\varphi = 2.25$ while the H_2 yield continues to increase over the entire tested range. The maximum yields for H_2 and CO occur at different φ and are 42% at $\varphi = 3.15$ and 56% at $\varphi = 2.25$, respectively. In contrast, equilibrium calculations predict that the peaks in conversion of H_2 and CO occur at the same φ ($\varphi \sim 2.9$).

As mentioned previously, the energy conversion efficiency is the percentage of chemical energy in the fuel that is contained in specific species in the exhaust. The total energy conversion efficiency is percent of the chemical energy in the fuel that is contained in the exhaust. Figure 36 and Figure 37 show the total energy conversion efficiency and species energy conversion efficiency as a function of φ and V for jet fuel.

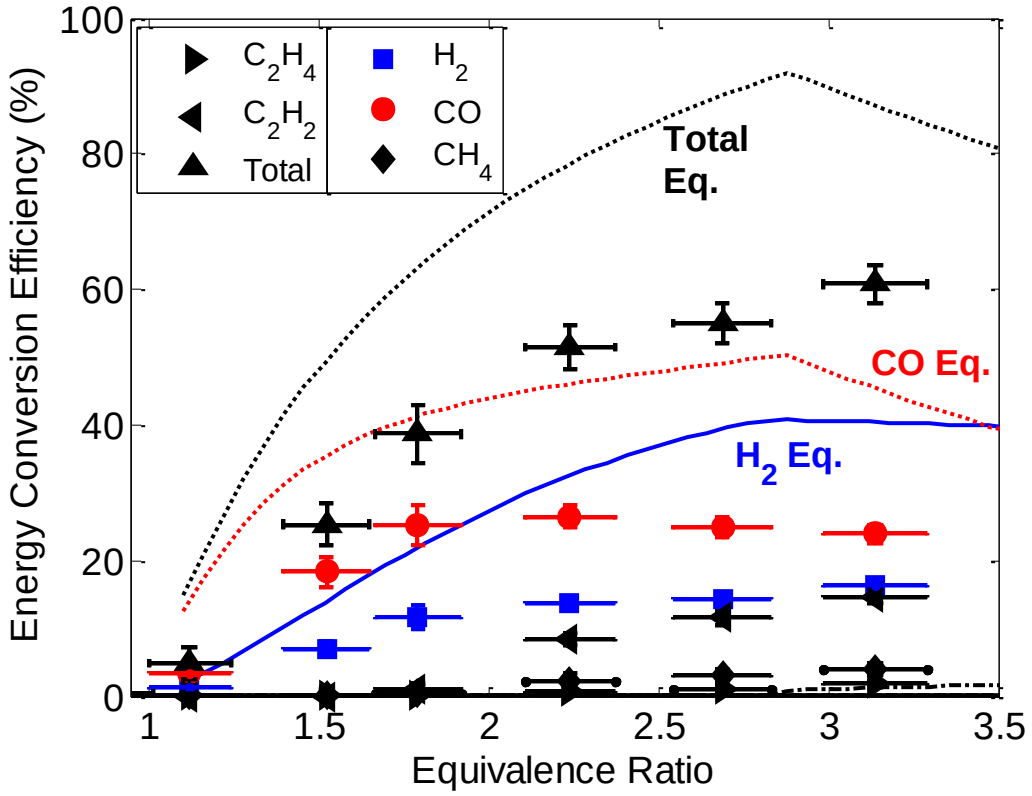

Figure 36. Energy conversion efficiency vs. equivalence ratio for jet fuel with inlet velocity = 34 cm/s. Downstream propagation observed for equivalence ratio > 2.5

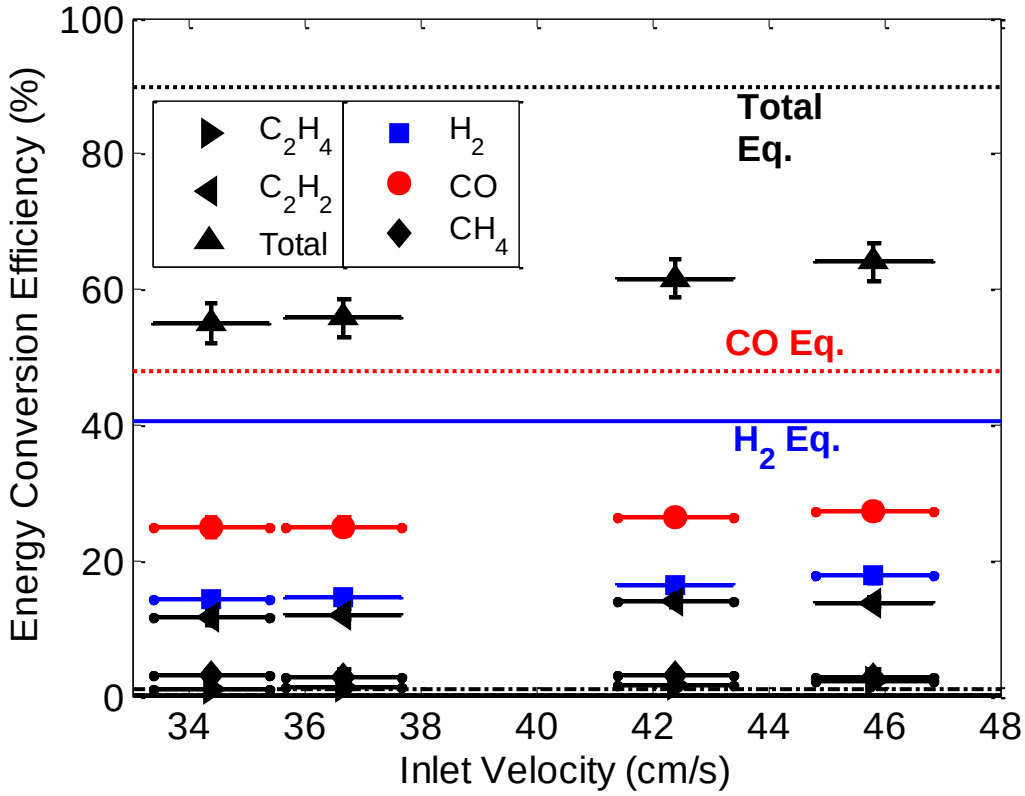

Figure 37. Energy conversion efficiency vs. inlet velocity for jet fuel with equivalence ratio = 2.7. Downstream propagation observed for all conditions

Similar to the trend observed in Figure 35, the experimental energy conversion efficiencies for CO, H_2 and the total are significantly lower than equilibrium (Figure 36). The total energy conversion efficiency increases with φ up to a maximum of 61% at φ = 3.15, meaning that 39% of the energy in the original fuel is lost to heat. Besides H_2 and CO, acetylene and, to a lesser degree, methane are the only energy-containing species that contributes substantially to the total energy conversion efficiency. This is in contrast to equilibrium which predicts almost no hydrocarbons in the products.

Figure 37 shows equilibrium and experimental energy conversion efficiency as a function of V for φ = 2.7. The experimental data show that V does not affect the energy conversion efficiencies (species specific or total) to a large degree over the tested range. Previous studies have shown that the energy conversion efficiency can depend strongly on inlet velocity; however, the tested range in this study was not as large as the tested ranges reported in previous studies.

2.3.3.3 Conversion of Butanol to Syngas

The potential of butanol for conversion to syngas was investigated through a similar set of experiments to those performed with jet fuel. Butanol differs substantially from jet fuel because it has a smaller molecular weight and is an alcohol, containing an oxygen atom in the molecule. In Figure 38, the yields of H_2 and CO are presented as a function of φ with V held constant at 30 cm/s.

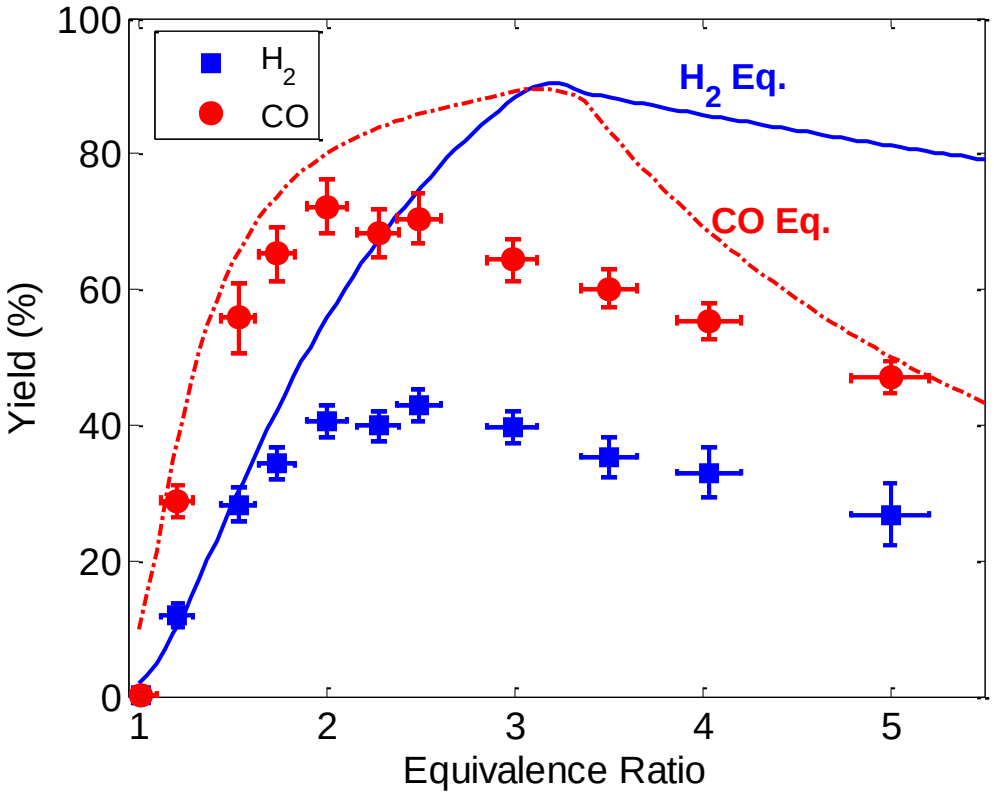

Figure 38. Hydrogen and carbon monoxide vs. equivalence ratio for butanol with inlet velocity = 30 cm/s. Downstream propagation observed for equivalence ratio > 2.5

The yields for H_2 and CO increase rapidly as φ is increased from stoichiometric. The peak CO yield (72 %) occurs at φ = 2, and the peak H_2 yield (43 %) occurs at φ = 2.5. As φ increases from these values, the yields for CO and H_2 decrease slowly. For both CO and H_2, the yields are very similar to the yields predicted by equilibrium until φ ≈ 2. At higher φ, the equilibrium yields are higher than the experimentally measured yields, though at φ = 5, the experimental value and equilibrium values for CO yield are nearly identical.

Figure 39 and Figure 40 show the energy conversion efficiency for the measured species and the total energy conversion efficiency as a function of φ and V, respectively. Both experimental data and equilibrium results are shown.

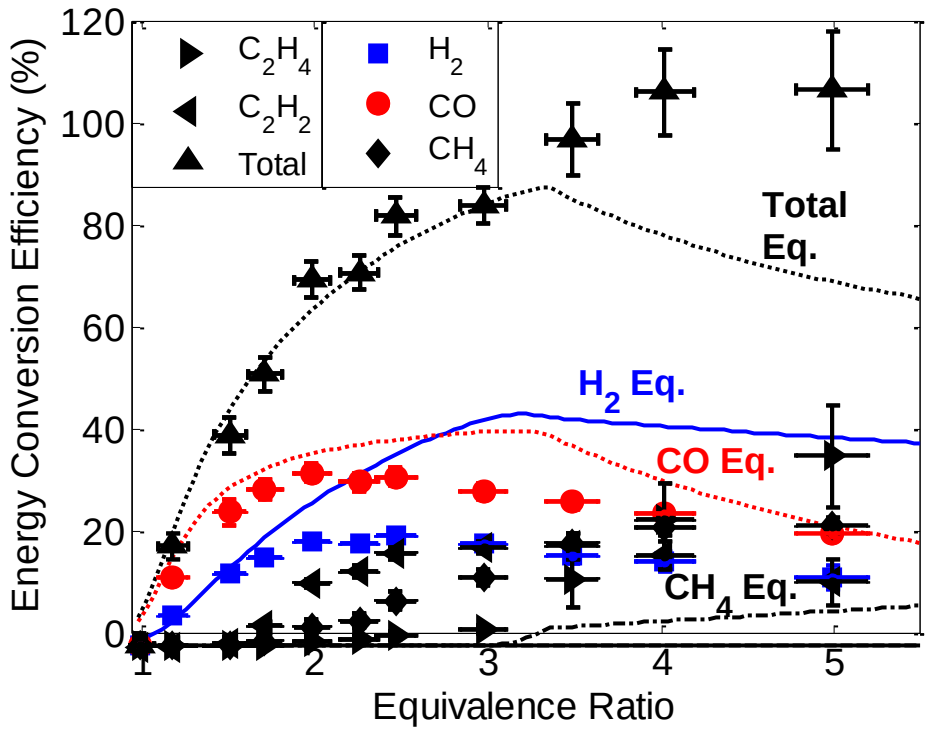

Figure 39. Energy conversion efficiency vs. equivalence ratio for butanol with inlet velocity = 30 cm/s. Downstream propagation observed for equivalence ratio > 2.5

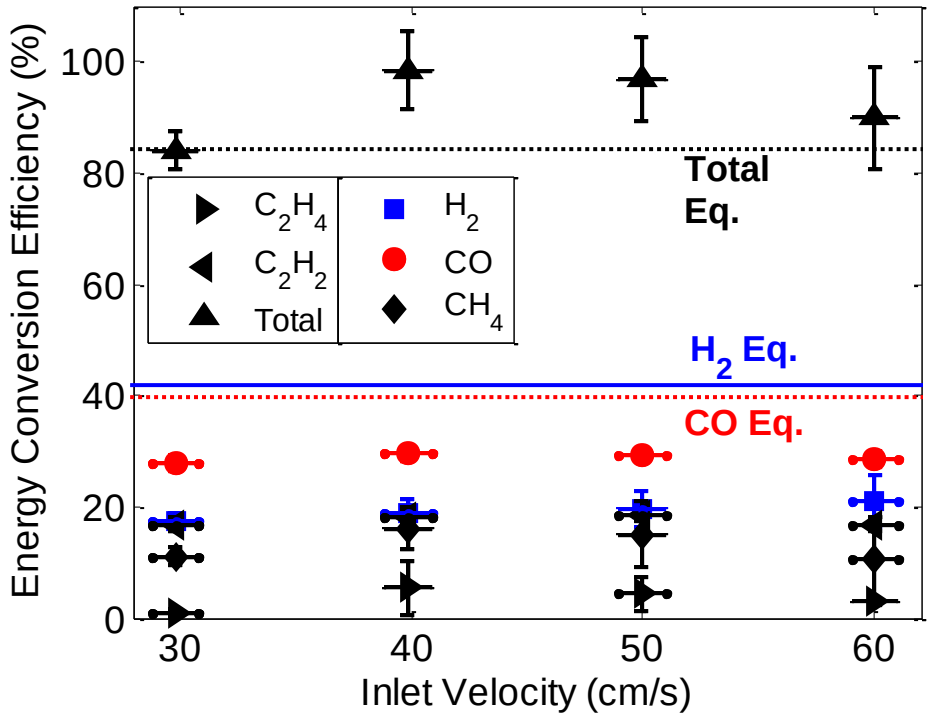

Figure 40. Energy conversion efficiency vs. inlet velocity for butanol with equivalence ratio = 3. Downstream propagation observed for all conditions

In Figure 39 the total energy conversion efficiency determined experimentally follows the equilibrium value until $\varphi > 3$ (where relatively fast downstream propagation was observed). As φ increases beyond 3, the experimental value for the total energy conversion efficiency increases until it slightly exceeds 100%. As explained in section 4.1, it is suspected that an imbalance in soot deposition and consumption at the time of exhaust gas sampling is the reason for the unrealistically high energy conversion efficiencies observed at $\varphi > 3.5$.

For conversion of butanol to H_2 and CO, lower φ are optimal since the conversion of energy from butanol to H_2 and CO peaks at $\varphi \approx 2$. At $\varphi \approx 2$, a significant amount (10%) of the chemical energy is in acetylene, and the contribution of acetylene to the chemical energy outflow increases to a maximum of 20% at $\varphi = 3.25$ and then decreases as φ increases. Methane and ethylene also contributed significantly to the chemical energy outflow as φ exceeded 2. The energy in methane peaks at $\varphi = 4$ with a maximum of 23%, while the energy in ethylene is nonzero at $\varphi = 3$ and rises steadily with φ up to a maximum of 36% at $\varphi = 5$. These results contrast with those for jet fuel (Fig. 5) which shows significantly less contribution from hydrocarbons to the energy content of the exhaust.

Figure 40 shows the energy conversion efficiencies as a function of V for butanol with $\varphi = 3$. Similar to the results for jet fuel, the energy conversion efficiencies for H_2 and CO do not change significantly as V is increased, but the total energy conversion efficiency does increase somewhat as V exceeds 30 cm/s. Exceeding the equilibrium value for total energy conversion efficiency and having near 100% conversion when the V was 40 cm/s and 50 cm/s is, again, likely the result of soot deposition/consumption imbalance and reaction zone propagation (see section 2.3.3.1).

2.3.3.4 Fuels Comparison

Thermodynamic analysis is often used to investigate fuel conversion to syngas [69, 119, 120]. In order to provide insight into the relative syngas production efficiencies

of a variety of fuels, equilibrium calculations were completed for a set of seven fuels with a range of molecular weights. The computed hydrogen yield and carbon monoxide yield as a function of φ for these fuels is shown in Figure 41 and Figure 42, respectively.

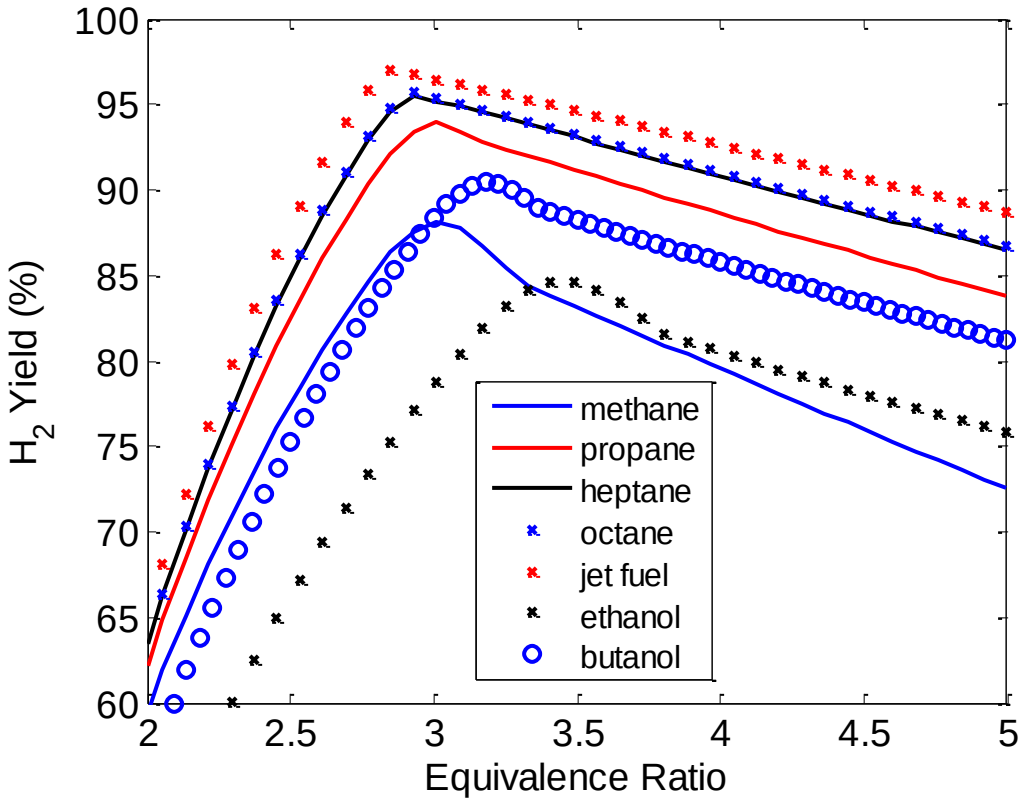

Figure 41. Hydrogen yield vs. equivalence ratio (equilibrium values)

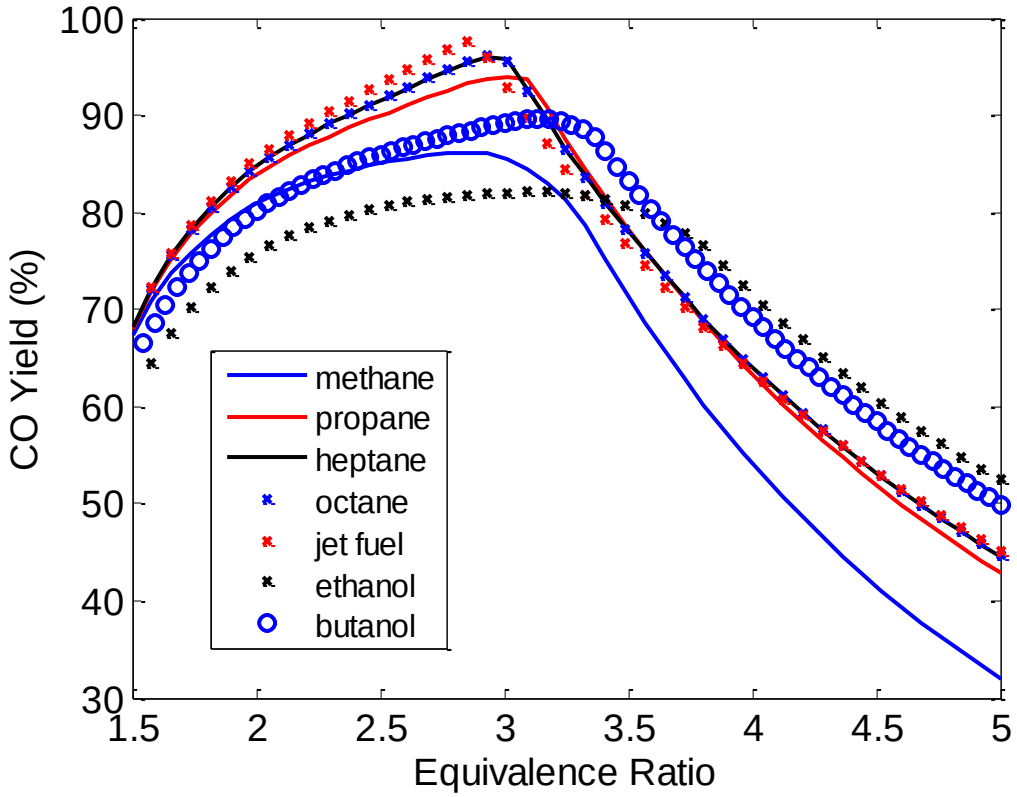

Figure 42. Carbon monoxide yield vs. equivalence ratio (equilibrium values)

The equilibrium data show a trend of increasing H_2 yield with increasing fuel molecular weight. The trend is the same for CO yield excluding the behavior of the oxygenated fuels at $\varphi > 3$. Based on equilibrium, jet fuel is expected to produce the highest yields of H_2 and CO, while ethanol should produce the lowest yields. Amongst the non-oxygenated fuels, methane should produce the lowest yields.

In earlier publications, the authors' group reported results of experiments converting methane [41], heptane [39], and ethanol [37] to syngas by filtration combustion. The filtration reactors that were used in these studies were similar to that

used in the current study, except that for methane where the reactor consisted of ceramic foam rather than a bed of alumina spheres. For each fuel, the operating conditions were different, so direct comparison across a range of V and φ is not possible. However, there are φ, V pairs that overlapped or near-overlapped between each of the fuels studied, so a limited comparison can be made amongst the fuels in terms of hydrogen and carbon monoxide yields. These data can be used to determine the accuracy of using equilibrium data to predict relative fuel performance. The hydrogen and carbon monoxide yields for given φ, V pairs are listed in Table 5.

Table 5. Comparison of hydrogen and carbon monoxide yields for various fuels (Representative uncertainty in yield values: ±5%, representative uncertainty in equivalence ratio: 0.1, representative uncertainty in inlet velocity: ±2 cm/s. Data for ethanol from [37], data for methane from [41], and data for heptane from [39])

Eq. Ratio	Vel (cm/s)	Meth H_2 %	Eth H_2 %	But H_2 %	Hept H_2 %	Jet H_2 %	Eth CO %	But CO %	Hept CO %	Jet CO %
2.5	55	73			65					
2	55	68	57							
3	55	73		45				66		
2.5	32±2	63		43	55	37		71	72	54
2	60		56		55		82		81	
3	60			47	77			66	85	
2	32±2		45	41		33	75	72		55
3	32±2			40		41		64		52

CO yield was not reported in the experiments with methane. However, H_2 yield can be compared with the various fuels. As the tables show, the H_2 yield for methane exceeded the H_2 yield that was observed with each of the other fuels. In terms of H_2 and CO yield, ethanol is next best, having a slightly higher yield of both H_2 and CO than butanol and heptane under the same operating conditions. Heptane has the next highest

conversion with yields higher than butanol. Jet fuel is, by far, the least efficient producer of syngas with both H_2 and CO yields less than those of all the other fuels except for the H_2 yield compared with butanol. Ten binary comparisons can be made amongst the fuels in terms of H_2 yield, and six can be made in terms of CO yield with these data. Among the ten H_2 yield comparisons and six CO yield comparisons only in two cases does a fuel with a larger molecular weight have a greater hydrogen yield than one with lower molecular weight (heptane vs butanol for both H_2 and CO). These data, then, suggest that syngas production efficiency generally decreases with molecular weight. Interestingly, this is the opposite of what is predicted by thermodynamic equilibrium (Figure 41 and Figure 42).

Experimental investigations of conversion of rich hydrocarbon mixtures have been conducted by other groups in the last few years, and these data allow a further comparison of the relative potential of fuels to be converted to syngas. Pedersen-Mjaanes, Chan, and Mastorakos [121] investigated the conversion of methanol, methane, octane and petrol to syngas in a 2-section heat recirculating reactor. They found methanol to have the highest maximum yield followed by methane and then octane and petrol [121]. Pastore and Mastorakos performed experiments with heptane and diesel in a 2-section reactor [59], and, in contrast to the trends observed in the work of the authors' group, they reported diesel to have a significantly higher rate of conversion than heptane in terms of the conversion of energy in fuel to energy in both H_2 and CO. Kennedy and coworkers at the University of Illinois at Chicago who have contributed substantially to the field of heat recirculating reactors and syngas production performed experiments with

methane, ethane, and propane in a filtration reactor very similar to the one used in the present experiments [53]. Their experiments showed nearly identical CO yields for each of the three fuels, but maximum H_2 yields increased in order of decreasing molecular weight. In a recent paper, the relative conversion efficiencies for experiments with methane, propane and heptane in a counterflow reactor were compared [122]. In those experiments, propane had the highest efficiency of conversion to H_2, followed by methane and then heptane. With these data from the literature ten binary comparisons can be made in terms of H_2 and CO yield. Of these ten comparisons, three are in agreement with equilibrium prediction (yield increase with molecular weight), five suggest that yield decreases with molecular weight, and two support neither trend. As with the filtration combustion experiments, these data suggest that the trend in syngas production efficiency as a function of fuel size is not predicted by equilibrium.

Based on the data reported in all of these studies, including the present study, the potential of fuels to be converted to syngas roughly decreases with increasing molecular weight. Currently, the available literature does not provide enough data to draw strong conclusions about fuel optimization for conversion to syngas, and there are multiple exceptions to this general trend indicating that there is a need for a comprehensive study of the effect of fuel on conversion where fuels are tested under identical conditions. The major conclusion of this fuels comparison is that equilibrium predictions of syngas production as a function of fuel size are inaccurate under most conditions. Since equilibrium is often used to predict general trends in syngas production, these data

suggest that care must be taken when interpreting the results of equilibrium computations.

Acknowledgements for Work on Experiments with Re-Designed Apparatus

Casey D. Zak, Daniel I. Pineda and Janet L. Ellzey contributed substantially to the work described in this section, which is based on a paper submitted to the International Journal of Hydrogen Energy [123].

2.4 Concluding Remarks Regarding the Conversion of Jet Fuel and Butanol to Syngas

The results of the conversion of butanol and jet fuel to syngas via non-catalytic transient filtration combustion were presented. Initial attempts to convert jet fuel showed degradation of porous media. The results of those initial experiments show that the selection of materials for a porous media reactor can depend significantly on the fuel that is being used. The reactor was redesigned and successful experiments were conducted with the new apparatus.

At maximum, about 42% of the hydrogen in jet fuel was converted to H_2 and 56% of carbon was converted to CO. The H_2 yield continued to increase with φ in the jet fuel experiments whereas in the butanol experiments the yields for H_2 and CO both reached peaks within the tested operating range. The peak CO yield for experiments with butanol was 72% and the peak H_2 yield was 43%. Most of the chemical energy exiting the reactor

was bound in H_2 and CO, but CH_4, C_2H_2 and C_2H_4 were observed in substantial amounts in experiments with both fuels, especially in experiments with butanol at high φ. In contrast, equilibrium predicted nearly negligible amounts of energy-containing compounds besides H_2, CO and solid carbon.

Soot production proved to be substantial in experiments with both fuels, with the qualitative observation of soot from both fuels exceeding the soot production observed in similar experiments with methane, heptane, and ethanol. Soot production limited the maximum testable φ for jet fuel experiments to $\varphi = 3.15$ since soot clogged the reactor when φ exceeded this value. An analysis of the carbon balance for jet fuel experiments showed that up to 40% of the carbon entering the system was deposited on the porous medium. Similarly for butanol, the carbon balance showed significant loss up to an $\varphi \sim 3$. At the most extreme φ, the reaction zone propagates downstream oxidizing some of the soot that has been deposited previously, resulting in an exhaust stream with more carbon atoms than are contained in the inlet fuel at the time of sample.

Equilibrium calculations and experimental results were analyzed to determine trends in fuel conversion efficiency as a function of fuel type. The equilibrium calculations predicted that larger fuel molecules would, generally, produce higher syngas yields, but the experimental results disagreed with this trend. Generally, experimental results show that smaller hydrocarbons produce higher syngas yields with jet fuel having the lowest hydrogen and carbon monoxide yields. The comparison of these equilibrium data with the experimental data available in the literature suggests that kinetic effects are very important in fuel conversion to syngas and equilibrium results should be interpreted

carefully when predicting syngas production from the combustion of very rich mixtures of fuel and air. Lastly, the demonstration of the conversion of jet fuel and butanol, along with previous demonstrations with methane, ethanol and heptane show the robustness of the non-catalytic filtration reactor.

3 RICH COMBUSTION FOR SYNGAS PRODUCTION: THE EFFECT OF PREHEAT ON BURNER-STABILIZED FLAMES

Generally, in heat-recirculating reactors both conduction and radiation are enhanced over gaseous values by the presence of a solid surface, and in some designs, such as a packed bed or filtration reactor, mass transfer is enhanced over the gas phase levels [124, 125]. The complexity of the transport processes in these reactors makes analysis and the determination of the critical design parameters difficult.

Previous research has shown that the stable operating range, defined as the sets of φ and inlet velocity (V) where stable combustion is attained, varies widely depending on the reactor design even when operating on the same fuel. For example, when operating on methane stable operation in a packed bed reactor was demonstrated up to φ = 5.0 [41] while for a counter-flow reactor the limit was at φ = 2.5 [60]. When the reaction front was stabilized at the interface of two sections of porous media the limit was φ = 1.9 [31].

The conversion of the reactants to syngas also depends on the reactor design. Experiments reforming methane to syngas with filtration reactors [41, 50], a counter-flow reactor [60] and another type of porous media reactor [119] showed a variety of syngas yields with maximum H_2 yields ranging from 40% to more than 70% amongst the different reactors. Furthermore, experiments reforming heptane to syngas with two different reactor types [39, 61] showed different reforming efficiencies. The filtration reactors typically produce the highest syngas yields, but since the stable operating conditions of the various reactors typically do not overlap, a direct comparison is difficult.

Several computational studies have shown the importance of conduction, radiation, and solid-to-gas heat transfer in these reactors [26, 32, 126, 127]. The significant outcome of these enhanced processes is that the reactants are preheated and will therefore react even at extreme equivalence ratios. In these devices, the preheat temperature is a function of both the properties of the reactor and the combustion process. In one study [6], the inlet mixture to a porous reactor was preheated externally to a controlled temperature but since additional heat transfer takes place within the reactor, the effective preheat temperature is difficult to discern. The development of an optimal design is challenging because the level of preheat required for conversion and the specific effect of preheat temperature on the conversion are unclear. An additional complication is that preheating sometimes occurs under conditions where mass transfer is substantially enhanced.

The purpose of the current work is to understand the effect of preheat temperature on the conversion of rich mixtures of methane/air to syngas. In order to examine the specific effect of preheat temperature, we investigated flames stabilized on flat flame burners. In contrast to heat recirculating reactors, flat flame burners allow the control and measurement of preheat temperature and do not have enhanced transport processes that complicate the analysis.

There has been very substantial work on premixed methane/air laminar flames stabilized by various methods including on flat flame burners. Most studies have focused on lean or near-stoichiometric conditions, though there are many published investigations of rich burner-stabilized flames as well. Most of the experiments with rich flames were

studies of detailed flame structure conducted at low-pressure [128]. It is known that kinetics can differ between low and high pressure [128, 129] so studies at high pressure are important to supplement the detailed low-pressure flame investigations. The studies at atmospheric pressure [130-133] have typically focused on flame structure or measurements of flame speed rather than the concentrations of species over a wide range of conditions as is reported in this work. In one exception [131], CO concentrations over a range of equivalence ratios were measured. Previous studies of rich premixed methane/air flames with preheated reactants have not included exhaust product measurements with the exception of NOx [134-138].

In this chapter, experimental measurements and computational predictions of exhaust products are reported for rich methane/air flames with and without preheated reactants. Chemical kinetic and flame models have not been validated extensively for very rich equivalence ratios [50, 139], therefore included are comparisons of various global flame characteristics such as standoff distance, flame temperature, and stable operating range to establish confidence in these models to make adequate predictions. The models are then used to compare to the experimental data from rich flames with and without preheated reactants and also to extend the range of temperature conditions that are investigated.

3.1 Analytical and Numerical Approach

In a laminar flame, such as that on a flat-flame burner, a reaction zone is sustained by heat and mass diffusion from the reaction zone to the unburnt region. The mathematical description of this type of reacting system requires solving the following conservation equations: mass, momentum energy and chemical species. These equations in full 3-D form are shown below.

Overall mass conservation

$$\frac{\partial \rho}{\partial t} + \nabla \cdot (\rho \boldsymbol{v}) = 0 \tag{8}$$

where $\boldsymbol{v} = bulk\ fluid\ velocity$ and $\rho = density$

Species conservation

$$\rho \frac{DY_i}{Dt} = \omega_i - \nabla \cdot (\rho Y_i \boldsymbol{V}_i) \tag{9}$$

where $Y_i = mass\ fraction\ for\ species\ i$, $\omega_i = net\ rate\ of\ formation\ of\ species\ i$, and $\boldsymbol{V}_i = diffusion\ velocity\ of\ species\ i$

Momentum conservation

$$\rho \frac{D\boldsymbol{v}}{Dt} = -\nabla \cdot \boldsymbol{P} + \rho \sum_{i=1}^{N} Y_i \boldsymbol{f}_i \tag{10}$$

where $\boldsymbol{P} = pressure\ tensor$ and $\boldsymbol{f}_i = body\ force\ on\ species\ i$

Energy conservation

$$\rho \frac{De}{Dt} = -\nabla \cdot \boldsymbol{q} - \boldsymbol{P}: (\nabla \boldsymbol{v}) + \rho \sum_{i=1}^{N} Y_i \boldsymbol{f_i} \cdot \boldsymbol{V_i} \tag{11}$$

where $\boldsymbol{q} = heat\ flux\ vector$

Solving this set of equations requires constitutive relations for transport phenomena and a description of the chemistry. The production and destruction of chemical species (ω_i) is described by the following:

Net rate of production of species i

$$\omega_i = \sum_{k}^{K} v_{ik} q_k \tag{12}$$

$$v_{ik} = v''_{ik} - v'_{ik} \tag{13}$$

Where $v'_{ik} = stoichiometric\ coefficient\ for\ species\ i\ in\ LHS\ of\ reaction\ k$ and

$v''_{ik} = stoichiometric\ coefficient\ for\ species\ i\ in\ RHS\ of\ reaction\ k$

The rate of reaction for reaction k is:

$$q_k = k_{f,k} \prod_{i=1}^{I} [X_i]^{v'_{ik}} - k_{b,k} \prod_{i=1}^{I} [X_i]^{v''_{ik}} \tag{14}$$

where $\kappa_{fk} = reaction\ rate\ coefficient\ for\ forward\ reaction\ of\ reaction\ k$ and

$\kappa_{b,k} = reaction\ rate\ coefficient\ for\ backward\ reaction\ of\ reaction\ k$

and the reaction rate coefficients are given by the modified Arrhenius equation as:

$$\kappa = reaction\ rate\ coefficient = AT^b \exp\left(\frac{-E_a}{RT}\right) \tag{15}$$

The rate of production of species i can be found by summing up the contributions from each of the individual reactions involving species i. The sum of all the individual elementary reactions that may contribute to the production or destruction of any species in the system is called a reaction mechanism. If the reaction rate coefficients are also known, then a chemical kinetic model can be obtained. A portion of a chemical kinetic model is shown in the following table:

Table 6. Portion of GRI 3.0 [140]

O+H2<=>H+OH	3.87E+04	2.7	6260
O+HO2<=>OH+O2	2.00E+13	0	0
O+H2O2<=>OH+HO2	9.63E+06	2	4000
O+CH<=>H+CO	5.70E+13	0	0
O+CH2<=>H+HCO	8.00E+13	0	0
O+CH2(S)<=>H2+CO	1.50E+13	0	0
O+CH2(S)<=>H+HCO	1.50E+13	0	0
O+CH3<=>H+CH2O	5.06E+13	0	0
O+CH4<=>OH+CH3	1.02E+09	1.5	8600
O+CO(+M)<=>CO2(+M)	1.80E+10	0	2385

The first column in this table shows the elementary reactions. The second, third and 4th show the values for A, b and E_a for the reaction rate coefficient as described by equation (15) for the given reaction. Given data like that shown in Table 6 for each of the individual reactions in a combustion system, the reaction rate coefficients can be found and then inserted into equation (14), which leads to the rates of production/destruction for each individual species as described by equations (12) and (13)

One dimensional solutions of these equations were obtained for burner-stabilized flames and laminar freely-propagating flames using Cantera [141] with GRI3.0 [140]. The Cantera codes that were used in the present study solved this set of equations use a finite difference scheme to form nonlinear algebraic equations from the partial differential equations. A hybrid Newton/time-stepping algorithm solves the equations and the grids are refined between solutions to add points in regions of high gradients.

For a burner-stabilized flame, the energy equation was solved with an upstream boundary condition of constant temperature and a downstream boundary condition of zero temperature gradient. The species conservation equation was solved with multicomponent transport. The upstream species boundary condition is zero concentration, and the downstream condition was zero gradient. The domain was 1 cm for all simulations.

For a freely-propagating flame, the energy equation was solved with upstream and downstream boundary conditions of zero temperature gradient. The species conservation equation was solved with multicomponent transport. The upstream and downstream species boundary conditions were zero gradient. The domain was 30 cm. The details of the burner-stabilized flame model and the freely-propagating flame model can be found in the Cantera documentation [141].

In addition to the detailed computational models, the analytical solution of Law [13] was used to compute the standoff distance as a function of operating conditions and to understand the basic behavior of burner-stabilized flames. Law's analytical solution to the problem of the burner-stabilized flame begins with governing equations (8 through

15) above. Full chemical kinetic models are not always used for combustion modeling; a global, semiglobal, or other reduced mechanism might be used because analytical solutions are not possible when using full kinetic models. In these reduced cases, the reaction rate coefficients are often for observed reaction rates rather than for the reaction rate of a realistic molecular process such as an elementary reaction. The first simplification that Law used in his model was reducing the reaction mechanism to a 1-step mechanism [142]:

$$v_f[F] + v_o[O] \rightarrow [P_1] + [P_2] \tag{16}$$

The governing equations are further simplified into a 1-dimensional, isobaric and adiabatic (except for heat loss to the burner) system. The oxidation reaction is considered to be irreversible, and the equations are nondimensionalized. In the next step, the problem is solved for steady state conditions and large activation energy, which leads to a singular perturbation problem. The solution to this perturbation problem yields the following nondimensional equations for flame temperature, standoff distance and heat loss:

$$\tilde{f}^2 = \left(\frac{\tilde{T}_f}{\tilde{T}_{ad}}\right)^4 exp\left[-\tilde{T}_a\left(\frac{1}{\tilde{T}_f} - \frac{1}{\tilde{T}_{ad}}\right)\right] \tag{17}$$

$$\tilde{f}\left[\tilde{T}_{ad} + (\tilde{T}_s - \tilde{T}_u)\right] - \tilde{L}_s = \tilde{f}\tilde{T}_f \tag{18}$$

$$\tilde{L}_s = \frac{\tilde{f}(\tilde{T}_f - \tilde{T}_s)}{e^{\tilde{f}\tilde{x}_f} - 1} \tag{19}$$

where the nondimensonal variables for mass flux, temperature, standoff distance and heat loss are given by:

$$\tilde{f} = \frac{f}{f^{\circ}}, \tilde{T} = \frac{T}{T_{ad} - T_u}, \tilde{x} = \frac{x f^{\circ}}{\rho D}, \tilde{L}_s = \frac{d\tilde{T}}{d\tilde{x}}$$

and f is the mass flux, f° is the laminar burning flux, T is the temperature, T_{ad} is the adiabatic flame temperature based on the unburned reactant temperature, T_u, x is the standoff distance, ρ is the density, and D is the mass diffusion coefficient.

To obtain dimensional values for the quantities of interest, the following dimensional versions of equations (17), (18) and (19) are used:

$$\left(\frac{f}{f^{\circ}}\right)^2 = \left(\frac{T_f}{T_{ad}}\right)^4 exp\left[-T_a\left(\frac{1}{T_f} - \frac{1}{T_{ad}}\right)\right] \tag{20}$$

$$\rho D \frac{dT}{dx} = f\left(T_{ad} + T_s - T_u - T_f\right) \tag{21}$$

$$e^{\frac{fx}{\rho D}} - 1 = \frac{f(T_f - T_s)}{\rho D \frac{dT}{dx}} \tag{22}$$

To obtain dimensional values for the quantities of interest, laminar burning fluxes and adiabatic flame temperatures obtained from Cantera solutions were also used. Two other parameters, the activation temperature, T_a, and the product, ρD, required dimensional values. Both of these parameters were set by calibration to experimental data. The activation temperature was set to 15098 K such that the flame temperature given by the analytical model matched the flame temperature, 1850 K, for methane/air at φ = 1.2, V = 11 cm/s as reported by [132]. Setting ρD = 5.5E-5 yielded the best fit to our experimental data for standoff distance at φ = 1.25. This value of ρD corresponded to the mass average value of ρD for a mixture of methane and air with φ = 1.25 at approximately 1025 K.

Using Law's solution, first the laminar flame speed, adiabatic flame temperature and activation temperature were used along with the mass flux to determine the flame temperature. The flame temperature, the adiabatic flame temperature, the surface temperature (which equals the unburned gas temperature), the density-diffusivity product and the mass flux were then used to determine a value for the temperature gradient at the surface. This temperature gradient was then used to determine the standoff distance in equation (22).

Equilibrium calculations for varying φ and initial reactant temperature were completed to compare with data from combustion processes that approach equilibrium in the limit of infinitely fast kinetics and adiabatic conditions [39, 59]. In these calculations, the initial temperature and φ were selected and enthalpy and pressure were held constant for equilibration. The equilibrium calculations provide insight into the thermodynamic properties of the mixtures, and equilibrium has been assumed to represent the species concentrations in the post-flame region of burner-stabilized flames [132, 143]. These calculations were performed in Cantera with thermodynamic data from GRI3.0. Solid carbon formation was included in all of the presented equilibrium calculations. These calculations show that no solid carbon is formed for methane/air mixtures until φ exceeds approximately 3.3.

The models are used to predict flame standoff distance in terms of the location of maximum CH concentration, flame temperature, stability limits and species yields. Experimentally, we define a stability limit as φ, V pair where if either is increased the flame ceases to be flat as described in detail in section 3.2.4. For the burner-stabilized

flame model, the limit is defined as the maximum V for a given φ that produces a converged solution. An additional limit comparison is based on the laminar flame speed of a mixture where the predicted laminar flame speeds are compared to the limiting velocities determined experimentally at each φ. Lastly, the models and experiments were compared in terms of exhaust species yields. A summary of the conditions for comparison is shown in Table 7.

Table 7. Conditions for comparing models and experiment. In each row the quantity of interest for comparison is listed for operating condition(s) given in the far left column.

	Measured Valued	**Calculated Value Burner Stabilized Flame**	**Calculated Value Free Flame**
Given φ, V	Standoff distance	Standoff distance	NA
Given φ, V	Flame temperature from [132]	Flame temperature	NA
Given φ	Maximum V at which flat flame was observed	Maximum V at which solution converged	Laminar flame speed for given φ
Given V	Maximum φ at which flat flame was observed	Maximum φ at which solution converged	φ at which laminar flame speed equals given V
Given φ, V	Species yields	Species yields	Species yield if laminar flame speed matches V at given φ

3.2 Experimental Approach

3.2.1 Experimental Apparatus

Experiments were performed with two different burners. Experiments without preheat were conducted on a water-cooled McKenna burner (Holthius & Associates),

which has a sintered porous bronze plate as the burner-surface. This burner is shown in Figure 43. The water flow was ~13 [g/s] for all experiments, efficiently cooling the burner surface. Because of the high thermal conductivity of the burner surface and the high flow rate of the cooling water, the temperature of the burner surface was constant at the water temperature during the experiments. The McKenna burner was used to establish a baseline with which to compare the experiments with preheated reactants and to determine the accuracy of the models since the McKenna burner is well-established for this comparison.

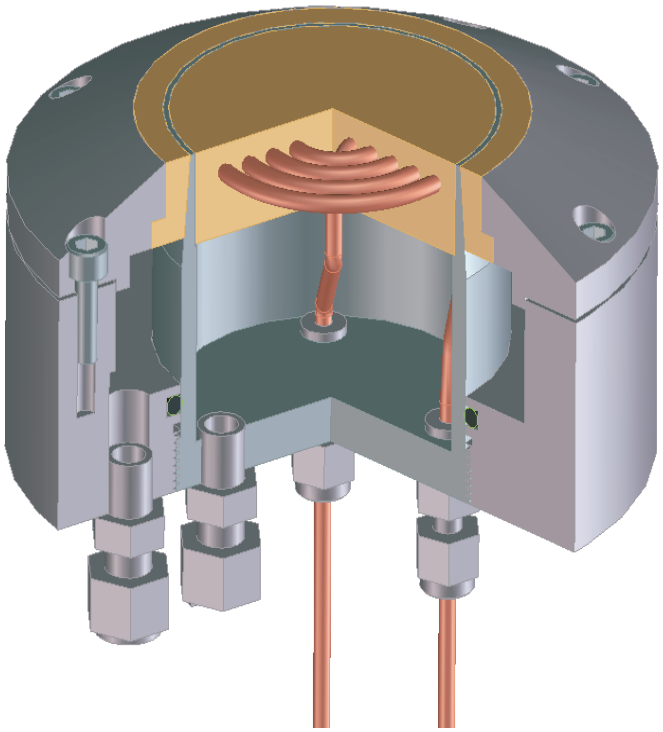

Figure 43. Graphic of the McKenna burner [144]

We constructed a second burner, similar in design and size to those used in other studies of flat flames [138, 145, 146], for experiments with preheated reactants. This burner was a square channel mullite ceramic matrix with 1.34 mm channels and 0.35 mm walls. The matrix was 51 mm long and 55 mm in diameter. A diagram of this burner is shown in Figure 44.

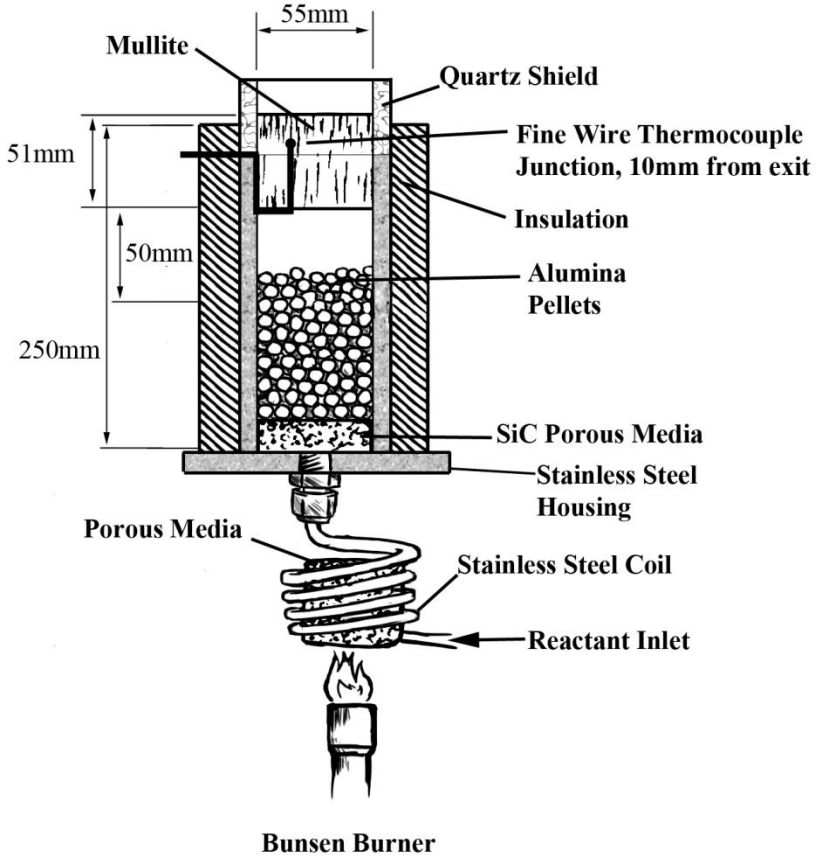

Figure 44. Diagram of ceramic burner

In all experiments, a quartz tube of 55 mm ID was used to shield the flames from external air. The quartz tubes were used instead of inert gas shielding because the exhaust gas samples were extracted from the center of the flame, where the quartz tube boundary had no effect. We found no observable difference in any measurements by running experiments with and without the quartz tube as a shield.

The flows were controlled with calibrated Hastings mass flow controllers. The air was compressed, dry laboratory air, and the methane was CP grade from Air Liquide. Preheating was accomplished by running the premixed methane/air through a helical coil of stainless steel heated by a Bunsen-burner before entering the reactor housing. The temperature of the reactants was monitored by a fine wire K-type thermocouple placed within the ceramic plug upstream of the preheat zone of a burner-stabilized flame. It was confirmed that fuel breakdown did not occur due to preheating before reaching the flame by sampling the gases after heating but without a flame.

3.2.2 CHEMILUMINESCENCE MEASUREMENT AND STANDOFF DISTANCE

In a hydrocarbon flame, fuel breakdown occurs and various intermediate species are created. In some cases the intermediate species are formed in excited states. The CH radical often is created in a higher electronic energy state than its ground electronic state, $^2\pi$. Though CH can be created in multiple high energy states the most common is $^2\Delta$. This excited CH, defined as CH*, relaxes from $^2\pi$ to $^2\Delta$ (with no change in vibrational energy levels) and releases a photon with an energy equal to the difference between the

energies of those two states. In this case, a photon is released with a wavelength of 431.42 nm [147]. Hai Wang of USC [148] suggested the following reaction mechanism for CH and CH*:

Table 8. Chemical kinetic mechanism for excited CH radical ([148])

	Reaction	A	b	Ea
1	C2H + O = CO + CH*	2.50E+12	0	0
2	C2H + O2 = CO2 + CH*	3.20E+11	0	1600
3	C2 + H2 = C2H + H	4.00E+05	2.4	1000
4	CH + CH = C2 + H2	5.00E+12	0	0
5	C + C + M = C2 + M	3.00E+14	0	1000.0
6	C + CH = C2 + H	5.00E+13	0	0
7	O + C2 = C + CO	5.00E+13	0	0
8	C2 + O2 = CO + CO	9.00E+12	0	980
9	C2 + OH = CO + CH*	1.11E+13	0	0
10	C + H + M = CH* + M	3.63E+13	0	0
11	CH* = CH	1.86E+06	0	0
12	CH* + N2 = CH + N2	3.03E+02	3.4	-381
13	CH* + O2 = CH + O2	2.48E+06	2.14	-1720
14	CH* + H2O = CH + H2O	5.30E+13	0	0
15	CH* + H2 = CH + H2	1.47E+14	0	1361
16	CH* + CO2 = CH + CO2	2.41E-01	4.3	1694.0
17	CH* + CO = CH + CO	2.44E+12	0.5	0
18	CH* + CH4 = CH + CH4	1.73E+13	0	167

This mechanism is used to determine the rate constant from the modified Arrhenius equation. As can be seen from the mechanism, there are 4 reactions that produce an excited CH molecule, three of them with C_2 species as reactants (reactions 1, 2 and 9) and one three-body reaction (reaction 10). When an excited CH is created it has many pathways to de-excite including spontaneous de-excitation (reaction 11). De-

excitation occurs quickly (typically between 10^{-6} and 10^{-8} seconds [147]) so CH* and CH should be spatially nearly coincident. This spatial coincidence is predicted by numerical simulation as described by Figure 45, which shows the normalized concentrations of CH and CH* as a function of distance from the burner surface for a simulation of a flame with $\varphi = 1.1$ and inlet velocity = 5 cm/s.

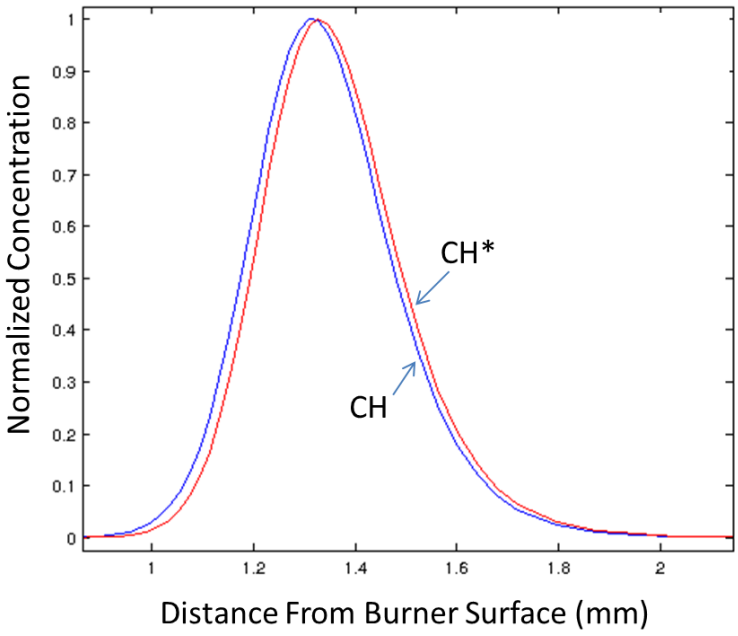

Figure 45. CH/CH* concentration vs distance from burner surface

As noted in the literature [149], CH and CH* are present in a thin region of a premixed flame and is nearly coincident with location of the reaction zone. Consequently, the standoff distance can be determined by measuring the distance between the burner surface and the maximum CH* concentration. A system built to measure the spatial location and intensity of CH* chemiluminescence, consisted of a digital webcam

(Logitech™ C910 HD), a vertical traverse with a micrometer head, and a LabVIEW™ control system, along with a 430±10 nm optical bandpass filter. The flow system and chemiluminescence measurement system is shown in Figure 46.

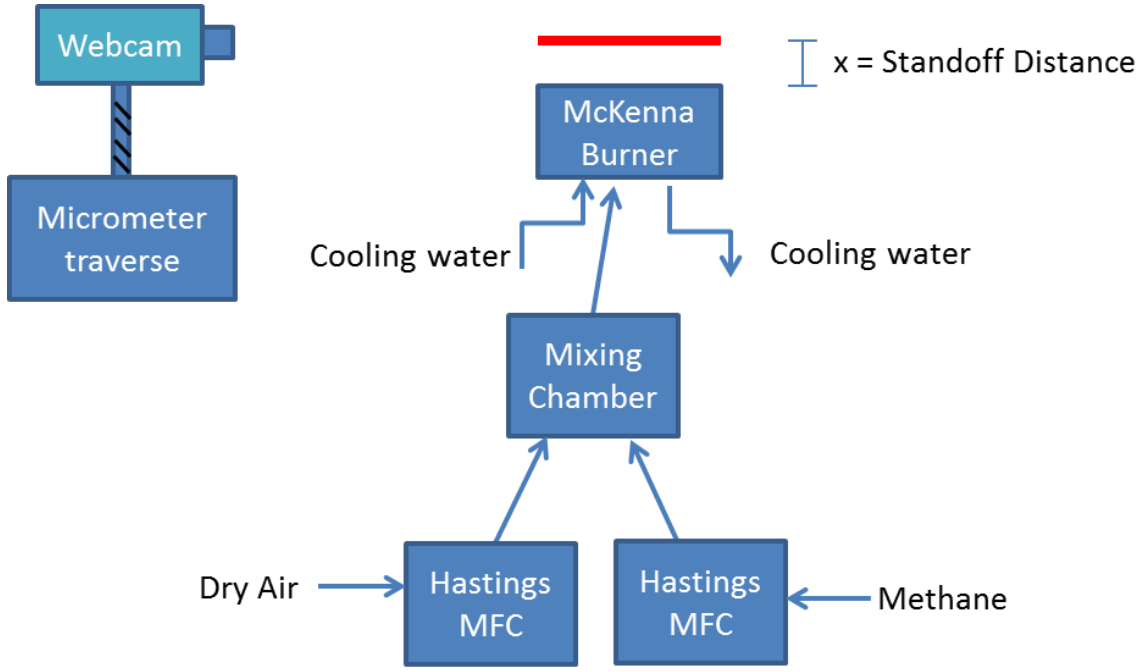

Figure 46. Diagram of flow system and chemiluminescence measurement system for flat flame burner

As described by Law [13], when the mass flux and mixture properties (φ, unburned gas temperature) are specified in equation (20), the flame temperature is determined and is independent from the surface temperature and standoff distance. Since the reaction zone is confined to a thin region at or very near the flame temperature, this flame temperature can be considered the controlling temperature for the chemical reactions and product species. Therefore the product species distributions for the ceramic

burner, which does not have a controlled surface temperature, the McKenna burner and the burner-stabilized flame model may be directly compared when the mass flux and mixture properties are identical. In addition they may be compared in terms of limit conditions because under limit conditions there is no thermal interaction between the flame and the burner surface.

The standoff distances are not compared to the modeling results for preheated reactants because the standoff distance is a function of the surface temperature, which is not controlled in these experiments using the ceramic burner. In contrast to the McKenna burner where the surface temperature is effectively controlled by the temperature of the cooling fluid, in the ceramic burner the surface temperature is a function of operating conditions. Stabilization is achieved through heat loss to the environment primarily by radiation from the burner surface. The required heat loss and burner surface temperature, then, determine the standoff distance.

3.2.3 SPECIES MEASUREMENT

Measurements of species concentrations in the exhaust were taken with a Varian (Agilent) CP-4900 gas chromatograph, which measures H_2, CO, nitrogen (N_2), carbon dioxide (CO_2), methane (CH_4), ethylene (C_2H_4), acetylene (C_2H_2) and select higher hydrocarbons. No compounds greater than C_2 were detected in any experiments. The sources of uncertainty were in the flow rates of methane and air, the calibration standards, and the gas chromatograph calibration. Uncertainties in species measurements were

calculated using a Student t distribution, and uncertainties for calculations were based on sequential perturbation (see appendix A).

The species results are reported in terms of dry species concentrations. The GC does not report the concentration of water in the products, and besides solid carbon and higher hydrocarbons, water is the only species that is not reported by the GC. Under conditions when solid carbon and large hydrocarbons are not expected to form, the dry mole fractions can be found by assuming that the difference between the concentrations (reported in mole %) and 100% is the concentration of water. Each of the reported species concentrations is then converted to a dry fraction by dividing the concentration by the sum of the concentrations reported by the GC.

The ideal way to measure the species at a specific time and location would be to freeze the reactions and count the number of moles of each species in a very small volume without disturbing the fields of concentration, temperature or velocity. The best approximation to this ideality when using a GC is to sample the gases through a quartz (inert) tube that is very small and efficiently cooled. Cooling the gases reduces the rate of reaction to a point where they are "frozen" so that the gas analyzed by the GC has the same molecular composition as it had at the point of sampling. The cooling of the gases within the tube, however, presents a problem because the temperature and velocity field cannot be significantly disturbed by the sample probe, especially if it is cold. In order to not disturb the fields, the sample probe was designed with a very thin tip (1 mm OD), and cooling took place approximately 1 cm from the tip (Figure 47). After the gases passed

through the cooling section of the sample probe, they entered a 0.75 m long piece of inert (Restek Silcosteel) tubing, and then entered the GC.

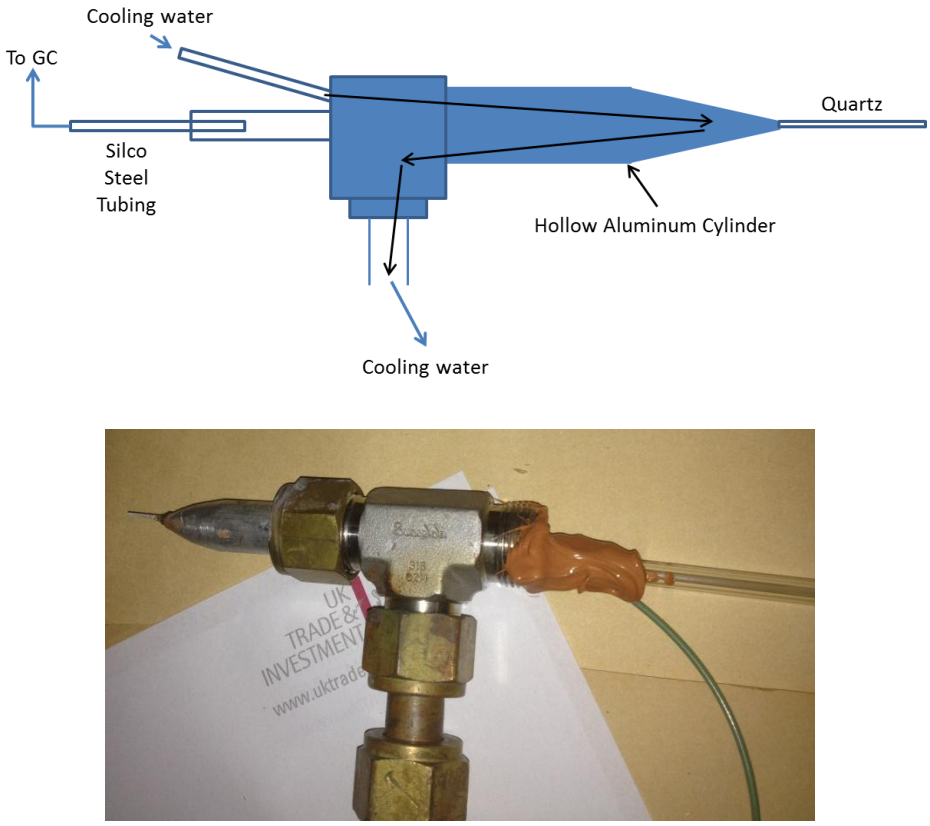

Figure 47. Diagram and image of water-cooled probe used for sampling gases in flat flame experiments

3.2.4 DETERMINATION OF FLAME FLATNESS

At blowoff, a flame loses its flatness, and at flashback, it is not visible. Since we wanted to compare our experimental results to one-dimensional computational models of burner-stabilized flames, it was important to establish a criterion for a "flat" flame that was also not in a flashback condition. In addition, the stability limit is defined as the φ,

V beyond which a flame would not be flat if either parameter was increased. These limiting conditions were found by perturbing φ and V while monitoring the flame flatness though CH* chemiluminescence imaging. Representative grayscale CH* chemiliuminescence images of one flame that is not flat and one flame that is flat are shown in Figure 48.

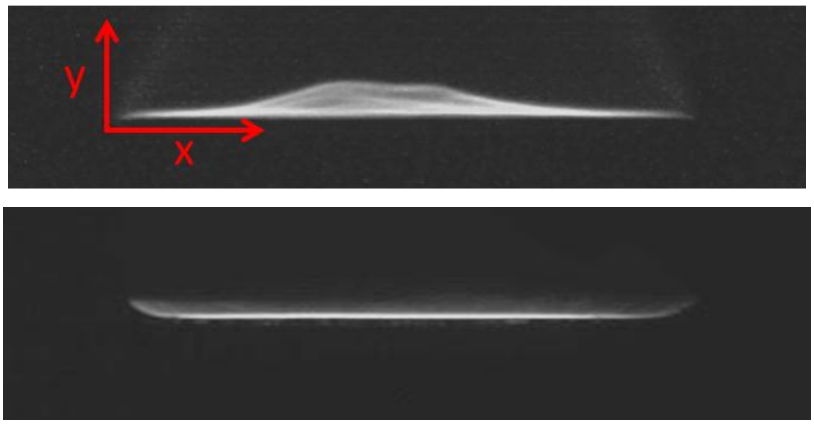

Figure 48. Pictorial diagrams describing the flatness metric used in this paper on a highly non-flat flame and a flat one.

The flame flatness was quantified by finding the variance of the full width (in y direction) at half maximum (FWHM) grayscale intensity along the x axis. By this definition, a perfectly flat flame has zero FWHM intensity variance. To find the FWHM intensity variance, the grayscale data was analyzed by a Matlab program using the following psuedocode with input being a 3D matrix of intensity, pixel number in x direction and pixel number in y direction;

for each pixel number in x

1. *find maximum intensity amongst all y pixels*
2. *find y pixel on each side of maximum that has intensity value equal to ½ the maximum intensity*
3. *find distance between two pixels found in step 2. Store this value as value of FWHM for given x pixel*

end for loop

find variance of all FWHM values

To determine the experimental limiting conditions (the conditions where increases in φ or V would produce a nonflat flame), velocity was held constant while φ was adjusted by increments of 0.005 for five different values of φ surrounding a suspected limit and images were taken to determine the FWHM variance for each condition. A limit value of φ was defined as a tested φ limit where the FWHM variance found in the set of five conditions at least doubled. A plot of FWHM variance vs. equivalence ratio (Figure 49) for a given inlet velocity (19.88 cm/s) describes how such a limit was found:

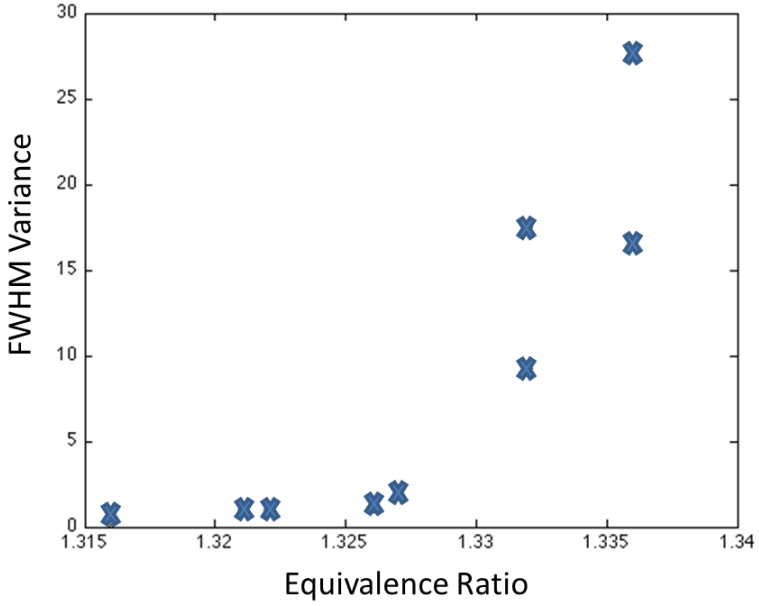

Figure 49. Variance of FWHM intensity of CH* chemiluminescence vs. equivalence ratio (V = 19.88 cm/s)

Figure 49 shows a clear, rapid increase in FWHM variance as the equivalence ratio increases from 1.33. From this figure one limit condition, V = 19.88 cm/s and phi = 1.33, was determined. From figures like these, we determined the limit conditions in the entire equivalence ratio/inlet velocity parameter space. Flames with operating conditions within the bounds of the limiting conditions were flat, and in this paper we only report measurements from flat flames.

3.3 Results and Discussion

Previous research on the conversion of rich fuel/air mixtures has shown that optimal production of syngas may occur beyond the conventional flammability limits.

Optimization, however, of reactor performance remains challenging because the level of preheat necessary is unclear. In the following sections, we discuss experimental, computational, and analytical results which provide some insight into the importance of preheating for conversion of rich methane/air mixtures.

3.3.1 Comparison of Experimental and Numerical Modeling Data

Since combustion models are not extensively compared to experimental data in the rich regime [139], we present comparisons of standoff distance, stability, and temperature in order to gain confidence in the predictions of the models, which are subsequently used to investigate a broader range of conditions than was investigated experimentally. In this section the computational models were compared to the results from experiments on the McKenna burner and the analytical model under non-preheated conditions.

Standoff distance

For a flat flame to stabilize on the surface of a burner, the burning velocity of the flame must match the inlet velocity. Matching of these velocities occurs because heat loss to the burner decreases the flame temperature and therefore decreases the burning velocity as described in detail in the literature [13, 150, 151]. The standoff distance, which we use for comparison between the model and experiment, is a fundamental

characteristic of burner-stabilized flames and has been used by other researchers for such comparison [152, 153].

Experimental, computational, and analytical results show that the flame standoff distance decreases with increasing inlet velocity, as shown in Figure 50. In the range of inlet velocities tested, the model and experiment agreed very well in both trend and magnitude, and the analytical model fits the data very well. This trend has been observed by other researchers and is explained in detail in the literature [137, 151].

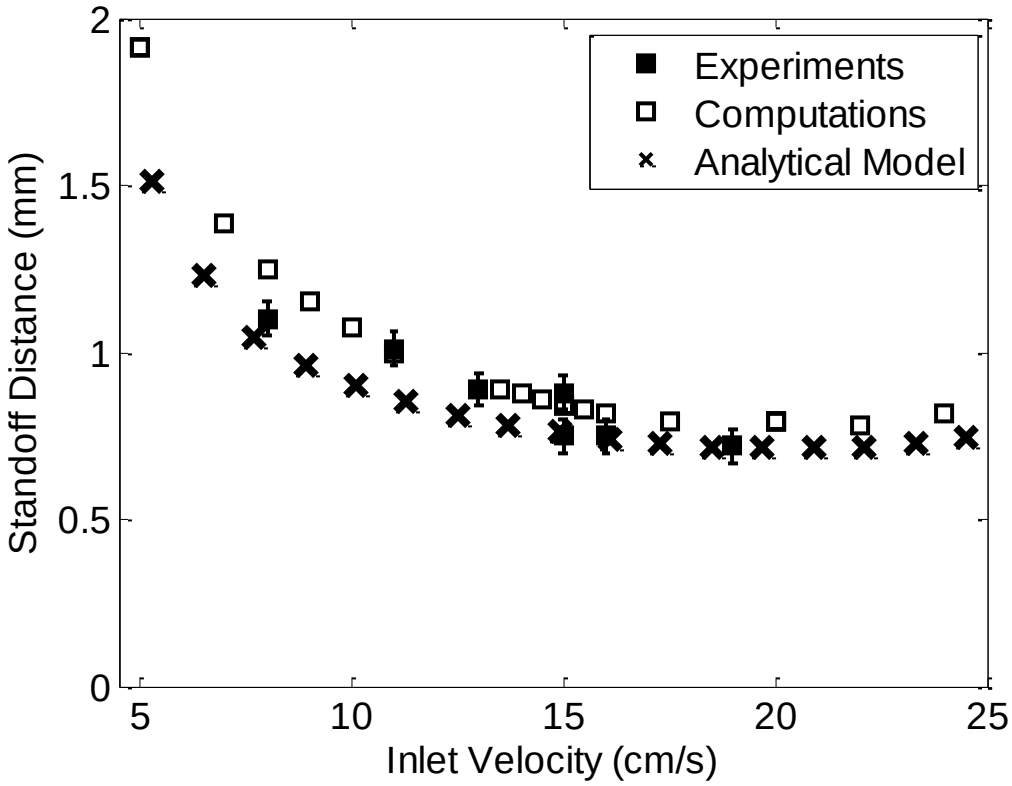

Figure 50. Standoff distance vs. inlet velocity at equivalence ratio = 1.25 ± 0.05

We also compared the modeling predictions with the experimental measurements of standoff distance as a function of φ while V was held constant at 15 cm/s (Figure 51). Again, the agreement between the experiments, the burner-stabilized flame model and the analytical model is very good. The same trend was observed by Furguson and Keck [150], and their standoff distance measurements were within about 1 mm of those reported here even though the reactant temperature in their experiments was 50 K greater than the temperature of the reactants in our experiments.

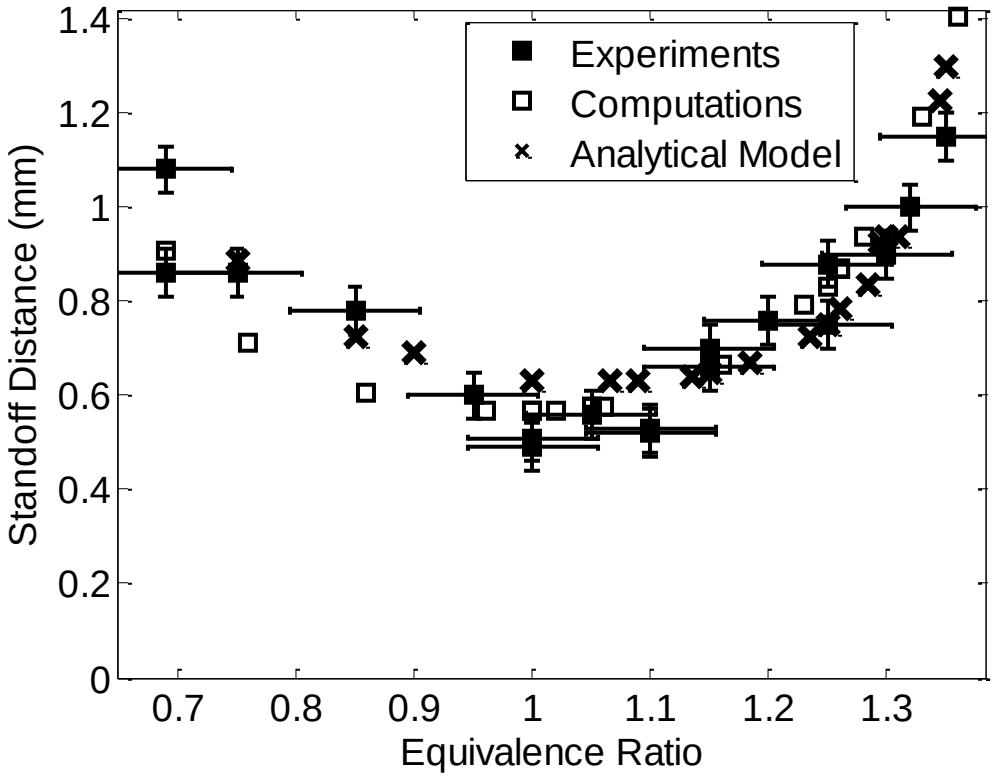

Figure 51.Standoff distance vs equivalence ratio at inlet velocity = 15 ± 0.2 cm/s

The standoff distance is one of the fundamental global parameters that characterize burner-stabilized flames. Over a range of V and φ, the burner-stabilized flame model was a very good predictor of standoff distance. Law's analytical model also fits the experimental and modeling data very well in trend and in magnitude except for a slight overprediction near stoichiometric.

Flame Temperature

Simulations of burner-stabilized flames are often conducted using experimental temperature profiles as inputs rather than solving the energy equation for the temperature profile. In our case, the energy equation was solved and the temperature profile was a simulation output. The model results for flame temperature were compared to experimental data from published CARS measurements [132].

Figure 52 and Figure 53 show experimental temperature data based on CARS measurements by [132] and computational data along with the adiabatic flame temperature for reference. As is clear from the figures, heat loss to the burner makes these flames have sub-adiabatic temperatures at all conditions. Significantly, the results from Cantera matched the experimental results well in trend at all tested conditions though the experimental data were slightly higher than the computational data. This difference can be explained by the radiative heat loss of about 10K per mm [136]

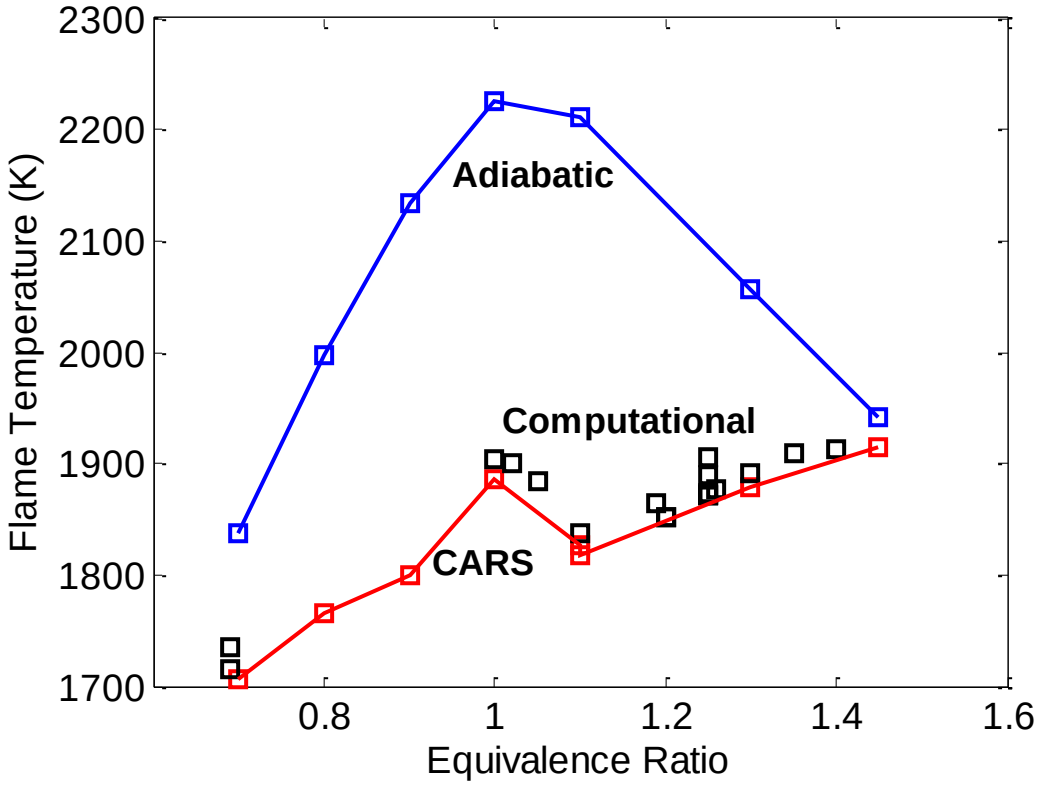

Figure 52. Flame temperature vs equivalence ratio (V = 11 cm/s)

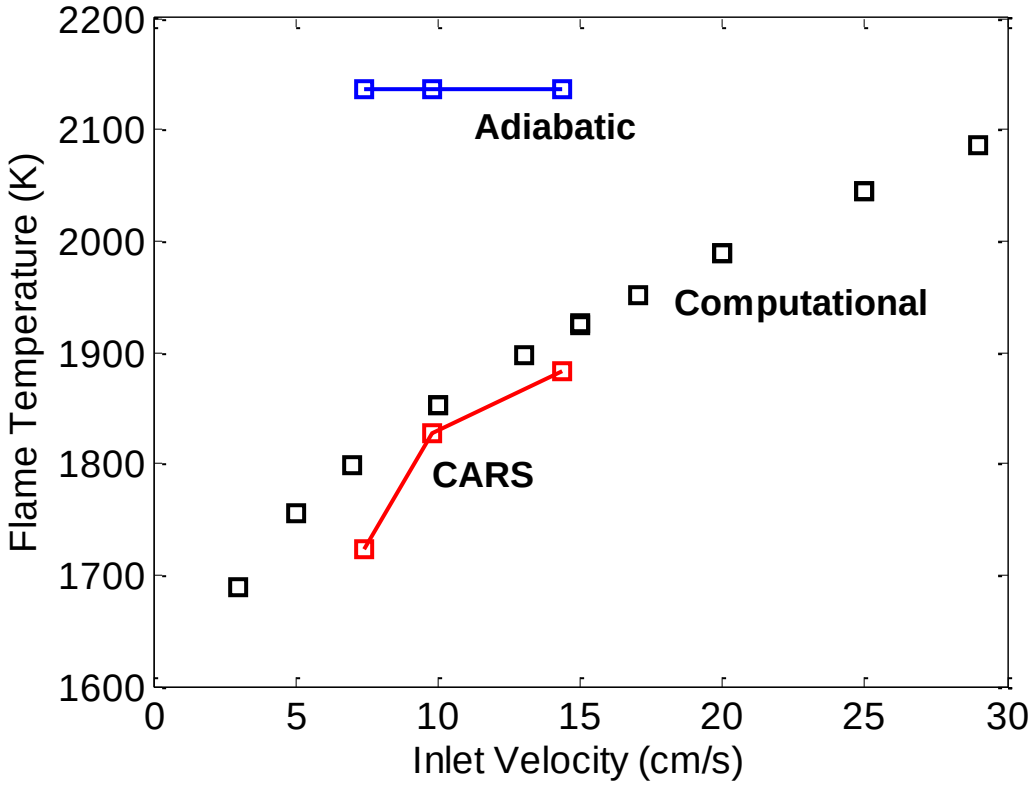

Figure 53. Flame temperature vs inlet velocity (φ = 1.2)

Limit conditions

We experimentally determined the limiting φ, V where a flat flame was stabilized as explained in section 3.2.4. These values are compared to the calculated laminar flame speeds in Figure 54. Also shown are the limiting φ, V pairs where converged solutions to the burner-stabilized flame model were found. On the rich side, where our focus is, the match between the experiments and computations is very good, except at the highest φ. On the lean side the trend is correct, but the magnitudes of the laminar flame speeds are

somewhat higher than the limiting inlet velocities found in the experiments and the burner-stabilized flame model. In the experiments the limiting velocities disagreed with the laminar flame speeds at near stoichiometric conditions. The burner-stabilized flame model predicted these near-stoichiometric limits as well; simulations of burner-stabilized flames with φ near stoichiometric failed to converge with inlet velocities close to the laminar flame speed.

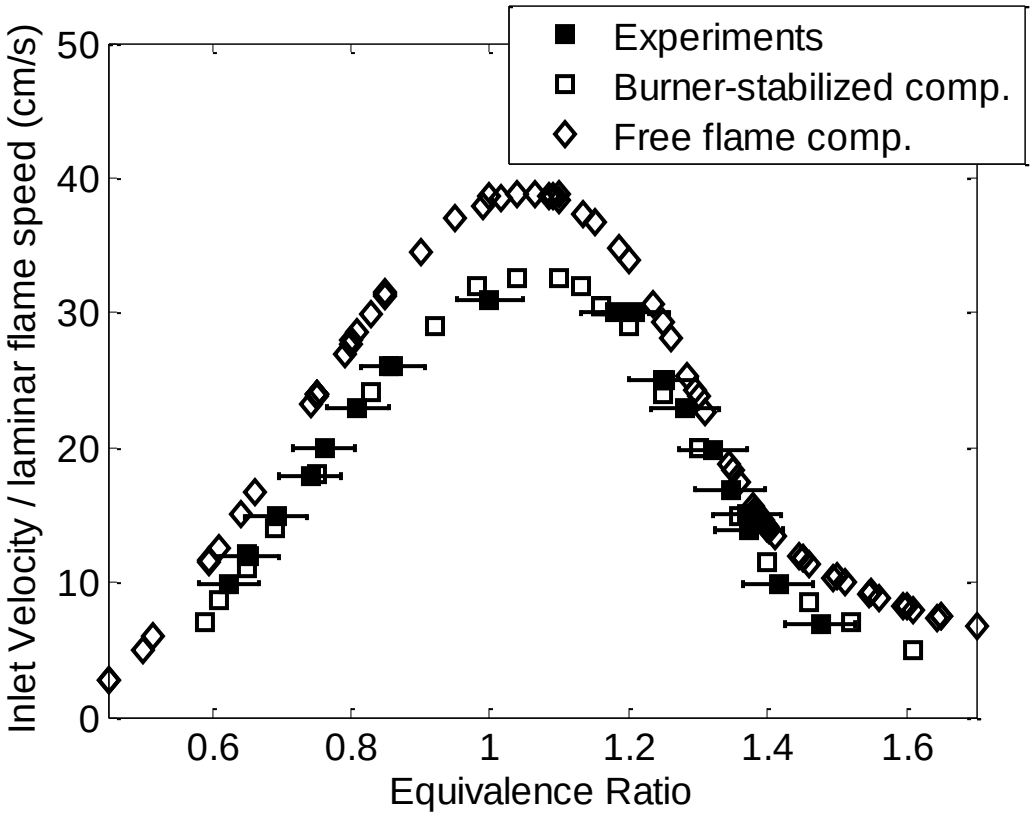

Figure 54. Limit inlet velocity and laminar flame speed vs equivalence ratio

These comparisons indicate that the computational model predicts flame standoff distance and temperature across a broad range of φ. In addition, the limits of operating

conditions corresponded well with the laminar flame speed determined from freely-propagating flame simulations. These comparisons establish confidence that the models can be used to predict the behavior of burner-stabilized flames especially at rich conditions.

3.3.2 Effect of Preheating on the Conversion of Rich Mixtures to Syngas

To provide a baseline for comparison to the results for flames with preheated reactants, experiments and simulations were conducted with reactants at standard conditions. These data are important also to complete the comparison between the models and experiments and to establish the similarity between the two burners used experimentally. Then data are presented for experiments and modeling of burner-stabilized flames with preheated reactants to show the effect of preheat on syngas production.

Comparison of McKenna and ceramic burner at baseline (unheated) conditions

As discussed in previously, the McKenna burner cannot withstand the preheat temperatures of interest in this study so we constructed a ceramic burner for this purpose. In Figure 55, the concentrations of H_2, CO and CO_2 are shown for experiments with both burners as well as predictions from burner-stabilized flame simulations, freely-propagating flame simulations, and equilibrium calculations. The error bars shown in

Figure 55 are the maximum uncertainties in the presented experimental data. The average uncertainty in the concentration measurements are as follows: ±0.29 for [H_2], ±0.32 for [CO], ±0.4 for [CO_2].

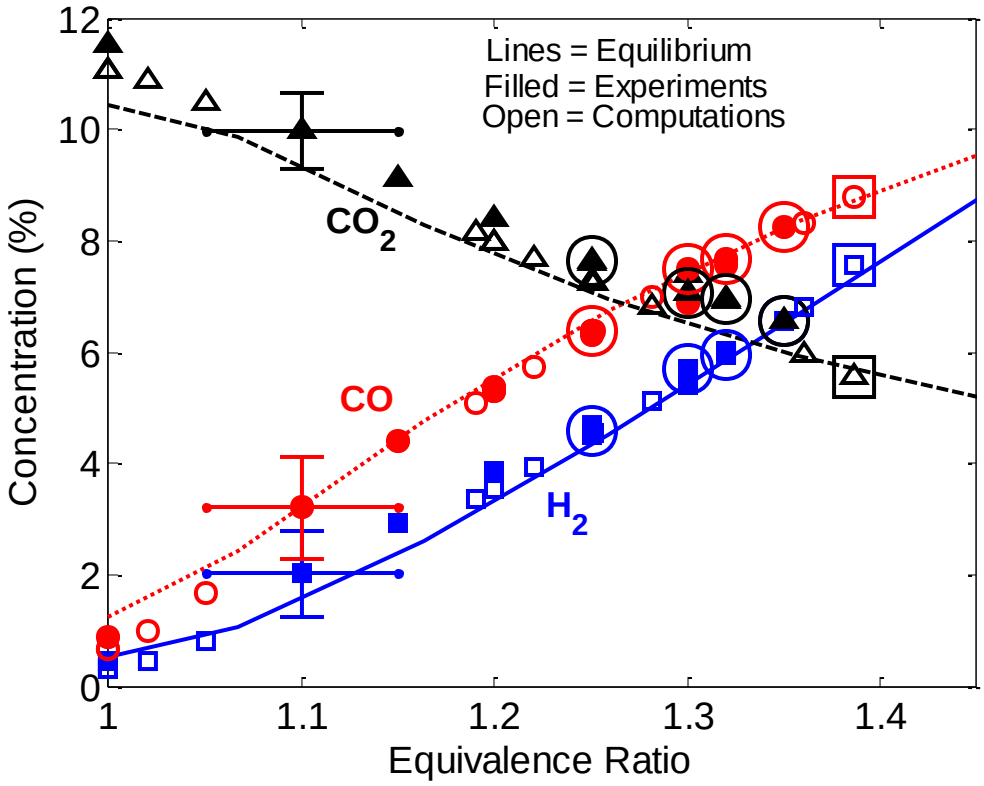

Figure 55. Concentration vs. equivalence ratio at inlet velocity = 15 ± 0.2 cm/s (circled points indicate ceramic burner data, all computational data are from burner-stabilized flame model except boxed points indicating free flame computations at φ = 1.38)

As Figure 55 shows, the experimental data from both reactors and the models match in concentration extremely well over the tested range of φ. The ceramic burner has a flashback limit, so data are presented for φ from 1.25 to 1.35 where flat flames were stabilized on the surface of the burner. At stoichiometric conditions, very nearly all of the

carbon in methane is converted to CO_2 and little CO is observed. As φ increases, the amount of carbon converted to CO_2 decreases as the amount converted to CO increases. Negligible amounts of small hydrocarbons were measured by the GC. Therefore, as φ is increased, more hydrogen in methane is converted to H_2 at the expense of H_2O. Both computations and experiments showed very nearly equilibrium levels of CO_2, CO and H_2. Lastly, the concentration of syngas increases monotonically with φ suggesting that even richer φ might improve syngas production if stable operation could be accomplished.

Concentrations for CO, CO_2 and H_2 are almost identical to the equilibrium values and are consistent with the trend of species concentrations seen in the burner-stabilized flame experiments and models. In the experiments if φ is increased, the standoff distance increases, but the flame remains flat (burner-stabilized) until the $\varphi \approx 1.32$ on the McKenna burner and $\varphi \approx 1.35$ on the ceramic burner. When φ is increased further, the flame becomes unstable because the laminar flame speed of the mixture approaches V; under this condition the flame can be considered nearly adiabatic, and the predictions of the freely-propagating flame model become appropriate for comparison. At 300 K, a free flame of methane and air has a laminar flame speed of 15 cm/s when $\varphi \approx 1.38$.

We measured species concentrations while varying V and holding φ constant at 1.25 to determine if the two burners and the model results were consistent across a range of V. These data are shown in Figure 56.

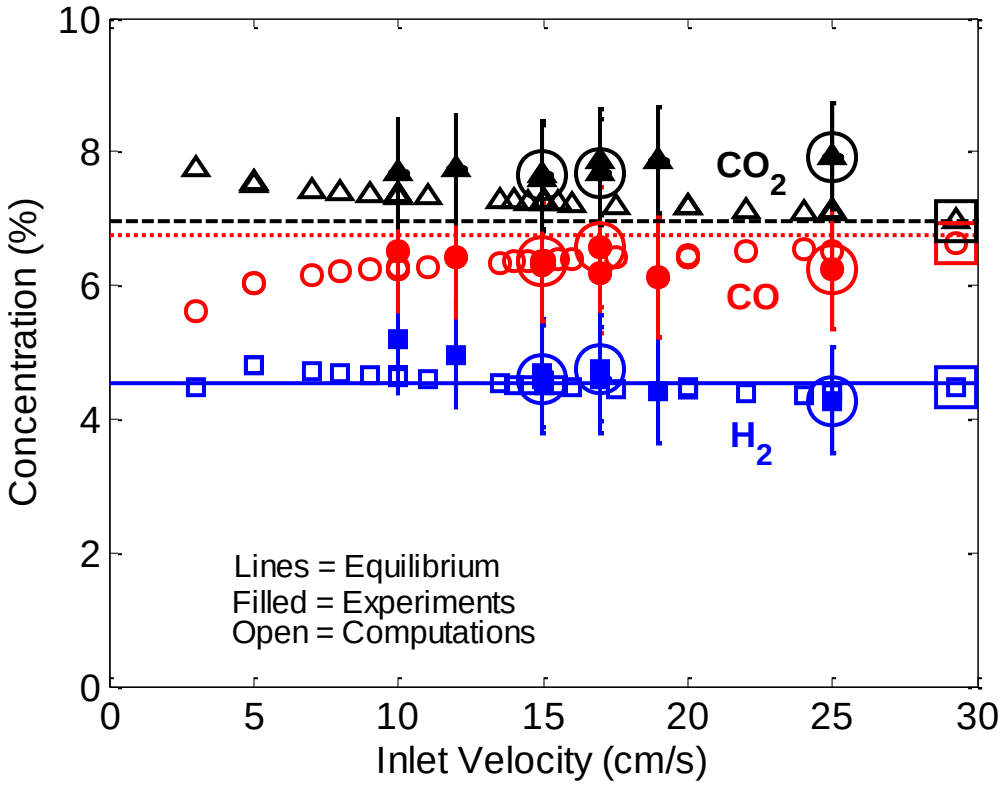

Figure 56. Concentration vs. inlet velocity at equivalence ratio = 1.25 ± 0.05 (circled points indicate ceramic burner data, all computational data are from burner-stabilized flame model except boxed points indicating free flame computations at V = 29 cm/s)

The computations predict almost no change in species concentration as a function of V in the range of inlet velocities that were tested experimentally. However, at very low inlet velocities the computations predict that more methane is converted to CO_2 at the expense of CO. The experiments show almost no change in concentration for both the McKenna burner and the ceramic burner. The equivalence ratio strongly affects species concentrations, as shown in Figure 55, and there is uncertainty in φ for all experimental data points when V is varied and φ is held constant. The uncertainties in species

concentration due to uncertainty in φ around φ = 1.25 are estimated as follows: ±0.8 for [H_2], ±0.9 for [CO] and ±0.8 [CO_2]. Because of these uncertainties, which are shown in Fig. 7 because they are larger than the raw measurement uncertainty, no variation in the experimental data as a function of inlet velocity is implied in Figure 56. Further explanation of this method for determining uncertainty is given in Appendix A.

The major conclusions from the previously presented data are that the ceramic burner and the McKenna burner produce nearly identical species concentrations across a range of φ and V. In addition, the burner-stabilized flame model and the free flame model were very accurate in predictions of standoff distance, limit conditions and [CO], [CO_2] and [H_2] at all φ and V tested.

Results from experiments and modeling with preheated reactants

Using the ceramic burner, we performed experiments with preheated reactants. Figure 57 shows concentration as a function of φ with V held constant at 25 cm/s and the reactants preheated to 617 K. Under unheated conditions on the ceramic burner for V = 25 cm/s the limit φ is 1.26.

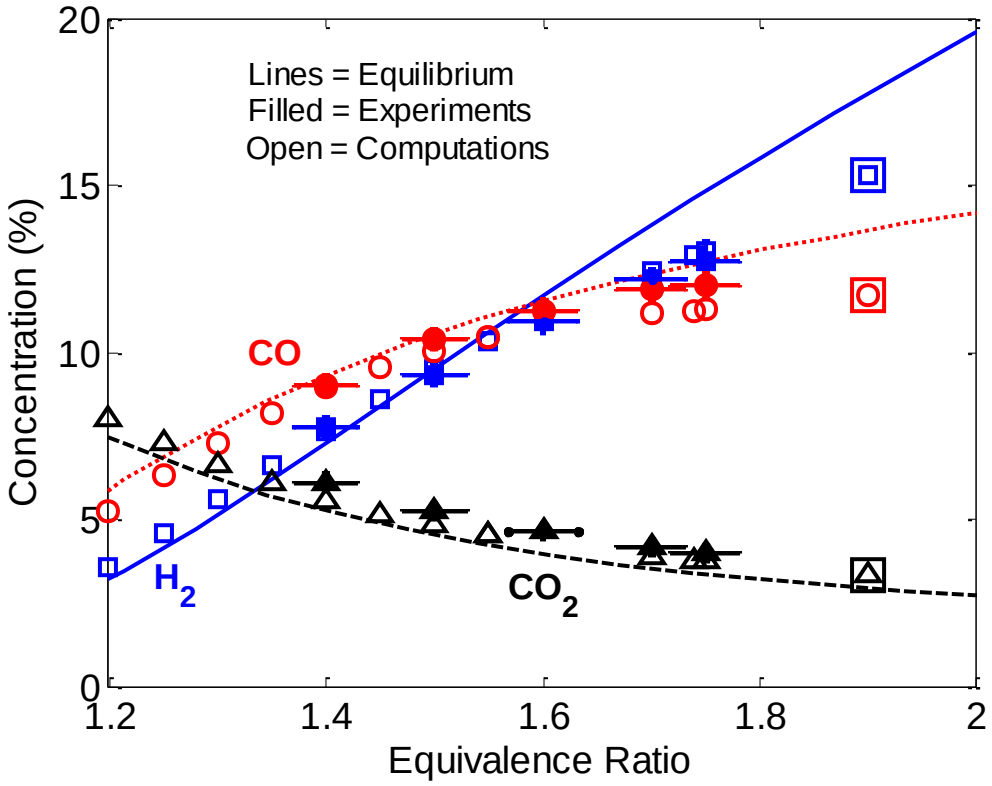

Figure 57. Concentration vs. equivalence ratio at inlet velocity = 25 ± 0.05 cm/s and reactant temperature = 617 ± 10 K (all computational data are from burner-stabilized flame model except boxed points indicating free flame computations at φ = 1.9, uncertainty in temperature is ± 10 K)

The burner-stabilized flame model matches the experimental data very closely. Under this preheat condition, a stable flame was obtained up to φ = 1.75, which is greater than the conventional flammability limit of 1.67 and significantly greater than the operating limit observed when reactants were unheated (φ = 1.26). The maximum [H_2] and [CO] achievable under unheated conditions at V = 15 cm/s were 6.5% and 8.3%, respectively, both occurring at φ = 1.35 as shown in Figure 57.

With reactants preheated, the maximum [H_2] was 12.7% and the maximum [CO] was 12%. These data show that preheating significantly extends the operating range of burner-stabilized flames such that the stable burning of mixtures that produce high syngas yields can be achieved. The data also show that the burner-stabilized flame model produces very good predictions of species at φ even beyond the rich flammability limit.

In section 3.3.1 it was shown that the limiting conditions for the experiments, the burner stabilized flame model and the laminar flame speed/equivalence ratio pairs were nearly coincident for flames with unheated reactants. As shown in Figure 57 with reactants preheated to 617 K the limiting equivalence ratio (φ = 1.75) for a converged solution with the burner-stabilized flame model is nearly identical to the experimental value as well. However, the mixture equivalence ratio (φ = 1.9) having a flame speed of 25 cm/s was significantly greater than the experimental and model limit for the burner-stabilized flame.

A difference between these data and the data with unheated reactants is that the experimental results and the computational results do not match the equilibrium values at the highest values of φ. Up to the maximum achievable φ for the burner-stabilized flame, the experiments and the model concentrations are very close to equilibrium for [CO_2], however [CO] begins to diverge from equilibrium slightly and [H_2] begins to diverge significantly when φ is greater than about 1.4. This divergence is somewhat unexpected since preheating should increase the rate at which the mixture reaches equilibrium relative to unheated conditions. However, under the preheated conditions, the φ that were accessible were all relatively high (φ > 1.4), and at high φ the heat release is low, thus

slowing the kinetic processes. Even though preheating increases the range of accessible φ by increasing reaction rates, the reaction rate increase is not great enough to allow full equilibration of the mixture. Lastly, the freely-propagating flame model shows even more substantial divergence from equilibrium for both [CO] and [H_2] while [CO_2] remains very close to the equilibrium value. The concentrations for the freely-propagating flame are consistent with the trend in concentration for the burner-stabilized flame. However, the difference between the limit φ for the burner-stabilized flame model and experiment and the φ having a flame speed of 25 cm/s casts doubt on the accuracy of the freely-propagating flame model under this preheated condition.

The effect of reactant temperature was investigated by preheating reactants while the equivalence ratio was held at 1.4 and the inlet velocity was held at 24 cm/s (Figure 58). The minimum temperature at which a stable flame was observed for these conditions was 365 K, and the maximum temperature to which reactants were preheated in experiments was 630 K.

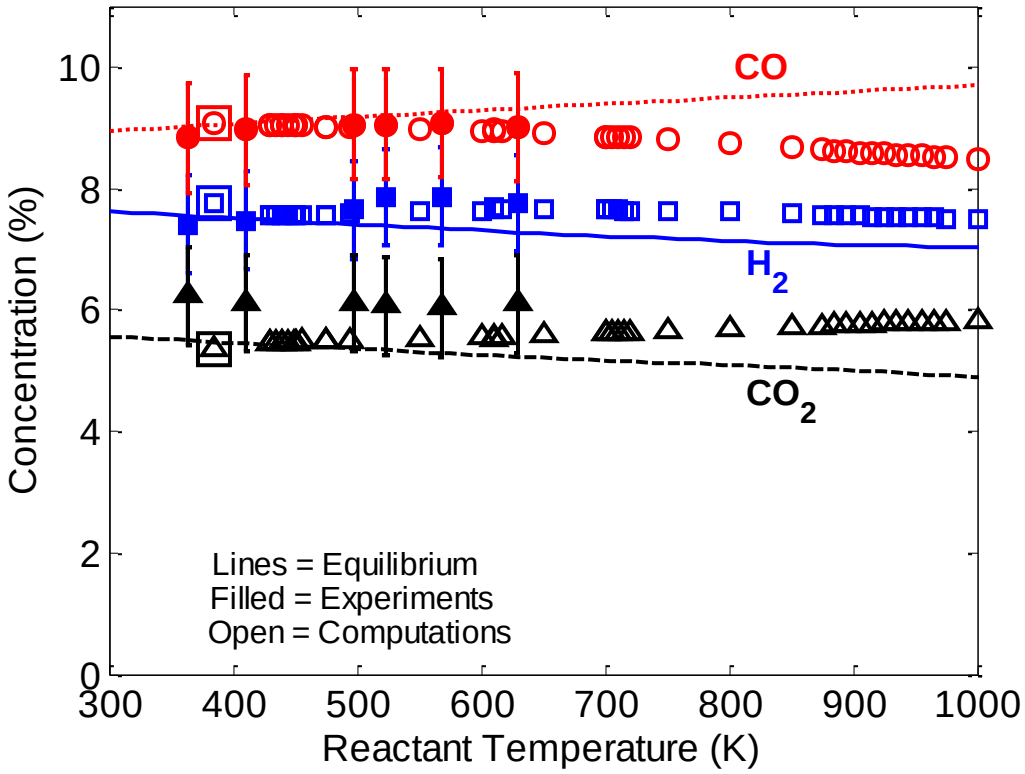

Figure 58. Concentration vs. reactant temperature at inlet velocity = 24 ± 2 cm/s and equivalence ratio = 1.4 ± 0.05 (all computational data are from burner-stabilized flame model except boxed points indicating free flame computations at temperature = 385 K)

In the range of temperature where there was overlap between the experiments and computations, the computations predicted [H_2] and [CO] very well while under-predicting [CO_2] slightly. As was shown in all of the previously presented data, the experimental results, burner-stabilized flame model and freely-propagating flame model had species concentrations nearly identical to the equilibrium values at unheated conditions. As the preheat temperature increases beyond 700 K, the difference between equilibrium and the burner-stabilized flame model increases for both [CO] and [CO_2],

however the difference between the model and equilibrium in terms of [H_2] does not increase significantly with temperature. Lastly, the overall yield of syngas ([H_2] and [CO]) remains constant with preheat temperature indicating that preheating is important for stabilizing a reaction, but not for improving syngas yield. The concentration uncertainties shown in this plot are due to uncertainty in equivalence ratio because these uncertainties are larger than the raw measurement uncertainties.

The minimum temperature at which a solution converged with the burner-stabilized flame model was within 90 K of the limit temperature, which is the minimum temperature at which a stable, flat flame was observed experimentally. The preheat temperature at which the freely-propagating flame model reported a flame speed of 25 cm/s was within 20 K of this limit temperature. The coincidence of this temperature amongst the models is another indication that the models are accurate in their prediction of flame characteristics at low reactant temperature conditions.

Lastly, Figure 59 shows concentrations of CO, H_2 and CO_2 from four sets of experiments with methane: unheated reactants on the McKenna burner, reactants preheated to 617K on the ceramic burner, and two previously-published results from experiments with filtration reactors [41, 43]. At the higher end of φ, the concentrations are basically identical between the sets of data, and at the lower end H_2 concentrations match though CO_2 concentrations and CO concentrations are higher and lower, respectively, for the McKenna experiments versus the filtration combustion experiments. Since these experiments were not all conducted under identical laboratory conditions, strong conclusions cannot be drawn. However, the data suggest that enhancement of

transport processes has no effect on syngas production at the higher, syngas producing equivalence ratios.

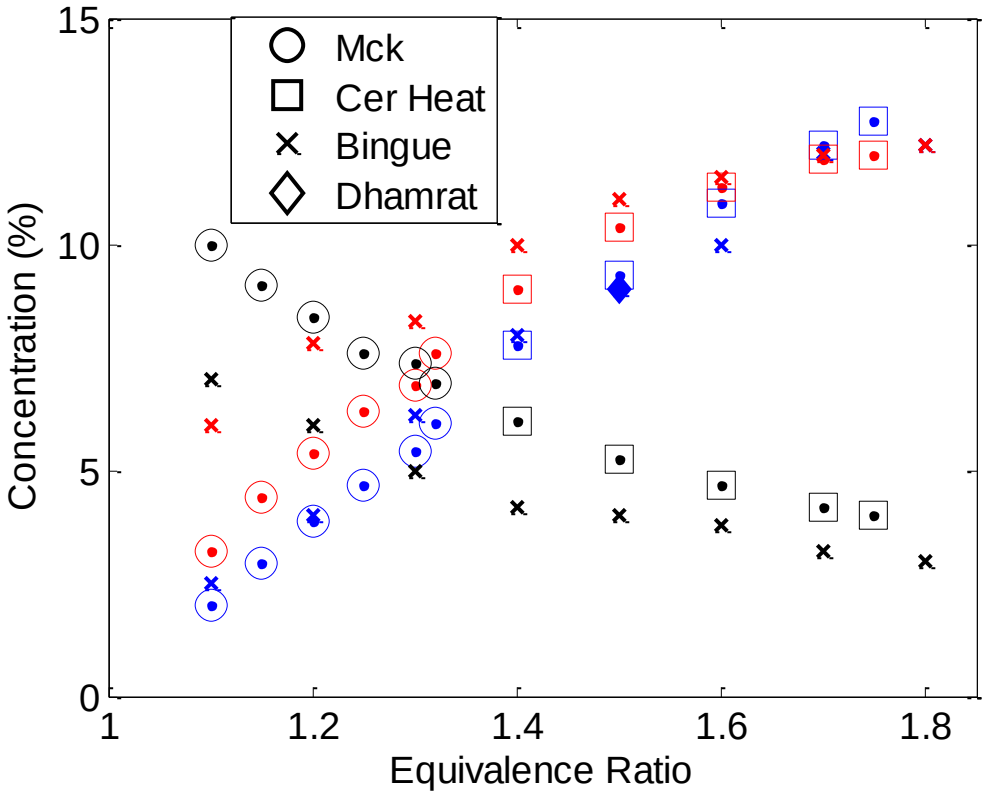

Figure 59. Comparison of concentrations for experiments with flat flame burners and filtration reactors. Bingue [43] and Dhamrat [41] data are from filtration combustion experiments.

3.4 Concluding Remarks Regarding the Effect of Preheat on Burner-Stabilized Flames

An experimental and modeling study of burner-stabilized flames was conducted to understand the effect of preheat on syngas production. First experiments were

conducted with unheated reactants so that confidence in the models could be gained for their prediction of combustion characteristics, especially species yields, at high equivalence ratios. The effect of preheat was investigated by preheating reactants up to 630 K while holding the inlet velocity and equivalence ratio constant.

The results showed that the burner stabilized flame model accurately predicts standoff distance, limit conditions and species yields for experiments with flat flame burners. Experiments with preheated reactants demonstrated that the operating limits for a flat flame burner increase substantially with increased reactant temperature, allowing the stable operation of the burner at richer equivalence ratios—where syngas yields are greater—than those achievable with unheated reactants. The specific effect of inlet temperature was investigated, and it was found that inlet temperature did not affect the yield of syngas under the tested range of temperatures. Burner-stabilized flames with preheated reactants showed deviations from equilibrium results in terms of species yields, in contrast with unheated conditions where equilibrium predicts species yields for burner-stabilized flames very well. The burner-stabilized flame model was able to predict the deviation from equilibrium when reactants were preheated to ~630 K. At high preheat temperatures, the limiting operating conditions of the experiment were well-predicted by the burner-stabilized flame model but not by the laminar flame speed.

These results have important implications with regards to heat recirculating reactors. First, the models, and therefore the kinetics mechanism, performed very well up to richest equivalence ratio examined of 1.75, which exceeds the conventional rich flammability limit. The only significant difference between the models and the

experiments was the difference between the limit equivalence ratio and the equivalence ratio where the laminar flame speed was 25 cm/s when the reactants were preheated to 617 K. This means that those working on reactor models for rich combustion should have confidence in GRI3.0 for predicting syngas production even beyond the rich flammability limit. In heat-recirculating reactors, preheat is accomplished by transport enhancement, which occurs in proximity to the reaction zone, as part of the reactor design. In the experiments described here, the preheat occurred far upstream of the reaction zone and was input from an external source. This experimental design provided a means to study the effect of preheat temperature independent of enhanced transport mechanisms and interaction with the reaction zone. The results show that preheat is necessary to attain stable operation at extreme equivalence ratios. This was the expected result since conditions (such as downstream propagation of the reaction zone in a filtration reactor) that enhance preheat have been observed in heat-recirculating reactors when mixtures expected to be unstable are burned. It was also found that further preheat does not enhance syngas production. This result aids in the design of heat recirculating reactors because it indicates that maximal heat recirculation may not be necessary for conversion of fuel to syngas.

4 CONCLUSIONS AND RECOMMENDATIONS

Two aspects of rich and ultra-rich combustion for syngas production were investigated in this study: the effect of fuel type and the effect of preheat. The effect of fuel type was studied by performing new experiments with butanol and jet fuel in a filtration reactor and comparing the results of these experiments with published experimental data from studies with other fuels and with equilibrium calculations. The effect of preheat was studied experimentally and numerically with burner-stabilized methane flames. The results of these studies advance the knowledge of rich and ultra-rich combustion for syngas production.

At present the study of rich combustion for syngas production is necessarily mostly experimental since chemical kinetic mechanisms that are well-validated for very rich conditions are not available. This is especially true for high molecular weight fuels like butanol and jet fuel because the number of species and reactions that is necessary to accurately model the chemistry grows exponentially with fuel size. A primarily experimental investigation of the conversion of jet fuel and butanol to syngas was undertaken to understand the potential of these fuels for conversion. With thee additional experimental data, a comparison amongst fuels for conversion was also conducted. Soot formation in jet fuel and butanol experiments complicated the analysis of the results. At maximum, about 42% of the hydrogen in jet fuel was converted to H_2 and 56% of carbon was converted to CO. The H_2 yield continued to increase with φ in the jet fuel experiments whereas in the butanol experiments the yields for H_2 and CO both reached peaks within the tested operating range. The peak CO yield for experiments with butanol was 72% and the peak H_2 yield was 43%. Significant soot formation was observed in

experiments with both fuels, but soot formation was so significant in the jet fuel experiments that it limited the range of experimental operating conditions. The comparison amongst fuels indicated that higher conversion rates are observed with smaller molecular weight fuels, generally. However, equilibrium calculations, which are often used to determine trends in fuel conversion, showed the opposite trend.

Combustion in heat-recirculating reactors is very complex with solid phase conduction and radiation, gas phase conduction and dispersion and convective coupling between the solid and gas phases. Additionally, filtration combustion, which was the focus of this study, is transient under many conditions, so measurements must be interpreted relative to the state of the system at a given time. In order to investigate preheat temperature, which is one important aspect of conversion in heat recirculating reactors, experiments were undertaken with burner-stabilized flames that are effectively 1-D and steady-state. An additional advantage to this experimental design is that the preheat temperature can be controlled as opposed to the situation in heat-recirculating reactors. An extensive set of model calculations were compared to the experimental data and used to investigate the effect of preheat temperatures that were beyond what was achievable experimentally. Throughout the range of operating conditions that were tested experimentally, the computational model was excellent in prediction of standoff distance, flame temperature, and species concentration. Experiments where the reactants were preheated showed a significant expansion of the stable operating range of the burner (increasing the equivalence ratio at which the flame blew off). However, increasing preheat temperature beyond what is required for stabilization did not improve syngas yields.

Based on the results of this work, recommendations for further study include, first and foremost, basic investigations of kinetics at high equivalence ratios. Though it was

shown that GRI3.0 predicted the behavior of premixed flames at relatively high equivalence ratios, this was a low bar to pass relative to examinations at very high equivalence ratios or with fuels that are significantly more complicated than methane. The second major recommendation is to investigate soot production in premixed flames of butanol and jet fuel. It was found that both fuels sooted significantly in experiments with a filtration reactor, but a filtration reactor is not ideal for investigating soot production because soot cannot be quantitatively measured in this configuration.

5 APPENDIX A: UNCERTAINTY

Uncertainty analysis relied upon the use of a Student-t distribution and sequential perturbation. The values of concentration reported by the GC were averaged, and the uncertainty was calculated by use of the student-t distribution [154]:

$$P_{\bar{x}} = \mp t \times \frac{S_x}{\sqrt{n}}$$

Where $P_{\bar{x}}$ is the uncertainty of the mean value, t is the tabulated value of the Student-t distribution, S_x is the standard deviation of the samples and n is the sample size. The distribution parameter, t is a function of the number of samples, n, and a confidence interval, C.

The implementation of this equation in Matlab is given by the following Matlab expression:

```
conf = .95;
dof = 1;
h2Unc = h2StdDev.*tinv(conf,dof)./sqrt(dof+1);
```

where `h2Unc` is the one-sided uncertainty bound, `h2StdDev` is the standard deviation of the concentration measurements for h2, `tinv` is the Matlab function that computes the value of t for the given confidence interval, `conf`, and degrees of freedom, `dof`. Degree of freedom is defined as n-1.

Systematic uncertainty included uncertainty in the GC calibration and the uncertainty in the calibration gas. The total uncertainty for each measurement was found from the following equation:

$$\delta_{y_i} = \sqrt{\delta_{y_i,meas}{}^2 + \delta_{y_i,GC\ cal}{}^2 + \delta_{y_i,GC\ gas}{}^2}$$

δ_{y_i} is the uncertainty in the measurement of the concentration of species, i. $\delta_{y_i,meas}$ is the uncertainty based on the Student-t distribution as described above. $\delta_{y_i,GC\ cal}$ is the uncertainty in the GC calibration, which is 1% of the calibrated range, and $\delta_{y_i,GC\ gas}$ is the uncertainty in concentration of the calibration gas. The value of $\delta_{y_i,GC\ gas}$ was 1% of the specified value for H_2, CO, CH_4, CO_2, N_2, C_2H_4 and C_2H_2 and was 5% of the specified value for all other species.

Uncertainties in flow rates resulted from uncertainties in the flow equipment. The air flow controllers are accurate to +/- 1% of full scale, the rotameters are accurate to 2% full scale and the rotameter indicator could be kept at a desired reading $\pm$ one tick. These errors combined to yield errors in equivalence ratio, inlet velocity and water fraction by the following representative equations for the mole flow rate of water:

$$moles/\min\ uncertinaty = \sqrt{SS}$$

$$SS = (moles/min_{set} - moles/min_{set+\Delta})^2 + (0.02 \times moles/min_{full\ scale})^2$$

where $moles/min_{set}$ is the desired value of moles per minute based on the specified rotameter setting, $moles/min_{set+\Delta}$ is the value of moles per minute that results from the rotameter indicating one tick higher than the specified setting, and $moles/min_{full\ scale}$ is the maximum flow rate of the rotameter.

The errors in flow rates and GC measurements were combined by sequential perturbation. The following set of equations describes how the uncertainty was found for

an arbitrary variable,Q, that is a function of 3 variables, each of which had its own uncertainty, Δ.

$$Q = Q(x, y, z)$$

$$\delta Q_x = Q(x + \Delta_x, y, z) - Q(x, y, z)$$

$$\delta Q_y = Q(x, y + \Delta_y, z) - Q(x, y, z)$$

$$\delta Q_z = Q(x, y, z + \Delta_z) - Q(x, y, z)$$

$$\Delta_Q = \sqrt{\delta Q_x{}^2 + \delta Q_y{}^2 + \delta Q_z{}^2}$$

The above procedure was used to find the uncertainty for all quantities, such as ethanol to hydrogen conversion efficiency, and water fraction, that were derived from other quantities with uncertainties.

The species concentrations depend on multiple variables. For an experiment where the temperature was held constant, the species concentration $[C]$ depended φ and V. When V is held constant and φ is varied, V is held constant only to within its uncertainty, . The same condition holds for when φ is held contant within its uncertainty, $d\varphi$, and V is varied. The data show that concentration of species correlated with φ at most values of φ. Therefore uncertainty in φ causes a significant uncertainty in $[C]$. After taking data a curve fit can be drawn that describes the functional relationship between $[C]$ and the dependent variables. Call this function $C = C(\varphi, V)$. Changes in $[C]$ resulting from changes in the independent variables can be estimated with the curve fit as [155]:

$$d[C] = \left[\left(\frac{\partial C}{\partial \varphi}\Big|_{V=const} d\varphi\right)^2 + \left(\frac{\partial C}{\partial V}\Big|_{\varphi=const.} dV\right)^2\right]^{1/2}$$

where $d\varphi$ is the uncertainty in φ and dV is the uncertainty in V

This method of finding the uncertainty in $[C]$ relies on a truncated Fourier expansion of the function, so this expression is only valid if C changes linearly within the range of $V \pm dV$ and $\varphi \pm d\varphi$. The uncertainty in equivalence ratio in the experiments described in this document was typically large enough that the concentration did not change linearly within the uncertainty of φ, so using this method would yield inaccurate estimates of the uncertainty in $[C]$. With a curve fit to the data, a more direct method of obtaining the changes in $[C]$ with the changes in φ and V can be obtained as described by the following graphic that describes the relationship between generic variables x and y.

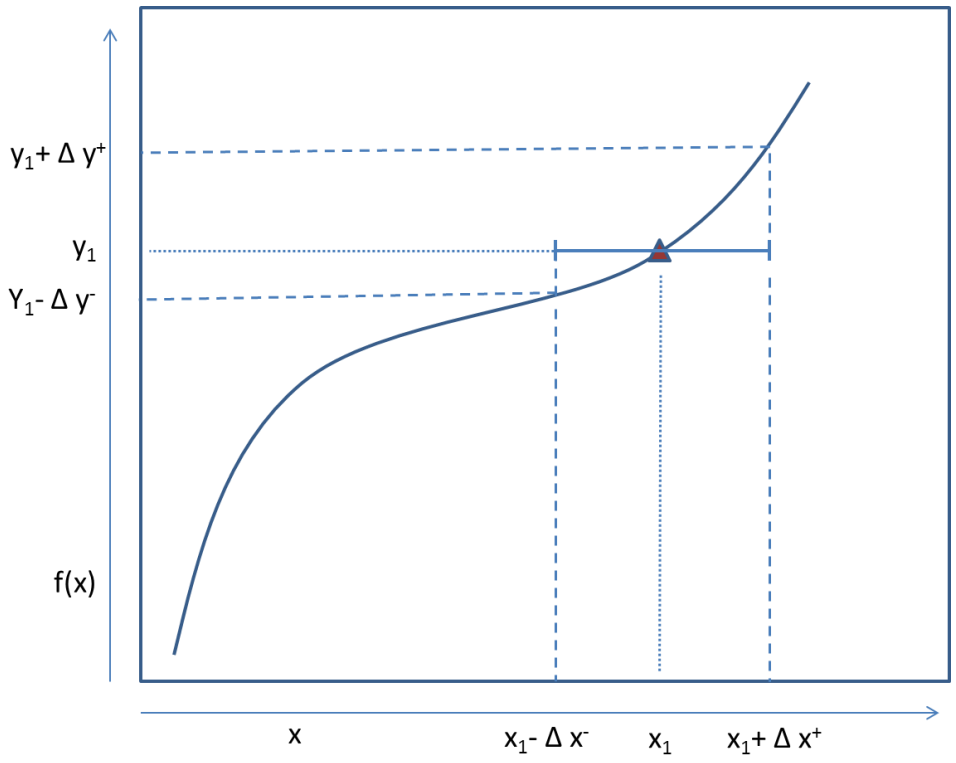

Figure 60. Graphic describing uncertainty for large uncertainty in independent variable

Figure 60 shows a graph of a dependent variable, y, vs the independent variable, x. The independent variable, x, has a fairly large uncertainties, Δx^- and Δx^+. The dependent variable, y, is not linear in the range $x_1-\Delta x^-$ to $x_1+\Delta x^+$. To find the uncertainty in y given the uncertainty in x, the values of y at the extents of the range around x1 are found. The value of y at x1 is then $y(x_1) = y_1$ with lower and upper bounds of $y_1-\Delta y^-$ and $y_1+ \Delta y^+$. This graphic is intended to illustrate the situation observed for the concentration as a function of equivalence ratio and the uncertainty in the concentration that is a consequence of the uncertainty in the equivalence ratio. Under some conditions, the raw concentration measurement uncertainty described above is smaller than the uncertainty due to uncertainty in equivalence ratio, so the larger of the two is shown on the plots where equivalence ratio is held constant.

Bibliography

1. Spath, P.L. and D.C. Dayton, *Preliminary Screening — Technical and Economic Assessment of Synthesis Gas to Fuels and Chemicals with Emphasis on the Potential for Biomass-Derived Syngas*, NREL, Editor. 2003, NREL: Golden, CO.
2. Carrette, L., K.A. Friedrich, and U. Stimming, *Fuel Cells - Fundamentals and Applications.* Fuel Cells, 2001. 1(1): p. 5-39.
3. Schoegl, I., *Production of Hydrogen-Rich Syngas via Superadiabatic Combustion*. 2009, Louisiana State University: Baton Rouge, LA.
4. Takanabe, K., K.-i. Aika, K. Seshan, and L. Lefferts, *Catalyst deactivation during steam reforming of acetic acid over Pt/ZrO2.* Chemical Engineering Journal, 2006. 120(1-2): p. 133-137.
5. Krummenacher, J.J., K.N. West, and L.D. Schmidt, *Catalytic partial oxidation of higher hydrocarbons at millisecond contact times: decane, hexadecane, and diesel fuel.* Journal of Catalysis, 2003. 215(2): p. 332-343.
6. Sobacchi, M.G., A.V. Saveliev, A.A. Fridman, L.A. Kennedy, S. Ahmed, and T. Krause, *Experimental assessment of a combined plasma/catalytic system for hydrogen production via partial oxidation of hydrocarbon fuels.* Int. J. Hydrogen Energy, 2002. 27: p. 635-642.
7. Al-Hamamre, Z. and A. Al-Zoubi, *The use of inert porous media based reactors for hydrogen production.* International Journal of Hydrogen Energy. 35(5): p. 1971-1986.
8. Holladay, J.D., J. Hu, D.L. King, and Y. Wang, *An Overview of Hydrogen Production Technologies.* Journal Name: Catalysis Today, 139(4):244-260; Journal Volume: 130; Journal Issue: 4, 2009.
9. Moon, D.J., J.W. Ryu, S.D. Lee, B.G. Lee, and B.S. Ahn, *Ni-based catalyst for partial oxidation reforming of iso-octane.* Applied Catalysis A: General, 2004. 272: p. 53-60.
10. Velu, S., X. Ma, C. Song, M. Namazian, S. Sethuraman, and G. Venkataraman, *Desulfurization of JP-8 Jet Fuel by Selective Adsorption over a Ni-based Adsorbent for Micro Solid Oxide Fuel Cells.* Energy & Fuels, 2005. 19(3): p. 1116-1125.
11. Lakhapatri, S.L. and M.A. Abraham, *Analysis of catalyst deactivation during steam reforming of jet fuel on Ni-(PdRh)-Al2O3 catalyst.* Applied Catalysis A: General. 405: p. 149-159.
12. Zabetakis, M.G., *Flammability Characteristics of Combustible Gases and Vapors*, B.o.M. US Dept. of the Interior, Editor. 1965: Washington, DC.
13. Law, C.K., *Combustion Physics*. 2006: Cambridge University Press.
14. Lewis, B. and G. Von Elbe, *Combustion, Flames, and Explosions of Gases*. 1961, New York: Academic Press.
15. Phillips, C., *JP-8 Aviation Turbine Fuel MSDS*, C. Phillips, Editor. 2012.
16. Williams, F.A., *Combustion Theory*. 1985: Benjamin/Cummings Pub. Co.

17. Liao, S.Y., D.M. Jiang, Z.H. Huang, Q. Cheng, J. Gao, and Y. Hu, *Approximation of flammability region for natural gas diluent mixture.* Journal of Hazardous Materials, 2005. 125(1â€“3): p. 23-28.
18. Weinberg, F.J., *Combustion Temperatures: The Future?* Nature, 1971. 233: p. 239.
19. Egerton, A., K. Gugan, and F.J. Weinberg, *The Mechanism of Smouldering in Cigarettes.* Combust. Flame, 1963. 7: p. 63-78.
20. Takeno, T. and K. Sato, *An Excess Enthalpy Flame Theory.* Combust. Sci. Tech., 1979. 20: p. 73-84.
21. Jones, A.R., S.A. Lloyd, and F.J. Weinberg, *Combustion in Heat Exchangers.* Proc. R. Soc. Lond. A, 1978. 360: p. 97-115.
22. *Advanced Combustion Methods*, ed. F.J. Weinberg. 1986: Academic Press, London, Orlando.
23. Babkin, V.S., V.I. Drobyshevich, Y.M. Laevskii, and S.I. Potytnyakov, *Filtration Combustion of Gases.* Fizika Goreniya i Vzryva, 1983. 19(2): p. 17-26.
24. Hardesty, D.R. and F.J. Weinberg, *Burners Producing Large Excess Enthalpies.* Combust. Sci. Tech., 1974. 8: p. 201-214.
25. Hackert, C.L., J.L. Ellzey, and O.A. Ezekoye, *Combustion and heat transfer in model two-dimensional porous burners.* Combustion and Flame, 1999. 116(1-2): p. 177-191.
26. Chen, C.-H. and P.D. Ronney, *Three-dimensional effects in counterflow heat-recirculating combustors.* Proceedings of the Combustion Institute, 2010. 33(2): p. 3285-3291.
27. Schoegl, I. and J.L. Ellzey, *Superadiabatic Combustion in Conducting Tubes and Heat Exchangers of Finite Length.* Combust. Flame, 2007. 151: p. 142-159.
28. Sathe, S.B., M.R. Kulkarni, R.E. Peck, and T.W. Tong, *An Experimental and Theoretical Study of Porous Radiant Burner Performance.* Proc. Combust. Inst., 1990. 23: p. 1011-1018.
29. Smucker, M.T. and J.L. Ellzey, *Computational and Experimental Study of a Two-section Porous Burner.* Combustion Science and Technology, 2004. 176(8): p. 1171 - 1189.
30. Vogel, B.J. and J.L. Ellzey, *Subadiabatic and Superadiabatic Performance of a Two-section Porous Burner.* Combustion Science and Technology, 2005. 177(7): p. 1323 - 1338.
31. Pedersen-Mjaanes, H., L. Chan, and E. Mastorakos, *Hydrogen production from rich combustion in porous media.* International Journal of Hydrogen Energy, 2005. 30(6): p. 579-592.
32. Barra, A.J. and J.L. Ellzey, *Heat Recirculation and Heat Transfer in Porous Burners.* Combust. Flame, 2004. 137: p. 230-241.
33. Alavandi, S.K. and A.K. Agrawal, *Experimental study of combustion of hydrogen-syngas/methane fuel mixtures in a porous burner.* International Journal of Hydrogen Energy, 2008. 33(4): p. 1407-1415.

34. Wood, S. and A.T. Harris, *Porous burners for lean-burn applications.* Progress in Energy and Combustion Science, 2008. 34(5): p. 667-684.
35. Babkin, V.S., *Filtrational Combustion of Gases. Present State of Affairs and Prospects.* Pure & Appl. Chem., 1993. 65(2): p. 335-344.
36. Bingue, J.P., A.V. Saveliev, and L.A. Kennedy, *Optimization of hydrogen production by filtration combustion of methane by oxygen enrichment and depletion.* International Journal of Hydrogen Energy, 2004. 29(13): p. 1365-1370.
37. Smith, C.H., D.M. Leahey, L.E. Miller, and J.L. Ellzey, *Conversion of wet ethanol to syngas via filtration combustion: An experimental and computational investigation.* Proceedings of the Combustion Institute, 2010. 33(2): p. 3317-3324.
38. Zhdanok, S., L.A. Kennedy, and G. Koester, *Superadiabatic Combustion of Methane Air Mixtures under Filtration in a Packed Bed.* Combust. Flame, 1995. 100: p. 221-231.
39. Dixon, M.J., I. Schoegl, C.B. Hull, and J.L. Ellzey, *Experimental and numerical conversion of liquid heptane to syngas through combustion in porous media.* Combustion and Flame, 2008. 154(1-2): p. 217-231.
40. Aldushin, A.P., *New Results in the Theory of Filtration Combustion.* Combust. Flame, 1993. 94: p. 308-320.
41. Dhamrat, R.S. and J.L. Ellzey, *Numerical and Experimental Study of the Conversion of Methane to Hydrogen in a Porous Media Reactor.* Combustion and Flame, 2006. 144: p. 698-709.
42. Leahey, D.M., *Computational Modeling of Fuel Reforming from Dry and Wet Ethanol-air Mixtures to Hydrogen in a Filtration Reactor, M.S. Thesis*. 2008, University of Texas at Austin: Austin, TX.
43. P. Bingue, J., A. V. Saveliev, A. A. Fridman, and L.A. Kennedy, *Hydrogen production in ultra-rich filtration combustion of methane and hydrogen sulfide.* International Journal of Hydrogen Energy, 2002. 27(6): p. 643-649.
44. Kennedy, L.A., J.P. Bingue, A.V. Saveliev, A.A. Fridman, and S.I. Foutko, *Chemical Structures of Methane-Air Filtration Combustion Waves for Fuel-Lean and Fuel-Rich Conditions.* Proc. Combust. Inst., 2000. 28: p. 1431-1438.
45. Mujeebu, M.A., M.Z. Abdullah, M.Z.A. Bakar, A.A. Mohamad, and M.K. Abdullah, *A review of investigations on liquid fuel combustion in porous inert media.* Progress in Energy and Combustion Science, 2009. 35(2): p. 216-230.
46. Howell, J.R., M.J. Hall, and J.L. Ellzey, *Combustion of Hydrocarbon Fuels within Porous Inert Media.* Prog. Energy Combust. Sci., 1996. 22: p. 121-145.
47. Mujeebu, M.A., M.Z. Abdullah, A.A. Mohamad, and M.Z.A. Bakar, *Trends in modeling of porous media combustion.* Progress in Energy and Combustion Science. 36(6): p. 627-650.
48. Futko, S.I., *Effect of Kinetic Properties of a Mixture on Wave Macrocharacteristics of Filtration Combustion of Gases.* Combustion, Explosion, and Shock Waves, 2003. 39(1): p. 11-22.

49. Foutko, S.I., S.I. Shabunya, S.A. Zhdanok, and L.A. Kennedy, *Superadiabatic Combustion Wave in a Diluted Methane-Air Mixture under Filtration in a Packed Bed.* Proc. Combust. Inst., 1996. 26: p. 3377-3382.
50. Drayton, M.K., A.V. Saveliev, L.A. Kennedy, A.A. Fridman, and Y. Li, *Syngas Production Using Superadiabatic Combustion of Ultra-Rich Methane-Air Mixtures.* Proc. Combust. Inst., 1998. 27: p. 1361-1367.
51. Bingue, J.P., A.V. Saveliev, and L.A. Kennedy, *Optimization of hydrogen production by filtration combustion of methane by oxygen enrichment and depletion.* Int. J. Hydrogen Energy, 2004. 29(13): p. 1365-1370.
52. Bingue, J.P., A.V. Saveliev, A.A. Fridman, and L.A. Kennedy, *Hydrogen production in ultra-rich filtration combustion of methane and hydrogen sulfide.* Int. J. Hydrogen Energy, 2002. 27: p. 643-649.
53. Toledo, M., V. Bubnovich, A. Saveliev, and L. Kennedy, *Hydrogen production in ultrarich combustion of hydrocarbon fuels in porous media.* International Journal of Hydrogen Energy, 2009. 34(4): p. 1818-1827.
54. Fay, M., R. Dhamrat, and J.L. Ellzey, *Effect of Porous Reactor Design on Conversion of Methane to Hydrogen.* Combustion Science and Technology, 2005. 177(11): p. 2171 - 2189.
55. Dmitrenko, Y., S. Zhdanok, R. Klyovan, and V. Minkina, *Methane-to-hydrogen conversion in the filtration-combustion wave of rich methane-air mixtures.* Journal of Engineering Physics and Thermophysics, 2007. 80(2): p. 304-310.
56. Dmitrenko, Y. and P. Klevan, *Hydrogen production in a reversible flow filtration combustion reactor.* Journal of Engineering Physics and Thermophysics. 84(6): p. 1296-1303.
57. Alabbadi, N., A. Al-Musa, Y. Dmitrenko, V. Martynenko, S. Shabunya, S. Al-Maiman, K. Al-Enazi, and M. Al-Zhuhani, *Conversion of methane to hydrogen in a reversible flow superadiabatic inert porous medium reactor.* Journal of Engineering Physics and Thermophysics. 84(6): p. 1287-1295.
58. Gavrilyuk, V.V., Y.M. Dmitrienko, S.A. Zhdanok, V.G. Minkina, S.I. Shabunya, N.L. Yadrevskaya, and A.D. Yakimovich, *Conversion of Methane to Hydrogen under Superadiabatic Filtration Combustion.* Theoretical Foundations of Chemical Engineering, 2001. 35(6): p. 589-596.
59. Pastore, A. and E. Mastorakos, *Rich n-heptane and diesel combustion in porous media.* Experimental Thermal and Fluid Science, 2010. 34(3): p. 359-365.
60. Schoegl, I. and J.L. Ellzey, *A mesoscale fuel reformer to produce syngas in portable power systems.* Proceedings of the Combustion Institute, 2009. 32(2): p. 3223-3230.
61. Belmont, E., S.M. Solomon, and J.L. Ellzey, *Syngas Production from Heptane in a Non-catalytic Counter-flow Reactor.* Combustion and Flame, 2012. In Press.
62. Liu, J., M. Wu, and M. Wang, *Simulation of the Process for Producing Butanol from Corn Fermentation.* Industrial & Engineering Chemistry Research, 2009. 48(11): p. 5551-5557.

63. Veloo, P.S., Y.L. Wang, F.N. Egolfopoulos, and C.K. Westbrook, *A comparative experimental and computational study of methanol, ethanol, and n-butanol flames.* Combustion and Flame. 157(10): p. 1989-2004.
64. Black, G., H.J. Curran, S. Pichon, J.M. Simmie, and V. Zhukov, *Bio-butanol: Combustion properties and detailed chemical kinetic model.* Combustion and Flame. 157(2): p. 363-373.
65. Dagaut, P., S.M. Sarathy, and M.J. Thomson, *A chemical kinetic study of n-butanol oxidation at elevated pressure in a jet stirred reactor.* Proceedings of the Combustion Institute, 2009. 32(1): p. 229-237.
66. Szwaja, S. and J.D. Naber, *Combustion of n-butanol in a spark-ignition IC engine.* Fuel. 89(7): p. 1573-1582.
67. Behrens, D.A., I.C. Lee, and C.M. Waits, *Catalytic combustion of alcohols for microburner applications.* Journal of Power Sources. 195(7): p. 2008-2013.
68. Nahar, G.A. and S.S. Madhani, *Thermodynamics of hydrogen production by the steam reforming of butanol: Analysis of inorganic gases and light hydrocarbons.* International Journal of Hydrogen Energy. In Press, Corrected Proof.
69. Wang, W. and Y. Cao, *Hydrogen production via sorption enhanced steam reforming of butanol: Thermodynamic analysis.* International Journal of Hydrogen Energy. 36(4): p. 2887-2895.
70. Wang, W. and Y. Cao, *Hydrogen-rich gas production for solid oxide fuel cell (SOFC) via partial oxidation of butanol: Thermodynamic analysis.* International Journal of Hydrogen Energy. 35(24): p. 13280-13289.
71. Lima da Silva, A. and I.L. MÃ¼ller, *Hydrogen production by sorption enhanced steam reforming of oxygenated hydrocarbons (ethanol, glycerol, n-butanol and methanol): Thermodynamic modelling.* International Journal of Hydrogen Energy. 36(3): p. 2057-2075.
72. Rass-Hansen, J., R. Johansson, M. Møller, and C.H. Christensen, *Steam reforming of technical bioethanol for hydrogen production.* International Journal of Hydrogen Energy, 2008. 33(17): p. 4547-4554.
73. Lee, I.C., J.G. St. Clair, and A.S. Gamson, *Catalytic partial oxidation of isobutanol for the production of hydrogen.* International Journal of Hydrogen Energy. 37(2): p. 1399-1408.
74. Cai, W., P.R.d.l. Piscina, and N. Homs, *Hydrogen production from the steam reforming of bio-butanol over novel supported Co-based bimetallic catalysts.* Bioresource Technology. 107(0): p. 482-486.
75. Humer, S., A. Frassoldati, S. Granata, T. Faravelli, E. Ranzi, R. Seiser, and K. Seshadri, *Experimental and kinetic modeling study of combustion of JP-8, its surrogates and reference components in laminar nonpremixed flows.* Proceedings of the Combustion Institute, 2007. 31(1): p. 393-400.
76. Cooke, J.A., M. Bellucci, M.D. Smooke, A. Gomez, A. Violi, T. Faravelli, and E. Ranzi, *Computational and experimental study of JP-8, a surrogate, and its components in counterflow diffusion flames.* Proceedings of the Combustion Institute, 2005. 30(1): p. 439-446.

77. Honnet, S., K. Seshadri, U. Niemann, and N. Peters, *A surrogate fuel for kerosene.* Proceedings of the Combustion Institute, 2009. 32(1): p. 485-492.
78. Dagaut, P., *Kinetics of jet fuel combustion over extended conditions: Experimental and modeling.* Journal of Engineering for Gas Turbines and Power-Transactions of the Asme, 2007. 129(2): p. 394-403.
79. Edwards*, T.I.M., *Cracking and Deposition Behavior of Supercritical Hydrocarbon Aviation Fuels.* Combustion Science and Technology, 2006. 178(1-3): p. 307-334.
80. Corporan, E., T. Edwards, L. Shafer, M.J. DeWitt, C. Klingshirn, S. Zabarnick, Z. West, R. Striebich, J. Graham, and J. Klein, *Chemical, Thermal Stability, Seal Swell, and Emissions Studies of Alternative Jet Fuels.* Energy & Fuels. 25(3): p. 955-966.
81. Ibarreta, A.F. and C.-J. Sung, *Optimization of Jet-A fuel reforming for aerospace applications.* International Journal of Hydrogen Energy, 2006. 31(8): p. 1066-1078.
82. Campbell, T.J., A.H. Shaaban, F.H. Holcomb, R. Salavani, and M.J. Binder, *JP-8 catalytic cracking for compact fuel processors.* Journal of Power Sources, 2004. 129(1): p. 81-89.
83. Shekhawat, D., D.A. Berry, D.J. Haynes, and J.J. Spivey, *Fuel constituent effects on fuel reforming properties for fuel cell applications.* Fuel, 2009. 88(5): p. 817-825.
84. Liu, D.-J., T.D. Kaun, H.-K. Liao, and S. Ahmed, *Characterization of kilowatt-scale autothermal reformer for production of hydrogen from heavy hydrocarbons.* International Journal of Hydrogen Energy, 2004. 29(10): p. 1035-1046.
85. Dreyer, B.J., I.C. Lee, J.J. Krummenacher, and L.D. Schmidt, *Autothermal steam reforming of higher hydrocarbons: n-Decane, n-hexadecane, and JP-8.* Applied Catalysis A: General, 2006. 307(2): p. 184-194.
86. Resini, C., C. Lucarelli, M. Taillades-Jacquin, K.-E. Liew, I. Gabellini, S. Albonetti, D. Wails, J. RoziÃ¨re, A. Vaccari, and D. Jones, *Pt-Al2O3 and Pt-Al2O3 catalysts for hydrogen production by dehydrogenation of Jet A-1 fuel: Characterisation and preliminary activity tests.* International Journal of Hydrogen Energy. 36(10): p. 5972-5982.
87. Pasel, J., J. MeiÃŸner, Z. PorÅ¡, R.C. Samsun, A. Tschauder, and R. Peters, *Autothermal reforming of commercial Jet A-1 on a scale.* International Journal of Hydrogen Energy, 2007. 32(18): p. 4847-4858.
88. Goud, S.K., W.A. Whittenberger, S. Chattopadhyay, and M.A. Abraham, *Steam reforming of -hexadecane using a catalyst: Kinetics of catalyst deactivation.* International Journal of Hydrogen Energy, 2007. 32(14): p. 2868-2874.
89. Gallagher, M.J., R. Geiger, A. Polevich, A. Rabinovich, A. Gutsol, and A. Fridman, *On-board plasma-assisted conversion of heavy hydrocarbons into synthesis gas.* Fuel. 89(6): p. 1187-1192.
90. Pastore, A. and E. Mastorakos, *Syngas production from liquid fuels in a non-catalytic porous burner.* Fuel. 90(1): p. 64-76.

91. Schmieder, R.W., *Radiotracer studies of soot formation in diffusion flames.* Symposium (International) on Combustion, 1985. 20(1): p. 1025-1033.
92. Saffaripour, M., P. Zabeti, M. Kholghy, and M.J. Thomson, *An Experimental Comparison of the Sooting Behavior of Synthetic Jet Fuels.* Energy & Fuels. 25(12): p. 5584-5593.
93. Shaddix, C.R., Ã.r.d.B. PalotÃ¡s, C.M. Megaridis, M.Y. Choi, and N.Y.C. Yang, *Soot graphitic order in laminar diffusion flames and a large-scale JP-8 pool fire.* International Journal of Heat and Mass Transfer, 2005. 48(17): p. 3604-3614.
94. Jensen, K.A., J.M. Suo-Anttila, and L.G. Blevins, *Measurement of Soot Morphology, Chemistry, and Optical Properties in the Visible and Near-Infrared Spectrum in the Flame Zone and Overfire Region of Large JP-8 Pool Fires.* Combustion Science and Technology, 2007. 179(12): p. 2453-2487.
95. Yao, M., H. Wang, Z. Zheng, and Y. Yue, *Experimental study of n-butanol additive and multi-injection on HD diesel engine performance and emissions.* Fuel. 89(9): p. 2191-2201.
96. Rakopoulos, D.C., C.D. Rakopoulos, E.G. Giakoumis, A.M. Dimaratos, and D.C. Kyritsis, *Effects of butanol/diesel fuel blends on the performance and emissions of a high-speed DI diesel engine.* Energy Conversion and Management. 51(10): p. 1989-1997.
97. Liu, H., C.-f.F. Lee, M. Huo, and M. Yao, *Combustion Characteristics and Soot Distributions of Neat Butanol and Neat Soybean Biodiesel.* Energy & Fuels. 25(7): p. 3192-3203.
98. Camacho, J., S. Lieb, and H. Wang, *Evolution of size distribution of nascent soot in n- and i-butanol flames.* Proceedings of the Combustion Institute, (0).
99. Echavarria, C.A., I.C. Jaramillo, A.F. Sarofim, and J.S. Lighty, *Burnout of soot particles in a two-stage burner with a JP-8 surrogate fuel.* Combustion and Flame. 159(7): p. 2441-2448.
100. Roesler, J.F., S. Martinot, C.S. McEnally, L.D. Pfefferle, J.L. Delfau, and C. Vovelle, *Investigating the role of methane on the growth of aromatic hydrocarbons and soot in fundamental combustion processes.* Combustion and Flame, 2003. 134(3): p. 249-260.
101. Elverum, P.J., J.L. Ellzey, and D. Kovar, *Durability of YZA ceramic foams in a porous burner.* Journal of Materials Science, 2005. 40(1): p. 155-164.
102. Mathis, W.M. and J.L. Ellzey, *Flame Stabilization, Operating Range, and Emissions for a Methane/Air Porous Burner.* Combust. Sci. Tech., 2003. 175(5): p. 825-239.
103. Davis, S., A. Belonoshko, A. Rosengren, A. van Duin, and B.r. Johansson, *Molecular dynamics simulation of zirconia melting.* Central European Journal of Physics. 8(5): p. 789-797.
104. Ansell, S., S. Krishnan, J.K.R. Weber, J.J. Felten, P.C. Nordine, M.A. Beno, D.L. Price, and M.-L. Saboungi, *Structure of Liquid Aluminum Oxide.* Physical Review Letters, 1997. 78(3): p. 464.

105. Howald, R.A. and I. Eliezer, *The thermodynamic properties of mullite.* The Journal of Physical Chemistry, 1978. 82(20): p. 2199-2204.
106. Mathis, W.M. and J.L. Ellzey, *Flame stabilization, operating range, and emissions for a methane/air porous burner.* Combustion Science and Technology, 2003. 175(5): p. 825 - 839.
107. Vasu, S.S., D.F. Davidson, and R.K. Hanson, *Jet fuel ignition delay times: Shock tube experiments over wide conditions and surrogate model predictions.* Combustion and Flame, 2008. 152(1-2): p. 125-143.
108. Hileman, I. James, Stratton, W. Russell, Donohoo, and E.G. Pearl, *Energy Content and Alternative Jet Fuel Viability*, American Institute of Aeronautics and Astronautics: Reston, VA, ETATS-UNIS. p. 12.
109. Babrauskas, V., *Ignition handbook : principles and applications to fire safety engineering, fire investigation, risk management and forensic science*. 2003, Issaquah, WA : [Bethesda, Md.] :: Fire Science Publishers ; Society of Fire Protection Engineers. viii, 1116 p. :.
110. Smith, C.H., C.D. Zak, D.I. Pineda, and J.L. Ellzey, *Conversion of Jet Fuel to Syngas via Filtration Combustion*, in *7th US National Meeting of the Combustion Institute*, C. Institute, Editor. 2011, The Combustion Institute: Atlanta, GA.
111. Smith, C.H., *Conversion of Wet Ethanol to Syngas via Filtration Combustion, M.S. Thesis*. 2009, University of Texas at Austin: Austin.
112. Goodwin, D.G. *Cantera*. 2002-2007 [cited.
113. Smith, C.H., D.M. Leahey, L.E. Miller, and J.L. Ellzey, *Conversion of Wet Ethanol to Syngas via Filtration Combustion: an Experimental and Computational Investigation*, in *6th U.S. National Combustion Meeting*, T.C. Institute, Editor. 2009, The Combustion Institute: Ann Arbor, MI.
114. Dixon, M.J., *Conversion of Liquid Heptane to Syngas through Combustion in Porous Media*, in *Department of Mechanical Engineering*. 2007, University of Texas at Austin: Austin, TX.
115. Stanmore, B.R., J.F. Brilhac, and P. Gilot, *The oxidation of soot: a review of experiments, mechanisms and models.* Carbon, 2001. 39(15): p. 2247-2268.
116. Warnatz, J., *Combustion : physical and chemical fundamentals, modeling and simulation, experiments, pollutant formation*. 4th ed. ed. 2006, Berlin ; New York :: Springer. xii, 378 p. :.
117. Dasch, C.J., *The decay of soot surface growth reactivity and its importance in total soot formation.* Combustion and Flame, 1985. 61(3): p. 219-225.
118. Tsurikov, M.S., K.P. Geigle, V. KrÃœGer, Y. Schneider-KœHnle, W. Stricker, R. LÃœCkerath, R. Hadef, and M. Aigner, *Laser-based Investigation of Soot Formation in Laminar Premixed Flames at Atmospheric and Elevated Pressures.* Combustion Science and Technology, 2005. 177(10): p. 1835-1862.
119. Al-Hamamre, Z., S. Voß, and D. Trimis, *Hydrogen production by thermal partial oxidation of hydrocarbon fuels in porous media based reformer.* International Journal of Hydrogen Energy, 2009. 34(2): p. 827-832.

120. Al-Hamamre, Z. and M.A. Hararah, *Hydrogen production by thermal partial oxidation of ethanol: Thermodynamics and kinetics study.* International Journal of Hydrogen Energy. 35(11): p. 5367-5377.
121. Pedersen-Mjaanes, H., L. Chan, and E. Mastorakos, *Hydrogen Production from Rich Combustion in Porous Media.* Int. J. Hydrogen Energy, 2005. 30: p. 579-592.
122. Belmont, E.L., S.M. Solomon, and J.L. Ellzey, *Syngas production from heptane in a non-catalytic counter-flow reactor.* Combustion and Flame, (0).
123. Smith, C.H., D.I. Pineda, C.D. Zak, and J.L. Ellzey, *Conversion of Jet Fuel and Butanol to Syngas by Filtration Combustion.* International Journal of Hydrogen Energy, 2012. Submitted.
124. Koch, D.L., R.G. Cox, H. Brenner, and J.F. Brady, *The Effect of Order on Dispersion in Porous Media.* J. Fluid Mech, 1989. 200: p. 173-188.
125. Hackert, C.L., J.L. Ellzey, O.A. Ezekoye, and M.J. Hall, *Transverse Dispersion at High Peclet Numbers in Short Porous Media.* Exp. Fluids, 1996. 21: p. 286-290.
126. Ronney, P.D., *Analysis of Non-Adiabatic Heat-Recirculating Combustors.* Combust. Flame, 2003. 135: p. 421-439.
127. Mishra, S.C., M. Steven, S. Nemoda, P. Talukdar, D. Trimis, and F. Durst, *Heat transfer analysis of a two-dimensional rectangular porous radiant burner.* International Communications in Heat and Mass Transfer, 2006. 33(4): p. 467-474.
128. Khose-Hoinghaus, K. and J.B. Jeffries, eds. *Applied Combustion Diagnostics*. Combustion: An International Series. 2002, Taylor & Francis: New York.
129. Hansen, N., T.A. Cool, P.R. Westmoreland, and K. Kohse-Hoinghaus, *Recent contributions of flame-sampling molecular-beam mass spectrometry to a fundamental understanding of combustion chemistry.* Progress in Energy and Combustion Science, 2009. 35(2): p. 168-191.
130. Marinov, N.M., W.J. Pitz, C.K. Westbrook, M.J. Castaldi, and S.M. Senkan, *Modeling of Aromatic and Polycyclic Aromatic Hydrocarbon Formation in Premixed Methane and Ethane Flames.* Combustion Science and Technology, 1996. 116-117(1-6): p. 211-287.
131. Schoenung, M. and R.K. Hanson, *CO and Temperature Measurements in a Flat Flame by Laser Ab orption Spectroscopy and Probe Techniques.* Combustion Science and Technology, 1980. 24(5-6): p. 227-237.
132. Weigand, P., R. Luckerath, and W. Meier, *Documentation of Flat Premixed Laminar CH4/Air Standard Flames: Temperatures and Species Concentrations*, D.I.o.C.T. (http://www.dlr.de/vt/PortalData/29/Resources/dokumente/ch4_air_flames.pdf), Editor. 2003: Stuttgart.
133. Gersen, S., A.V. Mokhov, and H.B. Levinsky, *Extractive probe/TDLAS measurements of acetylene in atmospheric-pressure fuel-rich premixed methane/air flames.* Combustion and Flame, 2005. 143(3): p. 333-336.

134. Kumar, K. and C.-J. Sung, *Laminar flame speeds and extinction limits of preheated n-decane/O2/N2 and n-dodecane/O2/N2 mixtures.* Combustion and Flame, 2007. 151(1â€“2): p. 209-224.
135. Liu, F.S. and O.L. Gulder, *Effects of pressure and preheat on super-adiabatic flame temperatures in rich premixed methane/air flames.* Combustion Science and Technology, 2008. 180(3): p. 437-452.
136. Bosschaart, K.J. and L.P.H. de Goey, *The laminar burning velocity of flames propagating in mixtures of hydrocarbons and air measured with the heat flux method.* Combustion and Flame, 2004. 136(3): p. 261-269.
137. Gibson, J., M. Ayoobi, and I. Schoegl, *Behavior of Preheated Premixed Flames at Rich Conditions.* Proc. Combust. Inst., 2012. 34(In Press).
138. Sepman, A., A.V. Mokhov, and H.B. Levinsky, *A laser-induced fluorescence and coherent anti-Stokes Raman scattering study of NO formation in preheated, laminar, rich premixed, methane/air flames.* Proceedings of the Combustion Institute, 2002. 29: p. 2187-2194.
139. Hidaka, Y., K. Sato, Y. Henmi, H. Tanaka, and K. Inami, *Shock-tube and modeling study of methane pyrolysis and oxidation.* Combustion and Flame, 1999. 118(3): p. 340-358.
140. Smith, G.P., D.M. Golden, M. Frenklach, N.W. Moriarty, B. Eiteneer, M. Goldenberg, C.T. Bowman, R.K. Hanson, S. Song, J.W.C. Gardiner, V.V. Lissianski, and Z. Qin, *GRI-Mech 3.0 URL* http://www.me.berkeley.edu/gri-mech/version30/. 1999.
141. Goodwin, D.G. (2012) *Cantera - An object-oriented software toolkit for chemical kinetics, thermodynamics, and transport processes*. http://code.google.com/p/cantera/
142. Chao, B.H. and C.K. Law, *Duality, Pulsating Instability, and Product Dissociation in Burner-Stabilized Flames.* Combustion Science and Technology, 1988. 62(4-6): p. 211-237.
143. Sutton, G., A. Levick, G. Edwards, and D. Greenhalgh, *A combustion temperature and species standard for the calibration of laser diagnostic techniques.* Combustion and Flame, 2006. 147: p. 39-48.
144. Associates, H. *Diagram of McKenna Burner*. 2012 [cited 2012 8/30/2012]; Available from: http://flatflame.com/.
145. Mokhov, A.V. and H.B. Levinsky, *A LIF and cars investigation of upstream heat loss and flue-gas recirculation as NOx control strategies for laminar, premixed natural-gas/air flames.* Proceedings of the Combustion Institute, 2000. 28(2): p. 2467-2474.
146. Cole, J.A., *A Molecular-Beam Mass-Spectrometric Study of Stoichiometric and Fuel-Rich 1,3-Butadiene Flames*, in *Chemical Engineering*. 1982, Massachusetts Institute of Technology: Cambridge.
147. Gaydon, A.G., *The spectroscopy of flames*. 2nd ed. ed. 1974, London :: Chapman and Hall. xii, 412, [2] p., [15] p. of plates :.

148. Wang, H., *CH* mechanism*, in *Personal Communication*, C.H. Smith and J.L. Ellzey, Editors. 2012.
149. Kathrotia, T., U. Riedel, A. Seipel, K. Moshammer, and A. Brockhinke, *Experimental and numerical study of chemiluminescent species in low-pressure flames.* Applied Physics B: Lasers and Optics. 107(3): p. 571-584.
150. Ferguson, C.R. and J.C. Keck, *Stand-off distances on a flat flame burner.* Combustion and Flame, 1979. 34(0): p. 85-98.
151. Kurdyumov, V.N. and M. Matalon, *The porous-plug burner: Flame stabilization, onset of oscillation, and restabilization.* Combustion and Flame, 2008. 153: p. 105-118.
152. Williams, B.A. and J.W. Fleming, *Comparison of species profiles between O2 and NO2 oxidizers in premixed methane flames.* Combustion and Flame, 1995. 100(4): p. 571-590.
153. Evertsen, R., J.A. Van Oijen, R.T.E. Hermanns, L.P.H. De Goey, and J.J. Ter Meulen, *Measurements of absolute concentrations of CH in a premixed atmospheric flat flame by cavity ring-down spectroscopy.* Combustion and Flame, 2003. 132: p. 34-42.
154. Devore, J.L., *Probability and statistics for engineering and the sciences*. 6th ed. ed. 2004, Belmont, CA :: Thomson-Brooks/Cole. xvi, 795 p. :.
155. Moffat, R.J., *Describing the uncertainties in experimental results.* Experimental Thermal and Fluid Science, 1988. 1(1): p. 3-17.